Article

Improvements for the Western North Atlantic, Caribbean and Gulf of Mexico ADCIRC Tidal Database (EC2015)

Christine Szpilka [1],*, Kendra Dresback [1], Randall Kolar [1], Jesse Feyen [2] and Jindong Wang [3,4]

[1] School of Civil Engineering and Environmental Science, University of Oklahoma, 202 W. Boyd Room 334, Norman, OK 73019, USA; dresback@ou.edu (K.D.); kolar@ou.edu (R.K.)
[2] NOAA/Great Lakes Environmental Research Laboratory, 4840 South State Road, Ann Arbor, MI 48108, USA; Jesse.Feyen@noaa.gov
[3] NOAA/National Ocean Service/Coast Survey Development Laboratory, 1315 East-West Highway, Silver Spring, MD 20910, USA; jindong.wang@gmail.com
[4] Earth Resources Technology, Inc., 14401 Sweitzer Lane, Suite 300, Laurel, MD 20707, USA
* Correspondence: cmszpilka@ou.edu; Tel.: +1-405-325-5911

Abstract: This research details the development and validation of an updated constituent tidal database for the Western North Atlantic, Caribbean and Gulf of Mexico (WNAT) region, referred to as the EC2015 database. Regional databases, such as EC2015, provide much higher resolution than global databases allowing users to more accurately define the tidal forcing on smaller sub-region domains. The database last underwent major updates in 2001 and was developed using the two-dimensional, depth-integrated form of the coastal hydrodynamic model, ADvanced CIRCulation (ADCIRC), which solves the shallow-water equations in the generalized wave continuity equation form. Six main areas of improvement are examined: (1) placement of the open ocean boundary; (2) higher coastal resolution using Vertical Datum (VDatum) models; (3) updated bathymetry from global databases; (4) updated boundary forcing compared using two global tidal databases; (5) updated bottom friction formulations; and (6) improved model physics by incorporating the advective terms in ADCIRC. The skill of the improved database is compared to that of its predecessor and is calculated using harmonic data from the National Oceanic and Atmospheric Administration Center for Operational Oceanographic Products and Services (NOAA CO-OPS) stations and historic International Hydrographic Organization (IHO) data. Overall, the EC2015 database significantly reduces errors realized in the EC2001 database and improves the quality of coastal tidal constituents available for smaller sub-regional models in the Western North Atlantic, Caribbean and Gulf of Mexico (WNAT) region.

Keywords: tidal constituent database; WNAT region; ADCIRC

1. Introduction

Small-scale regional hydrodynamic models are widely used to study many varied physical processes such as sediment transport [1–3]; storm surge inundation [4–6]; real-time surge forecast systems [7–10]; sea level rise [11–14]; passive fish and larval transport, as well as coupled ecological behavior [15–17]; combined hydrologic and hydrodynamic processes [9,18]; passive transport of oil spills [19] and coupled hydrodynamic-marsh interactions with biological feedback [20]. Each of these complex applications requires reliable tidal boundary forcing in order to provide accurate results. In particular, many coastal ocean models utilize tidal databases in order to specify the tidal boundary conditions in these regional studies. When no other data is available, the boundary conditions are

often selected from global tidal databases. However, while global tidal databases are highly accurate in the deep ocean, they often lack the resolution over continental shelves and in the shallower near-shore regions to adequately resolve the astronomical and associated nonlinear tides in the immediate coastal regions [21]. Therefore, it is necessary to create smaller-scale tidal databases that are able to resolve the near-shore environment. Over the past 25 years, three such databases have been developed for the eastern coast of the United States [22–24]. These regional databases use the finite element ADvanced CIRCulation model (ADCIRC) forced with a global tidal database at the open ocean boundary to develop the tidal profile within the domain.

Historically, the eastern (and gulf) coast of the United States has been modeled with a large domain that encompasses the entire Western North Atlantic, Gulf of Mexico and Caribbean Sea, herein referred to as the WNAT domain, and has traditionally had the open ocean boundary located at the 60° W meridian [22,25,26]. This larger domain provides easier forcing as the boundary lies mostly in the deeper Atlantic Ocean and includes only a small portion of the continental shelves near the coastline.

The first tidal database for the WNAT region, EC1991, was state of the art for its time and had 19,858 nodes and 36,653 elements with elements ranging from 7 km at the coastline to about 140 km in the deeper ocean. The bathymetry was extracted from the Earth Topography 5 min gridded resolution (ETOPO5) global bathymetric database. The EC1991 database included elevation and velocity harmonics for the O_1, K_1, Q_1, M_2, S_2, N_2 and K_2 constituents [22].

An updated version, EC1995, was created in order to take advantage of the National Ocean Service (NOS) hydrographic survey database for nearshore bathymetry, which has since been digitized [27]. The NOS bathymetric database includes raw sounding tracks from ship surveys and typically covers coastal areas out to the continental shelf in U.S. coastal waters. This updated version had 31,435 nodes and 58,369 elements and a minimum element size of 750 m in Perdido Bay between Alabama and Florida and a maximum element size of 105 km. The average coastal element size was about 5 km with regions of the Florida peninsula and the Gulf Coast west of the Mississippi River typically having 10 km resolution. The EC1995 database included elevation and velocity harmonics for the steady, O_1, K_1, M_2, S_2, N_2, M_4 and M_6 constituents.

The next generation, EC2001, database utilized a grid with 254,565 nodes and 492,179 elements and had a minimum element size of 200 m in the Mississippi River Delta region and a maximum element size of 29 km. The New Orleans area was the most highly resolved with average element sizes of 1 km and some areas of finer 500 m resolution. However, the remainder of the domain had typical coastal element sizes closer to 2–3 km. The original EC2001 database included elevation and velocity harmonics for the O_1, K_1, Q_1, M_2, S_2, N_2 and K_2 constituents [23]. As an intermediate update, a longer run of 410 days with additional P_1 tidal boundary forcing was recomputed in 2008, ec2001_v2e [24], to provide the NOS suite of 37 tidal constituents [28] for both species.

In comparison, the latest version, EC2015, database has 2,066,216 nodes and 3,770,720 elements with a minimum element size of 13 m in the Puerto Rico and Long Island Sound regions (as well as some small Florida channels) and a maximum element size of 46 km near the open boundary. With a few exceptions, the entire WNAT coastline (United States water only) has typical resolutions of 250–500 m with even more detail in inland channels and inlets. As per the 2008 update to the EC2001 database, the EC2015 database provides the computed amplitude and phase of elevation and velocity for the 37 standard NOS tidal constituents. Table 1 summarizes the grid features of the WNAT domain tidal databases.

Table 1. Summary of grid features for Western North Atlantic, Caribbean and Gulf of Mexico (WNAT) domain ADvanced CIRCulation model (ADCIRC) tidal databases.

Database Name	# of Mesh Nodes	# of Mesh Elements	Avg. Coastal Resolution (km)	Min. Coastal Resolution (m)	Max. Deep Ocean Resolution (km)
EC1991	19,858	36,653	7	1000	140
EC1995	31,435	58,369	5	750	105
EC2001	254,565	492,179	1 to 3	200	29
EC2015	2,066,216	3,770,720	0.25 to 0.5	13	46

In the next sections, we present the improvements that have been incorporated into this latest generation tidal database and the remaining challenges. We summarize the development of the EC2015 tidal constituent database; present a skill assessment for global, regional and site specific locations; and discuss how the database can and should be used. Limitations of the database are also discussed. In the interest of brevity, we will only present the skill assessment for these 8 primary constituents: M_2, S_2, N_2, K_2, O_1, K_1, P_1 and Q_1.

2. Materials and Methods

2.1. ADCIRC Computational Model

2.1.1. General Model Details

As mentioned before, the enhancements to this database will employ the ADCIRC regional hydrodynamic model. ADCIRC utilizes the full non-linear St. Venant (shallow water) equations, using the traditional hydrostatic pressure and Boussinesq approximations. The depth-averaged generalized wave continuity equation is used to solve for the free surface elevation, along with the non-conservative form of the momentum equation for the velocity components. The equations are discretized horizontally in space using continuous Galerkin, linear finite elements with equal-order interpolating functions (linear C^0), while time is discretized using an efficient, split-step, Crank-Nicholson algorithm with the nonlinear terms evaluated explicitly. There have been many papers written about the development and usage of the ADCIRC computational model, but basic details for the equations of ADCIRC can be found in [29–31].

One of the advances within ADCIRC since the East Coast database was last updated in 2001 is the addition of Manning's *n* friction representations. Users are able to specify specific quadratic friction coefficients, Chezy friction coefficients or Manning's *n* values throughout the domain [32]. For the Manning's *n* implementation, the *n* values are converted to an equivalent quadratic friction coefficient within ADCIRC before the bottom stress is calculated [30]. This equivalent quadratic friction coefficient is calculated for each node at every time step as

$$CF\left(t\right) = \frac{gn^2}{\sqrt[3]{depth + eta\left(t\right)}} \tag{1}$$

where *g* is the gravitational constant (9.81 m/s²), *n* is the Manning's coefficient, *depth* is bathymetric depth (m) and *eta*(*t*) is the water surface elevation at time *t* (m). Note that the computed quadratic friction coefficient, *CF*(*t*), can also be limited on the lower end by specifying the minimum *CF* value in the input file. Otherwise, the values can become quite small as the depth becomes large.

2.1.2. Model Input Parameters

Unless otherwise noted in the appropriate methods and results subsections, all of the ADCIRC model runs used the parameters in the following descriptions. The EC2015 tidal database was developed from a 410-day simulation run in order to capture the long-period non-linear tides. A smooth

hyperbolic tangent ramp function is applied to both the boundary forcing and the tidal potential forcing functions for the first 25 days. Then the model is allowed to run for another 20 days before the internal ADCIRC harmonic analysis is started for the final 365 days of the simulation. A one-minute interval is used for the internal harmonic decomposition. Tidal potential forcing is applied to the interior of the domain for the O_1, K_1, Q_1 and P_1 diurnal constituents and the M_2, N_2, S_2 and K_2 semidiurnal constituents. In addition to these eight constituents, the open ocean boundary is also forced with the Mm, Mf, M_4, MN_4 and MS_4 constituents. Nodal factors and equilibrium arguments were set for a 410-day run starting on November 17, 1991; this translates to the harmonic analysis occurring over the entire year of 1992, which is the middle of the current National Tidal Datum Epoch from 1983 to 2001. Unless otherwise noted, tidal forcing was extracted from the TPXO7.2 global tidal database [33].

A time-step of 1.0 s was used yielding a maximum Courant number of 0.76 in the U.S. Virgin Islands and of 0.3 along the Atlantic and Gulf coasts. The time weighting factors for the three-level implicit scheme in the GWCE form of the momentum equation are 0.35, 0.30 and 0.35 for the future, present and past time levels respectively. A two-level Crank-Nicholson scheme is used for the momentum equations. The lateral eddy viscosity coefficient was set equal to 5.0 m^2/s and a non-linear quadratic bottom friction scheme with a constant value of 0.0025 was used for all runs except for the variable bottom-friction comparisons. Specific friction settings for the Manning's *n* formulation and the variable *CF* runs are detailed in Section 2.2.5 below; for all variable friction tests, a lower limit of 0.0025 was used. A spatially variable but temporally constant GWCE, *G* or τ_0, parameter was used such that *G* is dependent upon the local depth and is set as follows: if the depth is $\geq$10, *G* is set to 0.005, if the depth is <10, *G* is set to 0.020.

Due to the large overall mesh domain, variable Coriolis forces were enabled. The non-linear finite amplitude option was utilized with wetting and drying enabled. With the newly expanded open ocean boundary, it was possible to enable the advective terms, as detailed in Section 2.2.6 below.

2.2. Improvements for the ADCIRC Tidal Database

The WNAT domain has been improved upon bit by bit over the past 25 years. As technology has progressed in that time, larger computational domains have been possible. Additionally, with advances in remote data collection methods, more accurate and plentiful data is now available for the bathymetric profile of the world's oceans and the location of coastlines. For the latest generation East Coast tidal database, six areas of improvement were examined:

1. Move the open ocean boundary out away from the Lesser Antilles
2. Improve the coastal resolution using the NOAA VDATUM product grids
3. Update the deep water bathymetry
4. Use the latest global tidal database products for forcing on the open ocean boundary
5. Compare three bottom friction schemes for improved accuracy
6. Improve the model physics by enabling the advective terms within ADCIRC

In the following subsections, we detail the methods used for each of these areas. Improvements realized in the harmonic constituent accuracy, as compared with CO-OPS and IHO field measurements, will be presented in the results section.

2.2.1. Open Ocean Boundary Placement

The open ocean boundary has been moved out from the traditional 60° W meridian that has been used for the past 25 years. Figure 1 shows the new extended model domain with the traditional boundary shown in red as a vertical line near the new boundary. The purpose of this expanded domain was to improve model stability by moving the open ocean boundary further away from the complexities of the Lesser Antilles island chain that separates the Caribbean Sea from the Atlantic Ocean. The traditional EC2001 domain becomes unstable near these islands when the quarter-diurnal

constituents (M_4, MS_4, and MN_4) are included in the boundary forcing. The EC2001_extended mesh was created at NOAA and has the same coastline and bathymetry in the interior as the EC2001 domain, but with a different boundary location.

There were two guiding principles for choosing this new open ocean boundary location: (1) to avoid any nearby amphidromic regions of the principal tidal constituents—M_2, S_2, N_2, K_1 and O_1; and (2) to create a smooth boundary with gradually changing element size. For elements closer to the coast, the element size was chosen to be smaller and then to gradually increase in size away from the coast. The new boundary curves to the west near Nova Scotia in order to create a smooth transition, without sharp corners, from the ocean boundary to the land boundary. It also prevents the introduction of the Gulf of St. Lawrence into the model domain. One other important design feature was to avoid having too small of elements across shelf breaks, particularly in the southern part of the boundary near the Lesser Antilles.

After a suitable boundary location was found, a one-year fully non-linear tidal simulation was performed to confirm the stability and robustness of the new boundary location. All thirteen of the TPXO7.2 global tidal model constituents were used to force the open boundary (M_2, S_2, N_2, K_2, K_1, O_1, P_1, Q_1, Mf, Mm, M_4, MS_4, and MN_4) during this stability test.
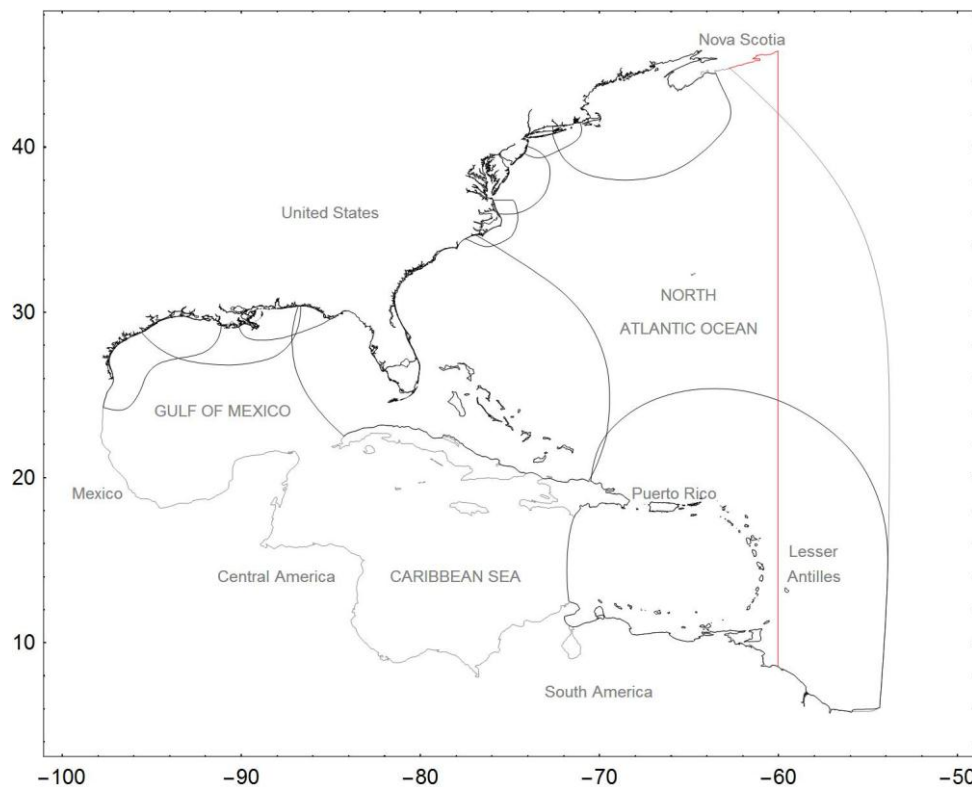
Figure 1. Location of new EC2001_extended model domain (shown in gray) compared to the traditional EC2001 boundary at the 60° W meridian (shown in red—remainder of shoreline is same as gray); and location of the nine VDatum domains (shown in black) used to update the coastal resolution and bathymetry in the EC2015 model. Note that the coarser gray shoreline is not visible underneath the black.

2.2.2. Increased Coastal Resolution

Each of the WNAT predecessors has gradually added more resolution along the coastline as data and computation capabilities were more readily available. However, this version marks a substantially increased level of coastal resolution for such a large study region. Recall from Table 1 that there are nearly 8 times the number of nodes in the EC2015 mesh when compared to the EC2001 mesh.

Over the past 15 plus years, NOAA has undertaken an ambitious study of the United States coastline to create a tool for transformation between different vertical datums. The VDatum (Vertical Datum) tool provides a single source for accurately and easily transforming geospatial data among different tidal, orthometric and ellipsoidal vertical datums along the United States coast. It allows the user to combine data from different horizontal and vertical reference systems into a common system in order to create integrated digital elevation models. The interested reader is referred to the VDatum website for more general information about the VDatum tool and for regional publications [34].

In order to create accurate tidal datum fields for the coastal regions, a series of highly resolved coastal grids were developed for each region of the East and Gulf Coast for the United States, as well as Puerto Rico and the U.S. Virgin Islands. Figure 1 shows the boundaries of the nine VDatum grids that are presently available in the WNAT domain, with the remainder of the EC2001_extended boundary shown to clearly illustrate the regions where VDatum meshes were used. Individual reports [35–43] for each of these domains are available on the VDatum website.

Notice that there are several areas of overlap between these regional VDatum subdomains. For each of these overlaps, the individual grids were carefully pieced together in such a way as to preserve the source grid with the highest coastal resolution. For the shelf regions within these overlaps, a transitional mesh was created at an appropriate distance from the shoreline that smoothly blended the triangulations of the two VDatum meshes. Finally, the bathymetry from the highest resolution source was reapplied onto the new triangulation. This process was repeated for each of the overlapping areas. A comparison of the East Coast of the United States from North Carolina to Maine in the EC2015 model and the previous EC2001 model is shown in Figure 2. Notice the inclusion of more inland channels, rivers and islands; as well as a more detailed shoreline.
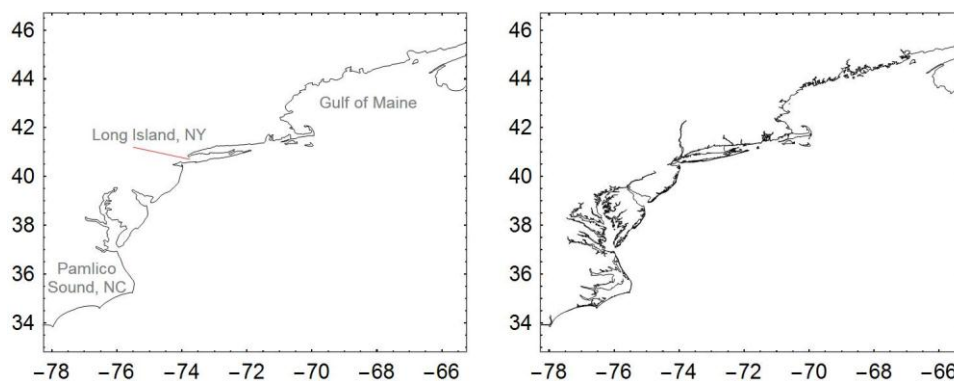
Figure 2. Comparison of coastal resolution in the EC2001 (**left**) and EC2015 (**right**) models from North Carolina to Maine.

It is important to note that the high-resolution meshes created for the VDatum project are in a Model Zero (MZ) vertical datum. The interested reader is referred to the VDatum Standard Operating Procedure manual [44]; but the basic idea is that small corrections are added/subtracted from the original charted bathymetry in an iterative manner until the simulation converges to a solution. The converged solution is verified against harmonic constituent data available within the region. This was necessary since the original bathymetric sources were all in different tidal datums and no tool existed to transform them into a unified vertical datum. The resulting vertical datum of the high resolution coastline is MZ. Although, model zero is not necessarily the same as mean sea level (MSL) due to non-linear dynamic effects, for our purposes, we have to assume that the VDatum coastline is approximately relative to MSL.

The next step was to replace the coastline of the newly created EC2001_extended mesh with this higher resolved coastline. During this step, we also compared localized truncation error analysis

(LTEA) meshes of various resolution for the Florida South Atlantic Bight region as we transitioned from the VDatum coastline into the deeper waters [45]. While exploring the various options, it was discovered that several smaller channels along the Georgia and Carolina coasts had not been included in the original VDatum mesh. We decided not to pursue the LTEA meshing at this time, due to the large grid size and time involved to process the size functions. Instead, any hydrologically significant channels were added using NOAA National Ocean Service (NOS) charts and sounding data. However, because these areas were outside of the original VDatum "wet" area, the proper conversion from the NOS sounding datum (usually MLLW or MLW) to the common MSL datum was estimated from the nearest wet conversion points output from the VDatum tool, typically at the mouth of the channel. In order to extrapolate the conversions up the length of the new channels, the slope of the surrounding channel topography was examined and average slope values (for each stream reach) were used to "march" the sounding datum to MSL conversions upstream from the channel mouth. At points in the channel where the surrounding topographic slope changed, a new reach slope value was used to continue marching upstream.

2.2.3. Updated Global Bathymetry

Once the improved coastline was merged into the EC2001_extended model, the next task was to update the bathymetry of all the non-coastal U.S. waters, which had last been updated in 2001. Two different global bathymetry sources were examined: the ETOPO$_1$ Global Relief Model from the National Geophysical Data Center and the SRTM30_PLUS model from the Scripps Institute of Oceanography.

The ETOPO$_1$ product is a 1 arc-minute global relief model of the Earth's surface. It integrates land topography and ocean bathymetry and was built from numerous regional and global data sets. Older two arc-minute and 5 arc-minute products are still available, although they have been deprecated by the latest model. The horizontal datum of ETOPO$_1$ is WGS84 geographic and the vertical datum is sea level. "More specific vertical datums, such as mean sea level, mean high water, and mean low water, differ by less than the vertical accuracy of ETOPO$_1$ (~10 m at best), and are therefore effectively equivalent" [46]. Various methods are available for obtaining the ETOPO$_1$ product from their website [47].

The SRTM30_PLUS product is a 30 arc-second global relief model of the Earth's surface, also derived from a wide variety of sources. However, rather than only being a compilation of existing bathymetric data sources, it also uses these data sources to modify global satellite bathymetry based on the latest altimeter-derived gravity models [48,49]. Depths are reported in meters and negative values indicate data points that are below sea level. Additionally, catalogs of the data sources and estimated errors in the depth and navigation for each point are available. Various methods of obtaining the data are available at their website [50].

After data was downloaded for each of these sources, the procedure was to create a bounding polygon of all water that was included in the various VDatum regional grids and only update the water that was outside of that polygon, see Figure 1 (all regions that are within the gray boundary but outside of the black boundaries were updated). This meant that most of the Gulf of Mexico and Caribbean coastline, including the southern coast of Cuba, Haiti and Jamaica had to be updated with global sources that were not necessarily meant to be used in shallow coastal regions. We compared both of the global sources and noticed that the ETOPO$_1$ product resulted in a great deal of oscillations in shallower regions (checkerboard type pattern from one point to the next), particularly along the southern coast of Cuba. In comparison, the SRTM30_PLUS product did not suffer as much with this issue, although it did exhibit occasional oscillations in shallower regions. In general, both products were developed for deeper water not coastal areas and the resolution and depth accuracy is not high enough to adequately resolve shallow coastal waters—with average errors in the 10 m range, all depths below 10 m are suspect. Overall, it was decided to use a single source for the updated bathymetry and the SRTM30_PLUS database was used as it exhibited fewer oscillations in the shallower, near-shore

regions. However, after interpolation of the global data set, there were nodes within the grid that were suspect—e.g., sharp change in bathymetry relative to surrounding nodes. The bathymetry at these suspect grid nodes was then hand-cleaned by interpolating from surrounding values in the mesh itself instead of directly from the global source. This removed most sharp oscillations along the non-US coastlines between topographic and bathymetric values, however, further inspection may reveal that some errors still exist.

2.2.4. Updated Open Ocean Forcing

Once an updated physical model had been developed for the entire WNAT region, it was necessary to extract tidal forcing information from available global tidal models at the open-ocean boundary. Since the last version of the East Coast ADCIRC tidal database in 2001, significant improvements have been made in the global tidal modeling community as well. Therefore, we compared two different choices for the boundary conditions: the TPXO7.2 model obtained from the Oregon State University Tidal Inversion Software (OTIS) and the Finite Element Solution FES2012 model from the French Tidal Group [33,51].

OTIS implements an efficient representer scheme for the general inversion calculation for tidal processing of TOPEX/Poseidon altimeter data going back to 2002. TPXO7.2 is a more recent version of a global model of ocean tides obtained from OTIS. The solution best fits, in a least-squares sense, the Laplace Tidal Equations and along-track averaged altimetry data [52,53]. TPXO products are updated as more altimetry and bathymetry data becomes available; since the beginning of the EC2001 project, they have since updated to TPXO8, but for consistency we wanted all of the model runs to have the same forcing so we continued to use TPXO7.2. Tides are provided as complex amplitudes of earth-relative sea-surface elevation for 13 constituents at a 1/4 degree resolution for the global ocean; software and accompanying data can be downloaded from their website [33].

Similarly, the French Tidal Group utilizes a global unstructured grid to model the tidal barotropic equations in a spectral configuration and then employs representer data assimilation from long-term satellite altimetry data to correct the tidal signals. FES products are provided on a 1/16 degree resolution for 32 tidal constituents over the global ocean. The most recent version is FES2012, which was produced by Noveltis, Legos and CLS Space Oceanography Division and is distributed by Aviso [51,54].

After extracting the tidal constituent information from each of these databases, a visual comparison was made of the amplitude and phase information that would be used as input into the ADCIRC model. Since the TPXO products only have information for 13 constituents, it was decided to use these same thirteen harmonic constituents to force the ocean boundary (diurnal—O_1 K_1 P_1 Q_1; semi-diurnal—M_2 S_2 N_2 K_2; quarter-diurnal—M_4 MS_4 MN_4; and long term—Mf Mm) in order to maintain a comparable forcing suite. In general, there were very few visual differences between these two models, particularly for the diurnal, semi-diurnal and long term constituents. What differences did exist were typically concentrated at the northern boundary near Nova Scotia (refer to Figure 1 for geographic locations within the WNAT domain). Similarly, among the quarter-diurnal constituents, most of the amplitude differences were focused along the boundary as it approached the coast of Nova Scotia. However, the phasing of the quarter-diurnal constituents was significantly different all along the boundary; note that the amplitudes of these constituents are often on the order of 10^{-3} to 10^{-2} m. Additionally, the phasing of the Q_1 constituent in each of the global products departed rapidly from each other as the boundary neared the Nova Scotia coast. A more quantitative comparison was made by calculating the maximum absolute difference in amplitude and phase over all 187 open ocean boundary nodes; these results are given in Table 2.

Table 2. Maximum absolute differences along the entire EC2015 boundary between the TPXO7.2 and FES2012 global tidal database products.

Constituent	Amplitude (cm)	Phase (Degrees)
O_1	1.28	20.20
K_1	2.26	10.95
P_1	1.25	34.62
Q_1	0.55	122.14
M_2	2.03	1.10
N_2	0.44	6.39
S_2	1.31	7.95
K_2	1.00	10.01
M_4	0.86	34.49
MS_4	0.95	58.66
MN_4	0.11	16.22
Mf	0.21	39.85
Mm	0.06	6.67

While interesting, this was not enough information to determine if one global model was better than the other. In the results section, we will present the actual ADCIRC harmonic differences due to the boundary forcing.

2.2.5. Bottom Friction Assignment

Finally, we examined three variations of the quadratic friction formulation for the EC2015 database: a constant *CF* version and two variable friction formulations. For the variable formulations, we used a merged combination of the *CF* values that had been developed for each of the VDatum regions and we also used the collaborative United States Geological Survey (USGS) usSEABED [55] database of core samples to assign appropriate Manning's *n* friction values.

Of the nine VDatum grids that fall within the EC2015 model domain, five had a variable quadratic bottom friction scheme. It was not necessary to be as rigorous in combining these friction values, as the areas of grid overlap did not have any conflicting friction values. Therefore, each VDatum region was simply mapped onto the EC2015 model and then combined canonically.

The usSEABED database contains three files for each region: "EXT—numeric data extracted from lab-based investigations, PRS—numeric data parsed from word-based data and CLC—numeric data calculated from the application of models or empirical relationship files" [55]. Each of these datasets has limitations and describes the data in different ways; they can be combined to create a more extensive coverage of the seafloor characteristics. For the EC2015 study, we had to limit the richness of the dataset in order to make it tractable for such a large study area. Therefore a relatively simple approach wherein the grain distributions within the "Gravel", "Sand", "Mud" and "Clay" columns of the original usSEABEDS data were aggregated into a single description based upon percentages in each class. This created a verbal distinction only between gravel, sand and silt that did not worry about actual grainsize distributions. Each larger coastal area was then assigned a descriptive designation with an associated shelf Manning's *n* value: muddy/silty: $n = 0.015$, sandy: $n = 0.022$ (upon visual examination, there were no large areas that were entirely gravel, just independent data points so no gravel appropriate Manning's *n* values were assigned in this stage). After a region was classified by bed type, depth-dependent linear interpolation was used to assign Manning's *n* values over each section of the coastal/shelf. For water depths between 5 m and 200 m, the shelf value was assigned; for depths greater than 200 m the post-Ike "deep ocean" value of 0.012 was assigned; finally, for depths less than 5 m, values were linearly interpolated from a value of 0.025 at zero depth to the shelf value at 5 m depth. This slightly larger zero-depth Manning's *n* value is meant to take into account the impeded flow characteristics due to extremely shallow water. After this process was completed, smaller

sub-regions were assigned estuary specific "shelf" values and very coarse sub-grids were defined over the sub-regions, then these sub-grids went through the linear depth interpolation process again with these new values. Only a few estuaries were assigned values different than their surrounding shelves. Table 3 provides the rough geographical shelf regions and specific estuaries that were used in this process, as well as the assigned shelf Manning's *n* values.

Table 3. Geographic regions used for Manning's *n* assignment from usSEABEDS data.

Geographic Region	Bed Description	Assigned Shelf Value
Louisiana/Texas	muddy/silty	0.015
Florida	sandy	0.022
Mexico/South America/Caribbean [1]	sandy	0.022
Atlantic Coast	sandy	0.022
Delaware/Chesapeake Bays	silty	0.015
Westernmost New York Sound	silty	0.015

[1] No data was available for these regions, so a general assumption was made.

This is a very simplified approach to assigning friction values given the rich dataset available. However, in the time available for the project, it was impossible to interpolate between each of the usSEABEDS data points and "smooth" the ensuing profile since there could be distances on the order of kilometers from a boulder site that was surrounded by sand. Without knowing the physical extents of the boulders, it is a judgement call how to transition from the one or two boulder indicated grainsizes to the surrounding sand bed. An area of future work would be an efficient interpolation scheme for such a diverse and scattered data set. Depending upon the water depth at an area of interest, it may not be as important as one might think however. If we look again at Equation (1) and note that initially $eta(t) = 0$, then we can compute the equivalent quadratic friction coefficient, as ADCIRC does internally. This allows a visual comparison between the Manning's *n* friction representation and the assigned VDatum friction representation. Figures 3 and 4 show regional views for the Gulf of Maine/New York Sound area and the Mississippi River delta area. For both Figures, panel (a) shows the bathymetric depth profile, panel (b) shows the assigned VDatum quadratic friction coefficients, panel (c) shows the simplified Manning's *n* assignment, and panel (d) shows the computed equivalent quadratic friction coefficient associated with (a) and (c).

Note that in both figures, the scales for panels (b) through (d) are the same. However, owing to the difference in regional bathymetry, the bathymetry scales for panel (a) in each figure are different. For the deeper Atlantic coast region, notice that although there is some variation in the Manning's *n* profile itself, the computed quadratic friction values do not show as much detail due to the overall deep bathymetry. Meanwhile, for the Louisiana region, the bathymetry scale is more abbreviated (from 0 m to 500 m with more detail in the first hundred meters) and there is more detail to the coastal *CF* values due to the shallower nature of that region.

Due to the inherent simplifications in the Manning's *n* assignments, a sensitivity study of the computed harmonic constituents to the assigned Manning's *n* values was conducted. The originally assigned Manning's *n* values were multiplied by factors of 90% and 110% and the resulting harmonic responses were compared. More details of this sensitivity study are given in the results section.

2.2.6. Inclusion of ADCIRC Non-linear Advective Terms

The final effort was to include the non-linear advective terms in the ADCIRC formulation; the interested reader is referred to [56] for details about the development of these terms and equations. In practice, these terms enter in by activating two flags in the input file. In past versions of the East Coast tidal database, the location of the open ocean boundary near the Lesser Antilles island chain caused instabilities if these terms were activated. Therefore, until the boundary was moved as part

of this study, it was not possible to include fully non-linear advection and compare how the tidal response varied due to these terms.
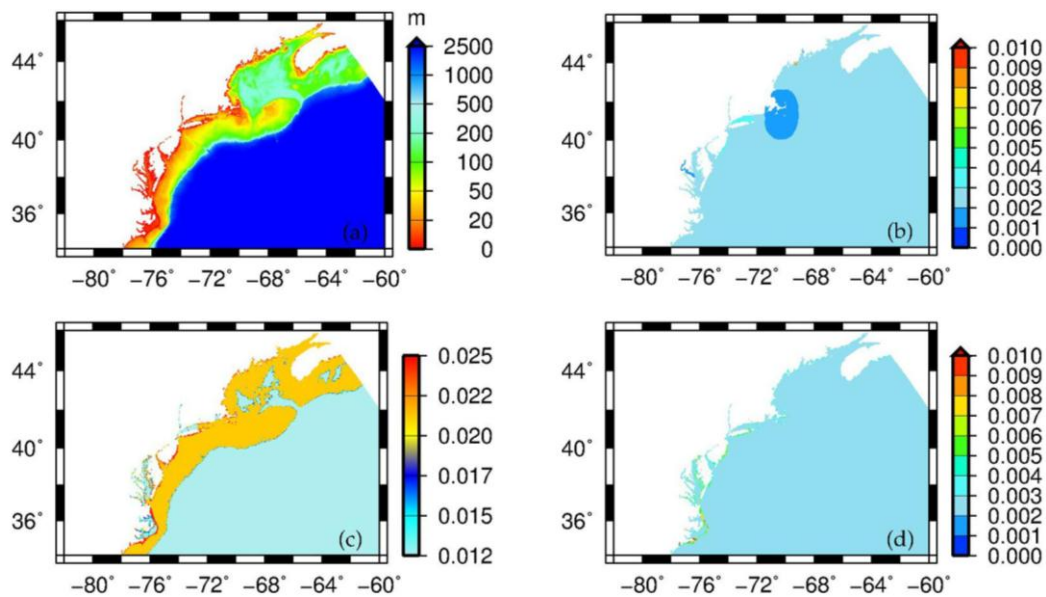
Figure 3. Comparison of bottom friction assignment for the Atlantic coastline from North Carolina to Maine: (**a**) bathymetry—scale from 0 m to 2500 m, (**b**) assigned Vertical Datum (VDatum) friction coefficient (*CF*) values, (**c**) assigned Manning's *n* values and (**d**) computed *CF* values from bathymetry and assigned Manning's *n* values.
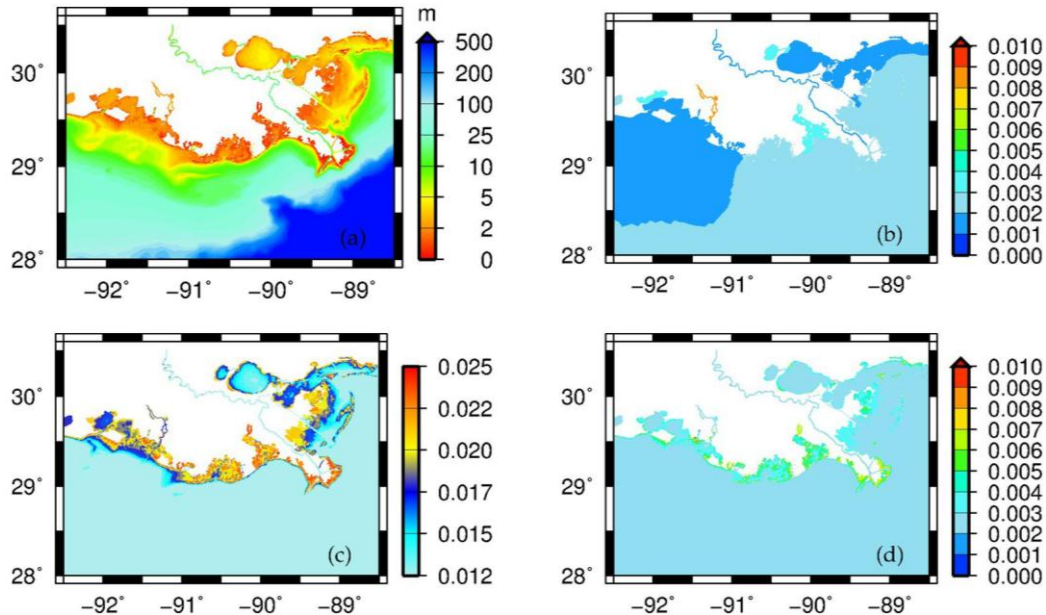
Figure 4. Comparison of bottom friction assignment for the Louisiana coastline: (**a**) bathymetry—scale from 0 m to 500 m, (**b**) assigned VDatum *CF* values, (**c**) assigned Manning's *n* values and (**d**) computed equivalent *CF* values from bathymetry and assigned Manning's *n* values.

2.2.7. Summary of Tidal Database Improvements

Six different areas of improvement have been presented for the EC2015 tidal database. Where possible, each model improvement was isolated to determine the accuracy improvement that was due only to that component of the project. However, the improved coastal resolution and

updated bathymetry were lumped into the final EC2015 release and were not studied individually. Table 4 provides a summary of the simulations that were completed for this study; including the run designation, description, mesh domain, inclusion of the advection terms, friction scheme and boundary forcing. For the boundary forcing, the textual label indicates which global tidal database was used and the number indicates how many constituents were used (e.g., TPXO-10 indicates that the TPXO7.2 global database was used with only 10 constituents—recall that the quarter-diurnal constituents create instability in the EC2001 domain for long-term simulations). For clarity, when reporting results, labeling figures and during the discussion, the results will be referred to by their run designation.

Table 4. Summary of model parameters for the model simulations completed in this study.

Run Designation	Description	Grid	Advection	Friction Scheme	Boundary Forcing [1]
EC2001	EC2001 extracted	EC2001	Off	0.0025	TPXO-10
EC2001-ext	EC2001 extended mesh	EC2001_ext	Off	0.0025	TPXO-10
FES1	FES 2012	EC2015	On	0.0025	FES-13
OTIS1	TPXO 7.2	EC2015	On	0.0025	TPXO-13
OTIS3	EC2015 release version	EC2015	On	VDatum	TPXO-13
OTIS3noadv	EC2015 advection off	EC2015	Off	VDatum	TPXO-13
OTIS4	Manning n	EC2015	On	Manning's n	TPXO-13
OTIS5	90% Manning n	EC2015	On	90% Manning	TPXO-13
OTIS6	110% Manning n	EC2015	On	110% Manning	TPXO-13

[1] The textual part of the label indicates which global tidal database was used, while the number indicates how many constituents were included.

The EC2001 tidal database was rerun with the most recent version of ADCIRC to ensure that we could expect a fair comparison with the EC2015 results. Error analysis confirmed that the new version of ADCIRC was recreating the harmonic constituents from the 2008 updated tidal database [23]. In subsequent sections, all reference to the EC2001 model indicate that constituents were directly extracted from the previous version of the database at the same locations as the recent improvements. In order to test the affects due solely to the boundary location, a new input file that mimicked the 2008 update, but used the new expanded boundary, was created; this run designation is given by EC2001-ext. The only difference in the input file is that boundary forcing was extracted from the TPXO7.2 global tidal database at the new boundary node locations.

A series of runs using the final EC2015 model domain (boundary placement, updated bathymetry and improved coastal resolution all lumped together) were conducted; all seven of these used the full thirteen-constituent suite of boundary forcing and six of them include the advective terms. The OTIS1 and FES1 simulations differ only in whether the TPXO7.2 or FES 2012 global tidal databases were used for the boundary conditions; a constant bottom friction was utilized in order to isolate the boundary forcing. Additionally, four variable bottom friction runs were conducted to compare the harmonic response to various friction schemes; OTIS3 used the merged VDatum friction, OTIS4 used the original Manning's n assignments, OTIS5 used the OTIS4 Manning's n values scaled by 90%, and OTIS6 scaled these by 110%. Finally, in order to test the advective terms, the OTIS3noadv simulation mimics the OTIS3 simulation but with the advective terms turned off.

2.3. Validation of the Improved ADCIRC Tidal Database

Two sources of harmonic constituent data were used to validate the new EC2015 tidal database. The analysis techniques used to compute model errors are also discussed in this section.

2.3.1. Validation Data

The Center for Operational Oceanographic Products and Services (CO-OPS) keeps a record of tidal benchmarks and harmonic data at stations throughout the United States [57]. Tidal harmonic data was available at 404 such stations in the EC2015 domain. Additionally, historical data from the International Hydrographic Organization (IHO) was used to provide wider coverage, specifically in the deeper regions beyond the continental shelves [58]. There is a higher measure of uncertainty in the IHO data, as information about the source of the constituents (e.g., length of analysis and data records) is not available; furthermore, the three-decimal digits precision of longitude and latitude coordinates used to locate the stations are sometimes insufficient to determine the physical location of the data collection. At the request of some of the participating countries, the bank was removed from public distribution in about 2002 [59]. Of the about 4190 IHO stations available worldwide, 277 fall within the EC2015 domain. For skill assessment purposes, all 681 stations (404 from CO-OPS and 277 from IHO) were classified by regional location (Atlantic, Gulf of Mexico, Caribbean Sea), as well as coastal proximity versus deep ocean.

The overall locations of the available 681 data stations are shown in Figure 5a; while Figure 5b,c and Figure 6 show zoomed views of the various regions. In all of these figures, the gray boundary depicts the new EC2015 model domain while the green boundary depicts the old EC2001 model domain; the data locations from CO-OPS are shown in blue while IHO data locations are shown in red; data locations shown with a cyan circle surrounding them are not wet in the EC2001 domain and are excluded from any error comparisons that specifically say that only wet stations were used; finally, sample regional scatter plots are provided in Appendix B for the 10 stations that are shown with a black X and indicated by station number.

Of these 681 stations, only 367 were considered wet in the EC2001 model, where by wet we mean that they are either within the domain itself (280) or were near enough to the boundary in the main water bodies that nearest neighbor data extraction (87) was valid. Stations that were far inland or within small channels are not extracted from the EC2001 database as they were not physically represented in the older database. All stations shown in Figures 5 and 6 without a cyan circle denote the location of these 367 stations where harmonics were extracted from the EC2001 database for comparison with the new EC2015 database. Appendix A provides a list of all 681 stations with the CO-OPS station designation (when applicable), lon/lat location, station name and assigned region (Table A1). Station numbers indicated with a single * are close enough to the boundary to use nearest element approximations within the EC2001 model, while those with a double ** are not located within the extents of the EC2001 model and are not used for statistics or station scatter plots when comparing results. Actual longitude and latitude coordinates were not shifted when extracting from the EC2001 database, as the nearest element is most likely where the station would have been manually shifted anyway.

2.3.2. Validation Methods

In order to determine which model best captured the tidal harmonic data at the available data stations, we looked at a variety of error measures. For each station, we examined scatter plots of measured and computed amplitude and phase for the eight primary tidal constituents (M_2, S_2, N_2, K_2, O_1, K_1, P_1 and Q_1). Ideally, the computed and measured values would have a one-to-one correspondence. Scatter plots were also made that included all 681 stations for each of these eight constituents and a least-squares linear regression was computed. Additionally, comparison scatters showing both the EC2001 and EC2015 models for these eight constituents were created using the 367 wet stations in the EC2001 tidal database.
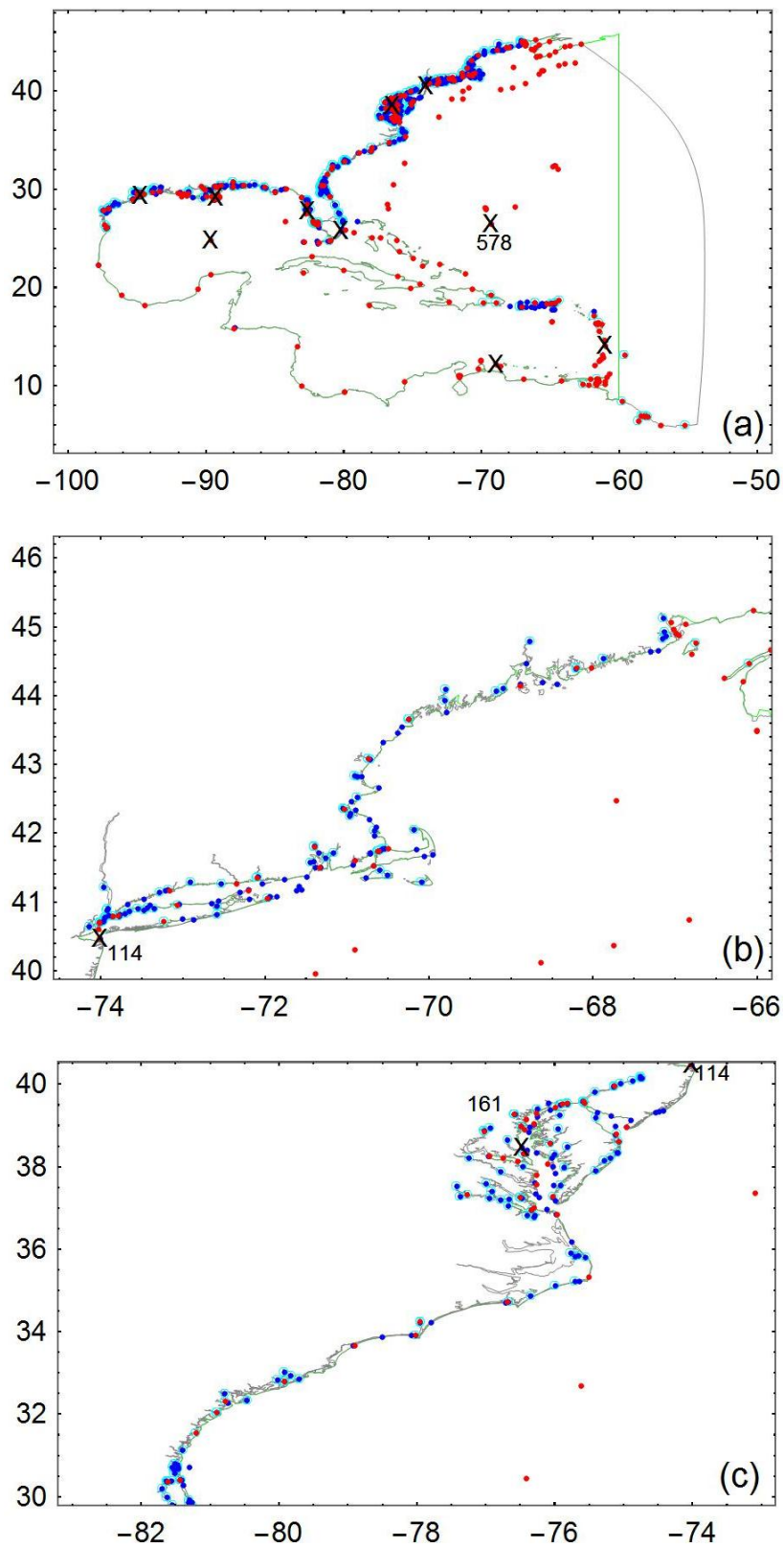
Figure 5. Locations for the stations available for validating the WNAT tidal databases: (**a**) global; (**b**) New York and Maine coast; and (**c**) Delaware down to Georgia. Blue points are from NOAA, red points are from IHO, cyan circles indicate stations that are in EC2015 (gray boundaries) but are not wet in EC2001 (green boundaries). Scatterplots are shown in Appendix B for points shown by an X.
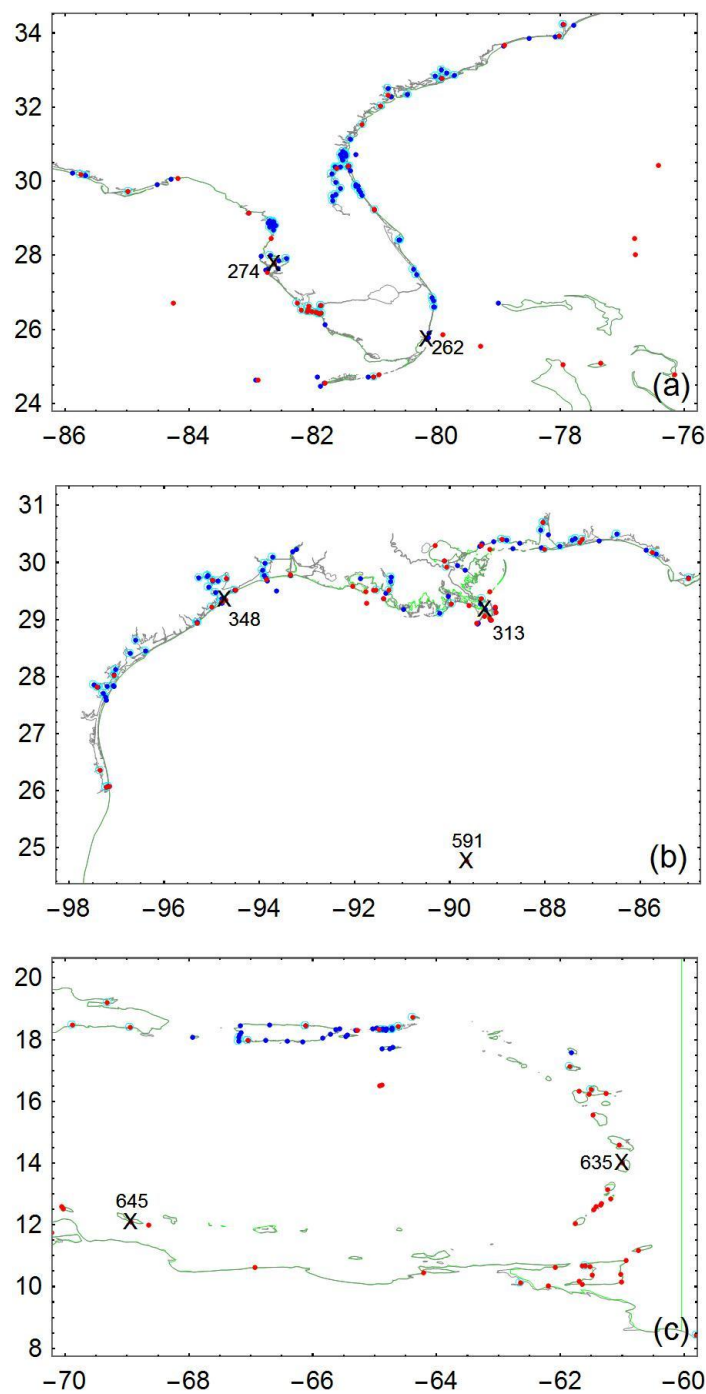
Figure 6. Locations for the stations available for validating the WNAT tidal databases: (**a**) Florida, (**b**) Gulf of Mexico and (**c**) Caribbean Sea. Blue points are from NOAA, red points are from IHO, cyan circles indicate stations that are in EC2015 (gray boundaries) but are not wet in EC2001 (green boundaries). Scatterplots are shown in Appendix B for points shown by an X.

In addition to these qualitative measures, three different error measures were calculated to quantify the skill of each model. For the phase, the mean absolute error was computed as

$$MAE = \frac{1}{8np} \sum_{e=1}^{np} \sum_{k=1}^{8} \left| \text{data}_{e,k} - \text{model}_{e,k} \right| \qquad (2)$$

where errors are summed over the number of data points for a particular region (*e*) as well as the number of constituents (*k*). To calculate the mean errors for an individual constituent, the second sum would only be computed for $k = 1$ and the 8 is removed from the denominator.

Due to some constituents having very small amplitudes, the mean relative error was computed for amplitudes only as

$$MRE = \frac{1}{8np} \sum_{e=1}^{np} \sum_{k=1}^{8} \frac{\left| \text{data}_{e,k} - \text{model}_{e,k} \right|}{\text{data}_{e,k}} \tag{3}$$

where the same summation rules apply. Note that if the errors are on the same order of magnitude as the data, the relative errors will be close to 100%. Additionally, a composite root mean square (RMS) error, combining the phase and amplitude error for each constituent into a single error metric, was calculated at each station as

$$A_E = \sqrt{0.5 \left(A_m^2 + A_o^2 \right) - A_m A_o \cos \left(\pi \left(h_m - h_o \right) / 180 \right)} \tag{4}$$

where A_m is the modeled amplitude in meters, A_o is the observed amplitude in meters, h_m is the modeled phase (degrees GMT) and h_o is the observed phase (degrees GMT). As before, the mean errors are calculated by summing over the number of data points for any particular region as well as the number of constituents,

$$MeanRMSE = \frac{1}{8np} \sum_{e=1}^{np} \sum_{k=1}^{8} \left(A_E \right)_{e,k} \tag{5}$$

In order to compare the skill of the new EC2015 model versus the previous EC2001 database, harmonic constituents were extracted from the 2001 database (2008 updated) at the stations that were within (or close enough to) the bounds of the EC2001 model. Mean errors were then computed for both databases at those 367 locations. However, mean errors were also calculated at all 681 stations for the new EC2015 database. Table 5 provides the total number of stations in each region that were used for statistics for each model; parenthetical numbers include only the stations that were physically within the EC2001 domain, not the nearest neighbors.

Table 5. Total number of validation stations available in each region for the most recent East Coast models.

Model	Atlantic Ocean	Deep Stations [2]	Gulf of Mexico	Caribbean	Global
EC2001	204 (151) [1]	31	90 (74)	73 (55)	367 (280)
EC2015	414	31	178	89	681

[1] Numbers in parentheses indicate how many were actually within the EC2001 domain while the first number includes those stations approximated with nearest neighbors. [2] The deep stations are also included in the Atlantic and Gulf of Mexico regional numbers.

3. Results

3.1. Results for the Various Improvements

In this section some of the model improvements are examined independently to determine how effective they are at increasing the tidal constituent accuracy. For brevity, only the regional mean RMS error comparisons are provided here. Full error analysis, as described in Section 2.3.2, will be provided in Section 3.2 when the EC2001 model is compared to the final release EC2015 model. Figure 7 presents the regional mean RMS errors for all nine simulations that were previously presented in Table 4. These mean errors were computed using only the 367 wet stations that are common to all model domains.
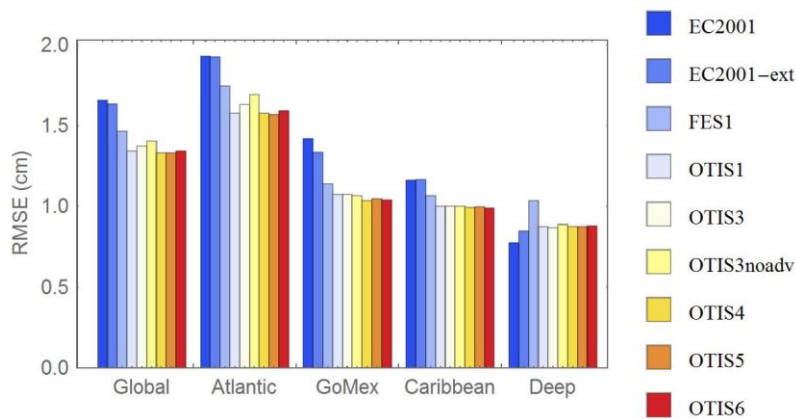
Figure 7. Comparison of regional root mean square (RMS) errors using the 367 wet stations for all nine study simulations summarized in Table 4.

3.1.1. Boundary Placement

As described in Section 2.2.1, the open ocean boundary has been moved out away from the Lesser Antilles Islands and the historical 60° W meridian that has been used for over 25 years. In order to test how much of an affect the new boundary placement has on the extracted harmonic constituents, the new EC2001_extended model was run with an identical input file as was used for the 2008 updates to the EC2001 tidal database, ec2001_v2e, [23]: a larger time step of 5.0 s is possible with these coarser meshes, the non-linear advective terms were turned off and only 10 forcing frequencies were used on the open boundary—the three quarter-diurnal constituents were not used in order to match the EC2001 simulation. All other parameters are as described in Section 2.1.2.

Concentrating only on the EC2001 and EC2001-ext results in Figure 7, we note that simply moving the boundary out away from the Lesser Antilles does not significantly improve the overall accuracy, although it does help the stability of the model. The Atlantic and Caribbean regional errors are unchanged, while the global errors are only slightly reduced. A moderate error reduction is realized in the Gulf of Mexico region and the deep stations actually have slightly higher mean errors.

3.1.2. Comparison of Open Ocean Boundary Forcing

Two different global tidal databases have been examined as input to the EC2015 model: FES12 and TPXO7.2. Looking at the FES1 and OTIS1 bars in Figure 7, we note that for all regions the OTIS1 simulation has less error than the FES1 simulation; these error reductions are most significant in the Atlantic region and deep water stations. Although the differences are rather small, it is obvious that the TPXO global database is providing more accurate results than the FES12 database.

3.1.3. Comparison of Bottom Friction Schemes

In this study, three different bottom friction schemes are compared: constant $CF = 0.0025$, VDatum quadratic friction coefficients and Manning's n formulation with n values estimated using the USGS usSEABEDS data. Due to the simplified assignment of the Manning's n values, sensitivity to the actual Manning's n specification was also examined.

Looking at the mean RMS errors for the OTIS1 through OTIS6 simulations (ignoring OTIS3noadv) in Figure 7, we note that there is actually very little difference in the mean errors for the Gulf of Mexico, Caribbean and Deep stations for any of the five friction simulations. Furthermore, we see that there is also little difference in the three Manning's n simulations (OTIS4 through OTIS6) in any of the regions. This is encouraging as it means that there is very little to no model sensitivity to small perturbations in the Manning's n values. Although a rather simplified approach for assigning these values was used, we should not be too concerned with the approach, assuming that representative values for each

region were chosen carefully. Finally, we note that the VDatum friction scheme (OTIS3) has slightly higher mean errors in the Atlantic region.

Examination of the individual constituents indicate that there is very little difference in the mean errors for the various friction simulations. The exception is the M_2 constituent which has slightly higher errors of about 0.3 cm for the OTIS3 simulation than all of the others. If one were to look at scatter plots of individual stations, then more substantial differences could be detected; however, on average, most constituents are insensitive to small changes in the bottom friction. Given the simplifications of the Manning's *n* assignments and the prior validation of the VDatum *CF* values during the VDatum model development, for this release (EC2015) we have chosen to implement the VDatum friction values.

3.1.4. Inclusion of Advective Terms

Finally, when examining the OTIS3 and OTIS3noadv error bars, we note that very little difference can be seen between the errors in the Gulf of Mexico and Caribbean regions. However, there are noticeable differences in the Atlantic Ocean and Deep stations, with the OTIS3noadv bars having slightly higher error than their counterpart. From this, we conclude that the addition of the advective terms does reduce the mean errors in the tidal constituent harmonics, particularly in the Atlantic coastal regions. While not shown here, it is noteworthy that these differences are more significant when all 681 stations are used to calculate the mean errors; this is due to the higher percentage of stations in the shallower coastal regions and narrow channels where the advective processes are more dominant.

3.2. Comparison of EC2015 and EC2001

For the EC2015 tidal database release, the VDatum friction formulation and TPXO7.2 boundary forcing with all 13 constituents was used; all other model input parameters are as given above in Section 2.1.2. For results and discussion, when we refer to EC2001 we mean the updated 2008 version [24]. Scatter plots of computed versus measured amplitudes and phases (and their linear best-fit) for the EC2001 and EC2015 databases are shown in Figure 8 for the dominant diurnal and semi-diurnal tidal signals: K_1 and M_2. Additionally, Table 6 provides the best fit statistics for all eight primary constituents at the 367 validation stations that are common to both databases.

Table 6. Summary of best-fit linear statistics for the 367 common validation stations in the EC2001 and EC2015 tidal databases.

	Harmonic Amplitudes							
Model	**Best-fit**	O_1	K_1	P_1	Q_1	M_2	S_2	N_2	K_2
EC2001	Slope	1.082	1.053	0.989	1.065	1.025	0.938	0.916	1.013
	R^2	0.973	0.964	0.956	0.959	0.989	0.959	0.971	0.943
EC2015	Slope	1.054	1.024	1.014	1.106	1.010	0.946	0.911	1.027
	R^2	0.984	0.978	0.964	0.960	0.996	0.975	0.980	0.964
	Harmonic Phases							
Model	**Best-fit**	O_1	K_1	P_1	Q_1	M_2	S_2	N_2	K_2
EC2001	Slope	0.988	0.995	0.981	0.967	0.980	0.959	0.976	0.960
	R^2	0.994	0.995	0.995	0.992	0.972	0.963	0.979	0.946
EC2015	Slope	0.983	0.975	0.988	0.955	0.986	0.951	0.986	0.964
	R^2	0.997	0.997	0.997	0.993	0.984	0.974	0.987	0.962

For a perfect fit of the validation data, both the slope and R^2 values would have a value of unity. Notice that although the slope may not be improved for all eight constituents, the R^2 value is closer to unity for all of them, indicating a tighter distribution. The larger apparent scatter in the diurnal amplitudes is due to their much smaller magnitudes, while the scatter in the semi-diurnal phases resides mostly in the Caribbean and Gulf of Mexico stations where the predominant constituents are

diurnal. Additionally, many of the CO-OPS validation stations on Puerto Rico have data records that are significantly less than one year.

Similarly, if we look at scatter plots of individual stations, we can compare how each of the databases performs for that point. Since there are 681 validation stations, only a few representative stations are provided herein. Figures B1–B5 in Appendix B provide plots for the 10 stations that were shown by a black X in Figures 6 and 7; plots are grouped together by region: Atlantic coast, Florida coast, Gulf of Mexico, Caribbean Sea and deep ocean stations. In order to illustrate the station differences due to the friction formulation, results for both the VDatum and Manning's *n* friction formulations are shown in these plots. Other than the bottom friction itself, all other ADCIRC parameters are the same for these two data sets. First, note that the different friction formulations typically affect the amplitude response of the model more than the phase (with the exception of station 313 at Pilottown, LA and station 645 at Curacao Willemstad). Recall that there are no river boundary conditions in these simulations, they are purely tidally driven. Therefore, stations such as Pilottown, LA that are located on a major river will not exhibit the proper harmonic response as they do not include the effects of riverine flow. Generally, the new EC2015 model is within the 5%–10% error bars for amplitudes and 10°–20° error bars for phase. For stations that are not, such as station 348 at Galveston Bay Entrance, where some constituents are overestimated while others are underestimated, a thorough examination of the nearby bathymetry may be warranted. While every effort was made to use the most recent bathymetry data available by incorporating the VDatum models, for some regions the only available NOS charts can be around 100 years old.
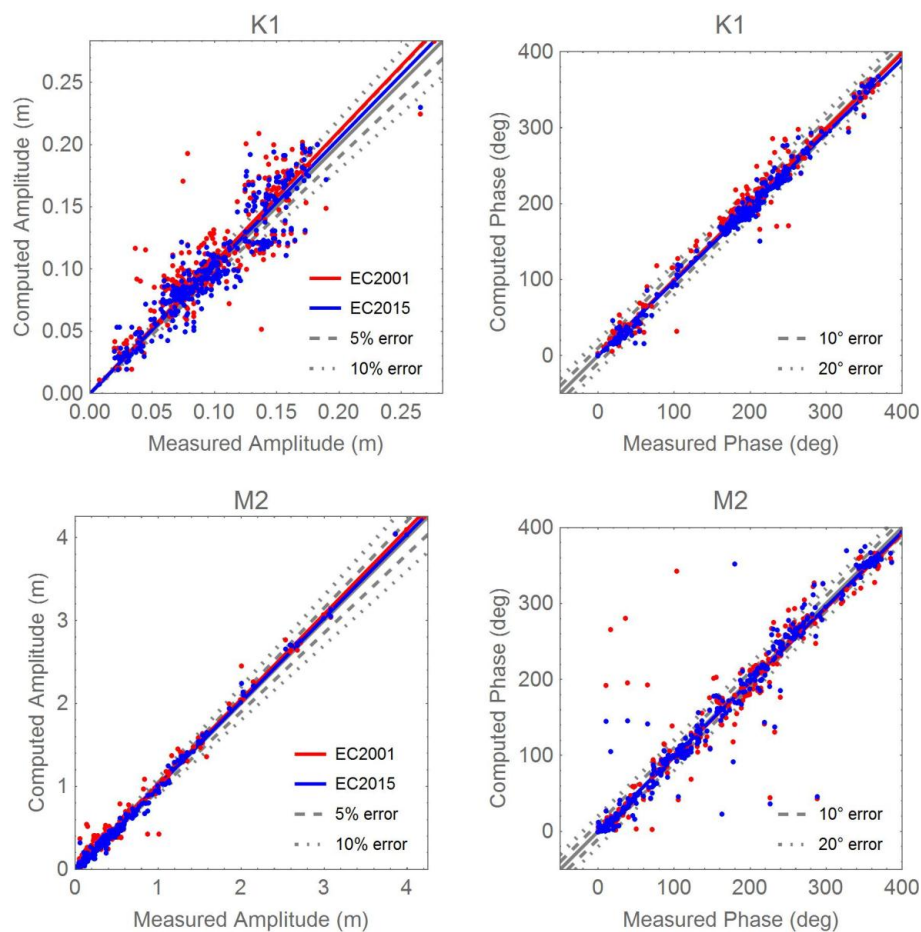
Figure 8. Comparison of scatter plots for the dominant constituents (K_1, M_2) for the EC2001 and EC2015 tidal databases using the 367 common validation data stations.

It is also instructive to see if there are sub-regional patterns in the errors (at the individual water body scale), which can help to guide future efforts at improving the tidal database. Plots of relative amplitude and absolute phase errors for the EC2015 model at each of the 681 stations are provided in Figures C1–C7 in Appendix C for the M_2 and K_1 constituents (same zoom views given in Figures 5 and 6). Plots are only provided for the dominant constituent in the sub regions: Gulf of Maine, Atlantic coast and Florida–M_2 and Gulf of Mexico and Caribbean Sea—K_1. Points shown in blue are underestimating the amplitudes (or exhibit a phase lag), while points shown in red are overestimating (exhibit a phase lead). The symbol shapes indicate to what degree the model is over/under estimating; we would like to see amplitude errors less than 10% and phase errors less than 20°. Several general trends can be gleaned from these plots:

- The M_2 amplitudes in the Gulf of Maine are slightly overestimated (generally less than 5% but a few as high as 20%) while those at the east end of Long Island Sound are overestimated about 10%–20%. Meanwhile stations along the remainder of the Atlantic coast down through Florida are underestimated by 5%–10% on average, with a few isolated stations overestimating. The Chesapeake Bay and Florida Key regions have several stations that are underestimated by more than 10%. For the 681 stations, 309 or roughly 45% of them have relative amplitude errors above the desired 10% threshold; most of these lie within the Gulf Coast and Caribbean regions where the semi-diurnal amplitudes are small and the remaining are fairly evenly distributed throughout the domain.

- The M_2 phases are generally lagged for the entire Atlantic coast and Florida region, with the exception of the Gulf of Maine (which exhibits slight 0%–5% phase leads). The most severe phase lags are often in the upper reaches of the estuaries, embayments and rivers. Of the 404 stations, only 111 (or 16%) have absolute phase errors greater than the desired 20°; most of these lie within the Chesapeake Bay, Gulf Coast and Caribbean regions.

- The amplitudes for the diurnal K_1 constituent are generally overestimated along the Gulf coasts and the Caribbean, although there are a few stations that are underestimated. While many of the Gulf of Mexico stations are outside of the desired 10% range, the majority of the Caribbean Sea stations are below this threshold. A higher number of the 681 stations (57%) fall outside of the desired 10% relative amplitude error range—of these stations, 60% are along the Atlantic coast where the semi-diurnal tides usually dominate and 30% are in the Gulf of Mexico with the remainder in the Caribbean Sea.

- Meanwhile, the phases for the K_1 constituent generally exhibit a phase lag in the Gulf of Mexico and Caribbean Sea basins and are typically more accurate. However, the stations along the northern Texas coast often exhibit phase leads. Only 8% fall outside of the desired 20° error range and two-thirds of those are along the Atlantic coast.

Finally, mean RMS errors for regions are shown in Figure 9, while mean absolute phase errors and mean relative amplitude errors are provided in Table 7. Looking primarily at the 367 validation stations that are common to both databases (blue diamonds for EC2001 and red circles for EC2015), we can draw several general conclusions.

- Globally, the greatest overall RMS improvement is realized in the M2 constituent (1.1 cm reduction). All of the constituents (except Q1) exhibit 2°–4° reductions in mean absolute phase error and 1%–7% reductions in mean relative amplitude errors. Overall, there is a 4% reduction in amplitude errors and about 2° in phase errors.

- For the Atlantic region, RMS error reductions of about 0.3 cm are gained in the O_1, K_1 and N_2 constituents and 1.4 cm for the M_2 constituent. In general, all of the constituents have 2°–3° reductions in mean absolute phase errors. However, the Q_1 and K_2 constituents actually have higher errors in the 2°–3° range. Additionally, with the exception of Q_1 which is roughly unchanged, the diurnal constituents exhibit 1 to 8% reductions in relative amplitude errors while the semi-diurnal have 3%–8% reductions in error.

- For the Gulf of Mexico, the greatest RMS error improvements are in the O_1 and K_1 (0.5 cm), M_2 (1.0 cm) and S_2 (0.3 cm) constituents. Mean absolute phase errors are improved by $1°$–$3°$ for the diurnal constituents and $3°$–$11°$ for the semi-diurnal (with the exception of S_2 which exhibits little change). Meanwhile, mean relative amplitude errors are reduced by 2%–6% for the diurnal constituents and by 8%–13% for the semi-diurnal (with the exception of Q_1 and M_2 which exhibit error increases of 2%–3%).

- For the Caribbean region, there are minor RMS error improvements of about 0.2 cm in the O_1, K_1 and S_2 constituents and 0.4 cm for M_2 while most of the other constituents are reduced by less than 0.1 cm. Mean absolute phase errors increase by $1°$–$2°$ for the diurnal constituents and decrease by $2°$–$9°$ for the semi-diurnal constituents. Mean relative amplitude errors decrease by 2%–11% for the diurnal constituents and 2% for M_2; while N_2 and K_2 increase by about 1%. Given these erratic trends, it is instructive to note that the data records used at CO-OPS to generate the harmonic constituent data in the U.S. Virgin Islands and Puerto Rico are often as small as 29 days.
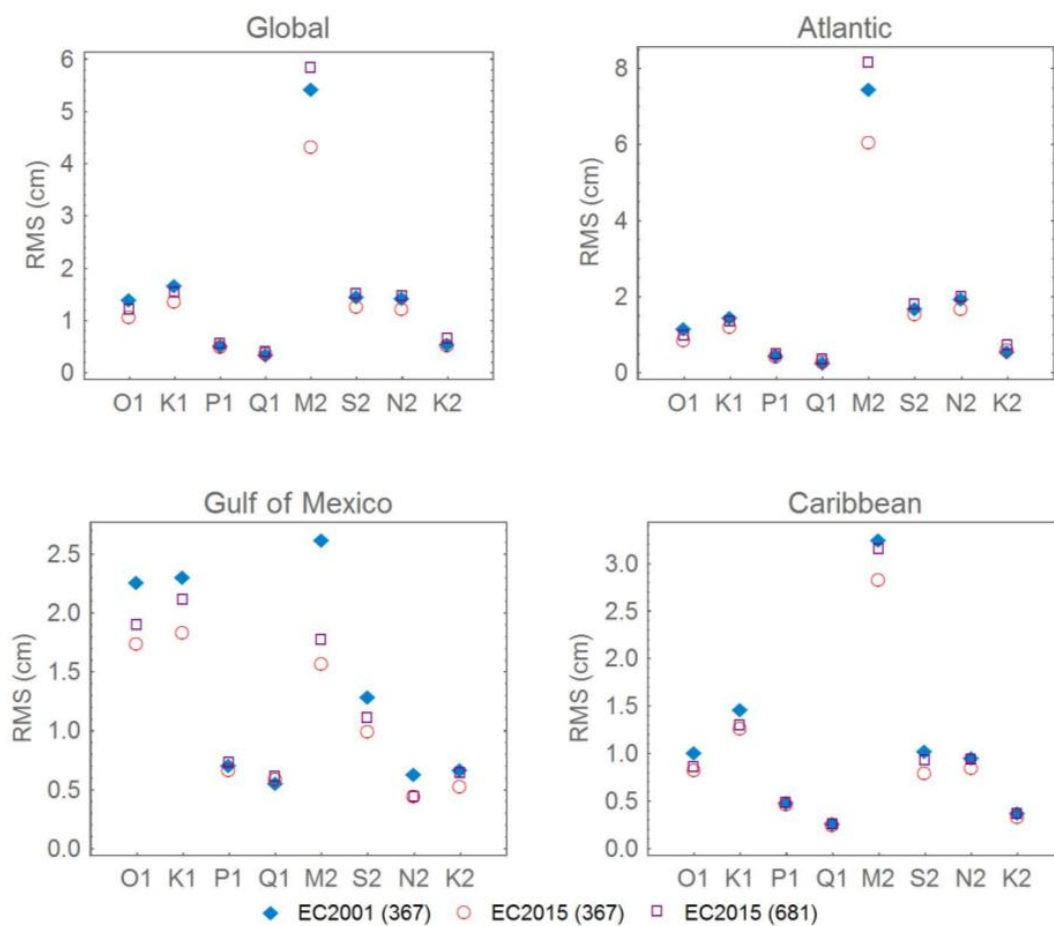
Figure 9. Mean RMS errors (cm) in harmonic constituents for the EC2001 and EC2015 ADCIRC tidal databases for each region of the WNAT model domain.

Table 7. Comparison of mean relative amplitude and mean absolute phase errors by region for each of the eight primary harmonic constituents and summed over all eight constituents for the EC2001 and EC2015 tidal databases: only common 367 wet validation stations used in the summations.

Mean Relative Amplitude Errors (%)								
Constituent	Entire Domain		Atlantic Ocean		Gulf of Mexico		Caribbean Sea	
	EC2001	EC2015	EC2001	EC2015	EC2001	EC2015	EC2001	EC2015
O_1	18.99	12.12	18.68	10.35	18.11	15.59	20.91	12.74
K_1	19.51	14.02	18.93	12.96	18.42	15.97	22.45	14.56
P_1	18.46	17.27	17.04	16.19	18.25	17.42	22.83	20.23
Q_1	21.79	21.00	19.89	20.34	21.26	24.56	28.86	17.50
M_2	23.39	20.65	13.39	8.50	38.31	39.81	32.95	30.98
S_2	23.77	18.08	17.01	12.76	37.83	24.54	25.33	25.06
N_2	22.57	19.20	14.76	11.97	39.76	31.60	23.66	24.72
K_2	31.40	25.06	20.01	11.78	61.82	54.28	33.73	34.71
All 8	22.40	18.29	17.42	12.98	30.90	27.23	26.16	22.49
Mean Absolute Phase Errors (deg)								
Constituent	Entire Domain		Atlantic Ocean		Gulf of Mexico		Caribbean Sea	
	EC2001	EC2015	EC2001	EC2015	EC2001	EC2015	EC2001	EC2015
O_1	10.37	8.49	11.02	9.41	9.30	6.53	9.87	8.34
K_1	8.87	7.47	9.21	7.73	8.44	6.27	8.49	8.25
P_1	9.59	7.66	9.52	7.55	8.90	6.71	10.69	9.17
Q_1	13.70	14.22	15.22	17.03	9.85	8.20	14.83	14.58
M_2	15.49	12.19	9.53	7.24	23.53	19.05	22.21	17.55
S_2	16.24	14.35	9.40	8.53	26.62	22.81	22.64	20.27
N_2	17.16	12.98	10.40	7.53	27.45	17.94	23.95	22.72
K_2	19.11	19.57	12.06	15.72	30.19	25.05	29.17	25.67
All 8	13.76	12.00	10.72	9.97	17.72	13.79	17.60	15.65

4. Discussion

Table 8 provides a summary of the global RMS errors for the eight primary constituents, as well as the mean regional errors summed over these constituents, for each of the nine model simulations done as part of this study (statistics computed using only the 367 common validation data points).

Table 8. Summary of RMS errors (cm) for the 367 common validation stations: global means for the eight primary constituents and regional means summed over all eight primary harmonic constituents.

Mean Global Constituent RMS Errors (cm)								
Run Designation	O_1	K_1	P_1	Q_1	M_2	S_2	N_2	K_2
EC2001	1.411	1.678	0.537	0.354	5.445	1.468	1.440	0.558
EC2001-ext	1.231	1.617	0.574	0.393	5.350	1.488	1.488	0.603
FES1	1.188	1.495	0.684	0.379	4.003	1.878	1.321	0.487
OTIS1	1.109	1.401	0.519	0.377	4.022	1.264	1.282	0.510
OTIS3	1.079	1.381	0.508	0.379	4.330	1.272	1.230	0.545
OTIS3noadv	1.048	1.366	0.504	0.378	4.653	1.266	1.208	0.534
OTIS4	1.108	1.375	0.517	0.373	3.980	1.263	1.282	0.503
OTIS5	1.104	1.382	0.516	0.374	3.972	1.264	1.275	0.506
OTIS6	1.118	1.372	0.521	0.372	4.028	1.264	1.296	0.500
Mean Regional RMS Errors (cm)					
Run Designation	Global	Atlantic Ocean	Gulf of Mexico	Caribbean Sea	Deep Ocean
EC2001	1.655	1.928	1.419	1.161	0.774
EC2001-ext	1.634	1.925	1.334	1.167	0.848
FES1	1.466	1.744	1.139	1.067	1.035
OTIS1	1.343	1.575	1.076	1.002	0.874
OTIS3	1.374	1.632	1.074	1.001	0.867
OTIS3noadv	1.405	1.691	1.066	1.000	0.888
OTIS4	1.332	1.577	1.035	0.995	0.875
OTIS5	1.331	1.569	1.046	0.999	0.873
OTIS6	1.341	1.593	1.038	0.991	0.878

Notice that the placement of the boundary did not significantly change either the individual constituents (greatest change was a less than 0.2 cm reduction for O_1) or the regional means, where the

greatest difference was less than 0.1 cm. Recall from Section 2.2.1 that this improvement was included primarily to increase the model stability for the long-term simulations of 410 days that were necessary for this study. While the slight model improvement is appreciated, it was not expected or required.

Meanwhile, the inclusion of the advective terms did not significantly affect the mean errors either. The largest difference was in the M_2 constituent, which exhibited 0.3 cm reductions of error when the advective terms were included in the simulation, and the largest regional change was for the Atlantic stations (less than 0.05 cm difference). While these are not significant error reductions, it is important to include as much of the model physics as possible. Furthermore, examination of scatter plots for individual stations shows that the inclusion of the advective terms can have significant influence on certain types of stations (rivers, channels, shallower estuaries, etc.) where we would expect the hydrodynamics to be more dominated by advection.

Turning now to the open ocean boundary forcing, we note that the simulation with TPXO 7.2 forcing is on average more accurate than the FES2012 forcing. The most significant difference is for the S_2 constituent, which exhibits 0.6 cm less error when the TPXO 7.2 product is used as the boundary condition, with the only other noticeable improvement being in the P_1 constituent (about 0.15 cm). Regionally, the reductions are about 0.15 cm for the deep and Atlantic stations. Interestingly, neither of these constituents has the highest phase or amplitude errors in Table 2. Visual examination of P_1 amplitudes and phases along the open boundary indicate that the FES2012 product has a considerable phase lag, compared to TPXO 7.2, for this constituent along the entire length and a noticeable departure for the amplitudes near the coast of Nova Scotia. However, there are no significant differences visible for the S_2 constituent. From this we infer that the non-linear interactions between the tides can indeed be very complex. Additionally, this highlights the need for accurate boundary conditions at any modeling level.

Finally, comparison of the various bottom friction schemes indicates that the bottom friction does not noticeably affect the overall statistical errors; there are very few differences across the OTIS1, OTIS3 and OTIS4 through OTIS6 simulations for constituents or regions. The exception to this is that the OTIS3 simulation is about 0.3 cm higher than all of the others for the M_2 constituent, with most of these errors occurring (on average) in the Atlantic region. However, as shown in Appendix B, individual stations can be significantly affected when the bottom friction is varied, from which we infer that overall statistical improvement could be gained by optimizing the friction scheme in each coastal embayment and estuary.

5. Conclusions

The results indicate that most of the reduction in harmonic constituent errors are due to the increased coastal resolution and updated coastal bathymetry. On average, very little overall improvement was realized solely from the bottom friction representation, inclusion of advective terms or new open ocean boundary location. However, these do contribute to the overall stability and robustness of the model, as well as having localized effects on the harmonic accuracy.

To put the errors in context, we also computed the mean RMS error (for all eight primary constituents) between the CO-OPS station data and the IHO data for the 63 stations that were available in both data sets. The mean error for all 63 stations was 0.72 cm, while the minimum and maximum error over all stations were 0.19 cm and 2.94 cm, respectively. On average, one could expect the data itself to be in error by about 0.7 cm at a given station, which is about half of the global RMS errors reported in Table 8. The measured to computed error measures reported throughout the paper include these errors in the data; thus, a significant portion of the reported errors stem from the uncertainty in the data itself.

Future improvements to the WNAT tidal database could include better bottom friction representations in individual water bodies that have not been optimized (e.g., the upper reaches of Chesapeake Bay, marshy areas along the Florida coast and other regions indicated by the figures

in Appendix C) and updated bathymetry for inlets and other important conveyances (e.g., Pamlico Sound inlets) as the VDatum models themselves are updated with more recent sounding data.

It is recommended that users of the EC2015 tidal database follow two basic guidelines: (1) choose your regional open ocean boundary location to be well outside of estuaries and bays and (2) make sure that your regional model bathymetry matches the database bathymetry at your boundary. Additionally, while harmonic information is available for 37 constituents, use caution when applying larger suites as only eight have been validated. Further guidelines and limitations are provided in Appendix D for the interested reader. The EC2015 tidal database is available on the ADCIRC website [24].

Author Contributions: R.K, K.D. and J.F. conceived the project and decided upon the six areas of improvement; J.W. created and validated the new EC2001_extended model domain and provided VDatum model grids and the most recent approved CO-OPS tidal constituent data; C.S. created the new EC2015 model domain, performed all of the ADCIRC model simulations to test the various improvements and analyzed the model results; K.D. modified the ADCIRC source code to allow internal harmonic analysis for large grids and the full suite of 37 constituents; C.S. wrote the paper.

Conflicts of Interest: The authors declare no conflict of interest. J.F. as a representative of the funding sponsor, was involved in designing the study. The funding sponsors had no role in the analyses or interpretation of data; in the writing of the manuscript, or in the decision to publish the results.

Appendix A

The locations, names and regional classification of all 681 validation stations are given herein; the last 277 stations are marked with IHO in the CO-OPS ID column to indicate that they are from the IHO bank of tidal constituents. Stations marked with a single asterisk are considered "wet" in the EC2001 model even though they are approximated by their nearest neighbor. Meanwhile, those marked with a double asterisk are not included in scatter plots or statistical error metrics for the EC2001 database since they are well outside the domain of the boundary or are in channels and other features that are not represented in the EC2001 model. Abbreviations for the region designations are as follows: Atlantic Ocean—A, Gulf of Mexico—G, Caribbean Sea—C, Deep water—D.

Table A1. Geographic location, name and regional classification for available validation stations.

ID	CO-OPS	Longitude	Latitude	Station Name	Region
1	2695540	−64.70331	32.37339	Bermuda Esso Pier, St. Georges Island	A
2	8410140	−66.98290	44.90460	Eastport, Passamaquoddy Bay	A
3 **	8410714	−67.10840	44.87045	Coffin Point, Coffin Neck	A
4 **	8410715	−67.13000	44.92330	Garnet Point, Hersey Neck	A
5 **	8410834	−67.14375	45.12889	Pettegrove Point, Dochet Island	A
6 **	8410864	−67.15167	44.82333	Gravelly Pt., Whiting Bay	A
7	8411060	−67.20917	44.65637	Cutler Farris Wharf, Little River	A
8	8411250	−67.29670	44.64170	Cutler Naval Base, Machias Bay	A
9 **	8412581	−67.87500	44.54000	Milbridge, Narraguagus River	A
10 **	8413320	−68.20500	44.39170	Bar Harbor, Frenchman Bay	A
11	8413825	−68.43500	44.17000	Mackerel Cove, Swans Island	A
12	8414249	−68.62093	44.19231	Oceanville, Deer Island	A
13 **	8414612	−68.77190	44.78765	Bangor, Penobscot River	A
14	8414721	−68.81330	44.47170	Fort Point, Penobscot River	A
15	8414888	−68.88840	44.16080	Pulpit Harbor, Penobscot Bay	A
16 **	8415490	−69.10170	44.10500	Rockland	A
17 **	8415709	−69.18170	44.07136	Thomaston, St George River	A
18	8417177	−69.78500	43.75500	Hunniwell Point, Kennebec River	A
19 **	8417208	−69.79708	44.08721	Richmond, Kennebec River	A
20 **	8417227	−69.80880	43.92500	Bath, Kennebec River	A
21 **	8418150	−70.24601	43.65608	Portland, Casco Bay	A
22 *	8418445	−70.33330	43.54000	Pine Point, Scarborough River	A
23 *	8418606	−70.38170	43.46170	Camp Ellis, Saco River	A
24 *	8419317	−70.56303	43.31966	Wells, Webhannet River	A
25 **	8419870	−70.74170	43.08000	Seavey Island, Portsmouth Harbor	A
26 **	8423898	−70.71167	43.07179	Fort Point, Newcastle Island	A
27 **	8440273	−70.90800	42.83600	Salisbury Point, Merrimack River	A
28 *	8440452	−70.82000	42.81670	Plum Island, Merrimack River Ent.	A
29 **	8440466	−70.87330	42.81500	Newburyport, Merrimack River	A
30 *	8441551	−70.61507	42.66033	Rockport Harbor	A
31 **	8442645	−70.87649	42.52295	Salem, Salem Harbor	A
32 **	8443187	−70.94330	42.45830	Lynn, Lynn Harbor	A
33 **	8443970	−71.04720	42.35750	Boston, Boston Harbor	A
34	8444162	−70.89170	42.32830	Boston Light, Boston Harbor	A
35 **	8444525	−70.95330	42.28000	Nut Island, Quincy Bay	A
36 **	8444788	−70.96670	42.24830	Shipyard Point, Weymouth Fore River	A
37	8445138	−70.72476	42.20099	Scituate, Scituate Harbor	A
38	8446009	−70.63873	42.08330	Brant Rock, Green Harbor River	A
39 **	8446121	−70.18216	42.04959	Provincetown, Cape Cod	A
40 **	8446166	−70.66789	42.03830	Duxbury, Duxbury Harbor	A
41 *	8446493	−70.66170	41.96000	Plymouth, Plymouth Harbor	A
42 **	8447173	−70.53500	41.77500	Sagamore, Cape Cod Canal	A
43 **	8447191	−70.56170	41.77000	Bournedale, Cape Cod Canal	A
44 *	8447241	−70.15550	41.75600	Sesuit Harbor, East Dennis	A
45 **	8447259	−70.59342	41.74585	Bourne Bridge, Cape Cod Canal	A
46 **	8447270	−70.61670	41.74170	Buzzards Bay, Cape Cod Canal	A
47 **	8447295	−70.62425	41.73500	Gray Gables, Buzzards Bay	A
48	8447368	−70.71500	41.71170	Great Hill	A
49 **	8447386	−71.16550	41.70580	Fall River, Hope Bay	A
50	8447416	−70.71941	41.69578	Piney Point, Wings Cove	A
51 *	8447435	−69.94887	41.68847	Chatham, Lydia Cove	A
52	8447495	−70.05670	41.66478	Saquatucket Harbor	A
53	8447712	−70.89981	41.59292	New Bedford, Clarks Point	A
54	8447842	−70.92830	41.53830	Round Hill Point	A
55	8447930	−70.67170	41.52330	Woods Hole, Buzzards Bay	A
56 **	8448157	−70.59870	41.45830	Vineyard Haven, Vineyard Hvn Hbr	A
57 **	8448558	−70.51150	41.38822	Edgartown, Martha's Vineyard	A

Table A1. *Cont.*

ID	CO-OPS	Longitude	Latitude	Station Name	Region
58 *	8448725	−70.76795	41.35461	Menemsha Harbor	A
59 **	8449130	−70.09438	41.28503	Nantucket Island, Nantucket Sound	A
60 *	8451552	−71.25500	41.63670	Bristol Ferry	A
61	8452660	−71.32670	41.50500	Newport, Narragansett Bay	A
62	8452944	−71.34330	41.71670	Conimicut Light, Narragansett Bay	A
63	8453742	−71.38670	41.49670	West Jamestown	A
64 **	8454000	−71.39978	41.80786	Providence, Providence River	A
65 *	8454049	−71.41100	41.58680	Quonset Point	A
66 **	8454538	−71.44346	41.57384	Wickford, Narragansett Bay	A
67	8455083	−71.49000	41.36330	Point Judith, Harbor Of Refuge	A
68	8458022	−71.76170	41.32830	Weekapaug Point, Block Island Sound	A
69	8459338	−71.55621	41.17404	Block Island Harbor, Old Harbor	A
70	8459479	−71.58000	41.22830	Sandy Point, Block Island Sound	A
71	8459681	−71.61064	41.16330	Block Island, Block Island Sound	A
72 **	8461490	−72.08975	41.36105	New London, Thames River	A
73 **	8463701	−72.53170	41.26830	Clinton, Clinton Harbor	A
74 **	8465705	−72.90830	41.28330	New Haven, New Haven Harbor	A
75 **	8467150	−73.18170	41.17330	Bridgeport, Bridgeport Harbor	A
76 *	8467373	−73.21330	41.15670	Black Rock Harbor, Cedar Creek	A
77 **	8467726	−73.28286	41.13249	Southport, Southport Harbor	A
78	8468799	−73.48000	41.03830	Long Neck Point, Long Island Sound	A
79	8510321	−71.85586	41.07199	Montauk Point Light	A
80 *	8510448	−71.93500	41.07330	Lake Montauk (U.S.C.G.)	A
81 **	8510560	−71.96000	41.04830	Montauk, Fort Pond Bay	A
82	8510719	−72.03191	41.25792	Silver Eel Pond, Fishers Island	A
83 *	8511171	−72.19000	41.03500	Threemile Harbor Entrance	A
84	8511236	−72.20521	41.17125	Plum Island Plum Gut Harbor	A
85	8511671	−72.30670	41.13670	Orient, Orient Harbor	A
86	8512668	−72.56170	41.01500	Mattituck Inlet, Long Island	A
87 **	8512735	−72.58170	40.93470	South Jamesport, Great Peconic	A
88 **	8512769	−72.58667	40.81830	Shinnecock Yacht Club, Penn. Creek	A
89 *	8512987	−72.64500	40.98170	Northville Fuel Dock, Long Island	A
90	8513825	−72.86830	40.73830	Smith Point Bridge, Narrow Bay	A
91 *	8514322	−73.00000	40.74780	Patchogue, Patchogue River	A
92 *	8514422	−73.04330	40.96500	Cedar Beach	A
93 **	8515586	−73.35330	40.90000	Northport, Northport Bay	A
94	8515786	−73.40000	40.95330	Eatons Neck, Huntington Bay	A
95 **	8515921	−73.43170	40.91000	Lloyd Harbor Lighthouse	A
96 **	8516061	−73.47000	40.87330	Cold Springs Harbor	A
97 **	8516299	−73.55000	40.90330	Bayville Bridge, Oyster Bay	A
98 **	8516614	−73.65500	40.86330	Glen Cove Yacht Club, Long Island	A
99 **	8516761	−73.70330	40.83170	Port Washington, Manhassset Bay	A
100 *	8516945	−73.76490	40.81030	Kings Point, Long Island Sound	A
101 **	8516990	−73.78170	40.79330	Willets Point, Little Bay, East River	A
102 **	8517276	−73.85670	40.78330	College Pt, Ft. Of 110Th St	A
103 **	8517847	−73.99517	40.70374	Brooklyn Bridge, East River	A
104	8518091	−73.67170	40.96170	Rye Beach, Amusement Park	A
105 **	8518639	−73.90625	40.80133	Port Morris, East 138Th St.	A
106 **	8518668	−73.94170	40.77670	Horns Hook, E. 90Th St. Hell Gate	A
107 **	8518687	−73.95830	40.75830	Queensboro Bridge, East River	A
108 **	8518699	−73.96956	40.71170	Williamsburg Bridge	A
109 **	8518750	−74.01436	40.70020	The Battery, New York Harbor	A
110 **	8518903	−73.92500	40.87830	Spuyten Duyvil Ck, Ent., Hudson R.	A
111 **	8518905	−73.91670	40.90330	Riverdale, Hudson River	A
112 **	8518924	−73.96330	41.21830	Haverstraw Bay	A
113 **	8519483	−74.14230	40.63980	Bergen Point West, Kill Van Kull	A

Table A1. *Cont.*

ID	CO-OPS	Longitude	Latitude	Station Name	Region
114 *	8531680	−74.00940	40.46690	Sandy Hook	A
115	8534720	−74.41830	39.35500	Atlantic City, Atlantic Ocean	A
116	8534770	−74.47670	39.33500	Ventnor City, Fishing Pier	A
117 *	8534836	−74.53330	39.30830	Longport, Risely Channel	A
118 *	8536110	−74.96000	38.96833	Cape May Canal, Delaware Bay	A
119 *	8536581	−74.89170	39.12830	Bidwell Creek Entrance, Del. Bay	A
120 *	8536931	−75.17500	39.23830	Fortescue Creek	A
121	8537121	−75.37500	39.30500	Ship John Shoal, Delaware River	A
122 **	8538886	−75.04300	40.01194	Tacony-Palmyra Bridge	A
123 **	8539094	−74.86970	40.08170	Burlington, Delaware River	A
124 **	8539487	−74.73670	40.13670	Fieldsboro, Delaware River	A
125 **	8539993	−74.75500	40.18830	Trenton Marine Terminal	A
126 **	8540433	−75.41000	39.81170	Marcus Hook	A
127 **	8545240	−75.14091	39.93333	Philadelphia (U.S.C.G.), Del. River	A
128 **	8545530	−75.13830	39.95330	Philadelphia (Pier 11 North), Del. R	A
129 **	8548989	−74.75170	40.13670	Newbold, Delaware River	A
130 **	8551762	−75.58830	39.58170	Delaware City, Delaware River	A
131 **	8551910	−75.57331	39.55870	Reedy Point, C&D Canal	A
132 *	8554399	−75.40000	39.18500	Mahon River Entrance, Del. Bay	A
133	8555889	−75.11333	38.98667	Brandywine Shoal Light, Del. Bay	A
134 *	8557380	−75.12000	38.78200	Lewes, Ft. Miles	A
135 *	8558690	−75.07000	38.61000	Indian River Inlet	A
136	8570280	−75.08330	38.32670	Ocean City, Fishing Pier	A
137 **	8570283	−75.09167	38.32833	Ocean City Inlet	A
138 **	8570536	−75.18909	38.21516	South Point, Chincoteague Bay	A
139 **	8570649	−75.28500	38.14830	Public Landing, Chincoteague Bay	A
140 **	8571091	−75.86330	37.97670	Crisfield	A
141	8571117	−76.02895	37.99826	Ewell, Smith Island	A
142	8571421	−76.03830	38.22000	Bishops Head, Hoopers Strait	A
143 **	8571559	−76.00500	38.30000	Mccreadys Creek, Fishing Bay	A
144 *	8571579	−76.26500	38.34170	Barren Island, Chesapeake Bay	A
145 **	8571773	−75.81930	38.48396	Vienna, Nanicoke River	A
146 **	8571892	−76.06818	38.57354	Cambridge, Choptank River	A
147 *	8572467	−76.37330	38.83670	Kent Point, Chesapeake Bay	A
148 **	8572669	−75.94500	38.91670	Hillsboro, Tuckahoe Creek	A
149 *	8572770	−76.35500	38.95670	Matapeake	A
150	8572955	−76.30110	39.03170	Love Point Pier, Kent Island	A
151 **	8573349	−75.92500	39.24500	Crumpton, Chester River	A
152 *	8573364	−76.24577	39.21333	Tolchester Beach, Chesapeake Bay	A
153 *	8573704	−76.06330	39.37170	Betterton, Sassafras River	A
154 **	8573903	−75.91670	39.50330	Town Point Wharf	A
155 **	8573927	−75.81000	39.52766	Chesapeake City	A
156 *	8574070	−76.09000	39.53670	Havre De Grace, Chesapeake Bay	A
157 **	8574459	−76.25500	39.38830	Pond Point, Bush River	A
158 **	8574680	−76.57833	39.26667	Baltimore (Fort McHenry)	A
159 **	8574683	−76.58500	39.26170	Fort McHenry Marsh, Patapsco R	A
160 **	8575512	−76.48099	38.98441	U.S. Naval Academy, Severn River	A
161	8577004	−76.47261	38.46579	Long Beach, Chesapeake Bay	A
162 *	8577188	−76.39640	38.39340	Cove Point	A
163 **	8577330	−76.45167	38.31667	Solomons Island, Patuxent River	A
164 **	8579542	−76.68333	38.65500	Lower Marlboro, Patuxent River	A
165 **	8579997	−76.93923	38.93240	Bladensburg, Anacostia River	A
166 **	8594900	−77.02167	38.87333	Washington, Potomac River	A
167 **	8630308	−75.40516	37.90701	Chincoteague Channel, South End	A
168	8632200	−75.98844	37.16519	Kiptopeke, Chesapeake Bay	A
169 *	8632366	−76.02450	37.26330	Cape Charles Harbor (U.S.C.G.)	A
170	8632837	−76.01500	37.53830	Rappahannock Light	A

Table A1. *Cont.*

ID	CO-OPS	Longitude	Latitude	Station Name	Region
171 **	8632869	−75.91670	37.55670	Gaskins Pt., Occohannock Creek	A
172	8633532	−75.99288	37.82926	Tangier Island, Chesapeake Bay	A
173	8635150	−76.96000	38.25170	Colonial Beach, Potomac River	A
174 **	8635257	−77.24297	38.21330	Rappahannock Bend	A
175 **	8635750	−76.46444	37.99590	Lewisetta, Potomac River	A
176 **	8635985	−76.78330	37.87330	Wares Wharf, Rappahannock R	A
177 *	8636580	−76.29000	37.61442	Windmill Point, Rappahannock R	A
178 **	8636653	−76.98996	37.58327	Lester Manor	A
179 *	8637289	−76.27330	37.34670	New Point	A
180	8637590	−76.22170	37.25670	New Point, Comfort Shoal	A
181 **	8637624	−76.50000	37.24670	Gloucester Point, York River	A
182 **	8637689	−76.47833	37.22667	Yorktown U.S.C.G. Training Center	A
183 **	8638339	−76.39911	36.82322	Western Branch	A
184 **	8638421	−76.66830	37.05670	Burwell Bay, James River	A
185 **	8638424	−76.66330	37.22000	Kingsmill, James River	A
186 **	8638433	−76.78330	37.18500	Scotland, James River	A
187 **	8638445	−76.91170	37.40330	Lanexa, Chicahominy River	A
188 **	8638450	−76.94330	37.23988	Tettington, James River	A
189 **	8638489	−77.37338	37.26686	Puddledock, Appomattox River	A
190 **	8638495	−77.42060	37.52451	Richmond River Locks, James River	A
191 *	8638610	−76.33000	36.94667	Sewells Point, Hampton Roads	A
192 **	8638660	−76.29202	36.82168	Norfolk Naval Shipyard	A
193	8638863	−76.11333	36.96667	Chesapeake Bay Bridge Tunnel	A
194	8639207	−75.96984	36.83180	Inside Channel, Rudee Inlet	A
195 **	8639348	−76.30172	36.77804	Money Point, S. Br. Elizabeth River	A
196	8651370	−75.74669	36.18331	Duck, Frf Pier	A
197 **	8652247	−75.76890	35.90370	Manns Harbor, Croatan Sound	A
198 **	8652437	−75.65645	35.84482	Oyster Creek, Croatan Sound	A
199 **	8652547	−75.70000	35.81170	Roanoke Marshes Light, Croatan S	A
200 **	8652587	−75.54936	35.79429	Oregon Inlet Marina, Pamlico S	A
201	8654400	−75.63500	35.22330	Cape Hatteras Fishing Pier	A
202 **	8654467	−75.70417	35.20950	U.S.C.G. Hatteras, Pamlico S	A
203 **	8654792	−75.98945	35.11564	Ocracoke Island	A
204 **	8655875	−76.34330	34.87500	Sea Level, Core Sound	A
205 **	8656483	−76.67000	34.72000	Beaufort, Duke Marine Lab	A
206	8656590	−76.71170	34.69330	Atlantic Beach Triple S Pier	A
207 **	8658120	−77.95330	34.22670	Wilmington, Cape Fear River	A
208	8658163	−77.78566	34.21330	Wrightsville Beach	A
209 **	8659084	−78.01830	33.91500	Southport	A
210	8659182	−78.08170	33.90170	Oak Island, Atlantic Ocean	A
211 *	8659897	−78.50670	33.86500	Sunset Beach Pier, Atlantic Ocean	A
212	8661070	−78.91830	33.65500	Springmaid Pier, Atlantic Ocean	A
213 **	8664022	−79.92138	33.00880	Gen. Dynamics Pier, Cooper R.	A
214 **	8664545	−79.83000	32.92670	Cainhoy, Wando River	A
215 **	8664941	−79.70670	32.85670	South Capers Island, Capers Creek	A
216 **	8665099	−80.02170	32.83670	I-526 Bridge, Ashley River	A
217 **	8665530	−79.92378	32.78170	Charleston, Cooper River Entrance	A
218 **	8667633	−80.78410	32.50250	Clarendon Plantation, Whale Br.	A
219 **	8668498	−80.46500	32.34000	Hunting Island Pier, Fripps Inlet	A
220	8668918	−80.73670	32.26670	Ribaut Island, Skull Creek	A
221 **	8670870	−80.90170	32.03373	Fort Pulaski, Savannah River	A
222 **	8677344	−81.39670	31.13170	St Simons Lighthouse	A
223 **	8679511	−81.51323	30.79781	Kings Bay	A
224 **	8679758	−81.47170	30.76330	Dungeness, Seacamp Dock	A
225 **	8679964	−81.54830	30.72000	St. Marys, St. Marys River	A
226 **	8720011	−81.46500	30.70830	Cut 1N, St Marys River Entr	A
227	8720012	−81.30170	30.71670	Cut 2N, St Marys River Entr	A

Table A1. *Cont.*

ID	CO-OPS	Longitude	Latitude	Station Name	Region
228 **	8720030	−81.46539	30.67171	Fernandina Beach, Amelia River	A
229 **	8720051	−81.52330	30.64330	Lanceford Creek, Lofton	A
230 **	8720098	−81.51500	30.56830	Nassauville, Nassau River East	A
231 **	8720211	−81.41330	30.40000	Mayport (Naval Sta.) St Johns R	A
232 **	8720218	−81.43000	30.39670	Bar Pilots Dock, St Johns River	A
233 **	8720219	−81.55830	30.38670	Dames Point, St. Johns River	A
234 **	8720220	−81.43170	30.39330	Mayport (Ferry) Saint Johns R	A
235 **	8720225	−81.63408	30.38337	Phoenix Park	A
236 **	8720242	−81.62000	30.36000	Longbranch, St Johns River	A
237 *	8720291	−81.38670	30.28330	Jacksonville Beach	A
238 **	8720357	−81.69164	30.19170	I-295 Bridge, West End, St Johns R	A
239 **	8720503	−81.62830	29.97830	Red Bay Point, St Johns River	A
240 **	8720554	−81.30000	29.91670	Vilano Beach (ICWW)	A
241 **	8720582	−81.30670	29.86670	State Road 312, Matanzas River	A
242	8720587	−81.26330	29.85670	St. Augustine Beach, Atlantic	A
243 **	8720625	−81.54832	29.80165	Racy Point, St Johns River	A
244 **	8720651	−81.25830	29.76830	Crescent Beach, Matanzas River	A
245 **	8720692	−81.22786	29.70453	State Road A1A Bridge	A
246 **	8720757	−81.20500	29.61500	Bings Landing, Matanzas River	A
247 **	8720767	−81.68170	29.59500	Buffalo Bluff, St. Johns River	A
248 **	8720774	−81.63170	29.64328	Palatka, St. Johns River	A
249 **	8720832	−81.67520	29.47675	Welaka, St. Johns River	A
250 *	8721020	−81.00500	29.22830	Daytona Beach (Ocean)	A
251 **	8721604	−80.59350	28.41580	Trident Pier, Port Canaveral	A
252 **	8721608	−80.60152	28.40871	Canaveral Harbor Entrance	A
253 **	8722125	−80.37170	27.63170	Vero Beach, Indian River	A
254 **	8722208	−80.32500	27.47170	North Beach Causeway, Indian R	A
255 **	8722548	−80.06670	26.84330	Pga Boulevard Bridge, Palm Beach	A
256 **	8722588	−80.05096	26.77000	Port Of W. Palm Beach, Lake Worth	A
257 **	8722669	−80.04670	26.61330	Lake Worth (ICWW)	A
258	8722670	−80.03330	26.61170	Lake Worth Pier, Atlantic Ocean	A
259 *	8723080	−80.12000	25.90330	Haulover Pier, N. Miami Beach	A
260	8723170	−80.13154	25.76830	Miami Beach (City Pier)	A
261	8723178	−80.13000	25.76330	Miami Beach, Government Cut	A
262	8723214	−80.16180	25.73140	Virginia Key, Biscayne Bay	A
263 *	8723962	−81.01670	24.71830	Key Colony Beach	G
264 *	8723970	−81.10500	24.71170	Vaca Key, Florida Bay	G
265 *	8724580	−81.80790	24.55570	Key West	G
266	8724635	−81.87830	24.45330	Sand Key Lighthouse	G
267	8724671	−81.92153	24.71828	Smith Shoal Light, Fl	G
268	8724698	−82.92000	24.63170	Loggerhead Key, Dry Tortugas	G
269 *	8725110	−81.80750	26.13170	Naples, Gulf Of Mexico	G
270 **	8725520	−81.87120	26.64770	Fort Myers, Caloosahatchee River	G
271	8726347	−82.76000	27.60170	Egmont Key, Tampa Bay	G
272	8726364	−82.72670	27.61500	Mullet Key, Tampa Bay	G
273	8726384	−82.56210	27.63870	Port Manatee, Tampa Bay	G
274	8726520	−82.62690	27.76060	St. Petersburg, Tampa Bay	G
275 *	8726607	−82.55376	27.85778	Port Tampa, Old Tampa Bay	G
276 **	8726667	−82.42500	27.91333	Csx Rockport, Mckay Bay Entrance	G
277	8726724	−82.83170	27.97830	Clearwater Beach, Gulf Of Mexico	G
278 **	8726738	−82.68500	27.98830	Safety Harbor, Old Tampa Bay	G
279 **	8727235	−82.63830	28.69170	Johns Island, Chassahowitzka Bay	G
280 **	8727274	−82.63830	28.76170	Mason Creek, Homosassa Bay	G
281 **	8727277	−82.69540	28.77170	Tuckers Island, Homosassa River	G
282 **	8727293	−82.60330	28.80063	Halls River Bridge, Halls River	G
283 **	8727306	−82.65830	28.82500	Ozello	G
284 **	8727328	−82.66670	28.86330	Ozello North	G

Table A1. *Cont.*

ID	CO-OPS	Longitude	Latitude	Station Name	Region
285	8727333	−82.72330	28.87000	Mangrove Point, Crystal Bay	G
286 **	8727336	−82.63500	28.88170	Dixie Bay	G
287 **	8727348	−82.63829	28.90505	Twin Rivers Marina, Crystal River	G
288 **	8727359	−82.69170	28.92330	Shell Island, Crystal River	G
289	8727520	−83.03170	29.13500	Cedar Key, Gulf Of Mexico	G
290 *	8728229	−84.29000	30.05870	Shell Point, Walker Creek	G
291 *	8728360	−84.51170	29.91500	Turkey Point	G
292 **	8728690	−84.98138	29.72670	Apalachicola, Apalachicola River	G
293 **	8729108	−85.66694	30.15228	Panama City, St. Andrew Bay	G
294	8729210	−85.87830	30.21330	Panama City Beach, Gulf Of Mexico	G
295 **	8729501	−86.49330	30.50330	Valpariso, Boggy Bayou	G
296	8729678	−86.86500	30.37670	Navarre Beach	G
297 **	8729905	−87.35670	30.41860	Millview, Perdido Bay	G
298 **	8729941	−87.42881	30.38694	Blue Angels Park, Perdido Bay	G
299 **	8731439	−87.68428	30.27982	Gulf Shores, Icww	G
300 *	8733821	−87.93453	30.48664	Point Clear, Mobile Bay	G
301	8735180	−88.07500	30.25000	Dauphin Island, Mobile Bay	G
302 **	8735391	−88.08800	30.56517	SH 163 Bridge, Dog River	G
303 **	8737048	−88.04010	30.70830	Mobile State Docks, Mobile River	G
304	8741196	−88.53330	30.34000	Pascagoula Point, Miss. Sound	G
305 *	8742221	−88.66670	30.23830	Horn Island, Mississippi Sound	G
306 **	8743281	−88.79830	30.39170	Ocean Springs	G
307 **	8744117	−88.90330	30.41175	Biloxi, Bay Of Biloxi	G
308	8745557	−89.08170	30.36000	Gulfport Harbor, Mississippi Sound	G
309	8747437	−89.32578	30.32639	Bay Waveland Yacht, Bay St. Louis	G
310	8747766	−89.36670	30.28170	Waveland, Mississippi Sound	G
311	8760417	−89.04447	29.20075	Devon Energy Facility, North Pass	G
312	8760551	−89.14000	28.99000	South Pass	G
313	8760721	−89.25830	29.17830	Pilottown	G
314	8760849	−89.35120	29.27330	Venice, Grand Pass	G
315	8760922	−89.40750	28.93220	Pilot Station East, SW Pass	G
316	8760943	−89.41830	28.92500	Pilot Station, SW Pass	G
317 *	8761305	−89.67325	29.86811	Shell Beach, Lake Borgne	G
318 *	8761529	−89.83500	29.94500	Martello Castle, Lake Borgne	G
319	8761819	−90.03830	29.40170	Texaco Dock, Hackberry Bay	G
320 *	8761927	−90.11342	30.02717	U.S.C.G. New Canal, Lake Pont.	G
321 **	8762075	−90.20860	29.11430	Port Fourchon, Belle Pass	G
322	8763535	−90.97600	29.17390	Texas Gas Platform, Caillou Bay	G
323 **	8764025	−91.23000	29.74330	Stouts Pass At Six Mile Lake	G
324 **	8764044	−91.23750	29.66750	Berwick, Atchafalaya River, La	G
325	8764227	−91.33810	29.45500	Lawma, Amerada Pass	G
326	8764311	−91.38500	29.37170	Eugene Island	G
327	8765251	−91.88000	29.71336	Cypremort Point	G
328 *	8767816	−93.22167	30.22364	Lake Charles, Calcasieu River	G
329	8767961	−93.30069	30.19031	Bulk Terminal #1	G
330	8768094	−93.34289	29.76817	Calcasieu Pass, East Jetty	G
331 **	8770475	−93.93130	29.86670	Port Arthur, Sabine Naches Canal	G
332 **	8770520	−93.88170	29.98000	Rainbow Bridge, Neches River	G
333 **	8770539	−93.89500	29.76670	Mesquite Point	G
334 **	8770559	−94.69040	29.71330	Round Point, Trinity Bay	G
335 **	8770570	−93.87010	29.72840	Sabine Pass North	G
336 **	8770597	−93.72170	30.09830	Orange (Old Navy Base)	G
337 **	8770613	−94.98500	29.68170	Morgans Point, Barbours Cut	G
338 **	8770625	−94.86830	29.68000	Umbrella Point, Trinity Bay	G
339 **	8770733	−95.07830	29.76500	Lynchburg Landing, San Jacinto R	G
340 **	8770743	−95.09000	29.75670	Battleship Texas, Houston Ship Ch	G

Table A1. *Cont.*

ID	CO-OPS	Longitude	Latitude	Station Name	Region
341 **	8770777	−95.26580	29.72580	Manchester, Houston Ship Ch	G
342	8770822	−93.83694	29.67806	Texas Point, Sabine Pass	G
343 **	8770933	−95.06670	29.56330	Clear Lake	G
344 **	8770971	−94.51330	29.51500	Rollover Pass	G
345 **	8771013	−94.91830	29.48000	Eagle Point, Galveston Bay	G
346	8771081	−93.64000	29.49830	Sabine Offshore	G
347 **	8771328	−94.78000	29.36500	Port Bolivar, Bolivar Roads	G
348	8771341	−94.72483	29.35733	Galveston Bay Ent North Jetty	G
349 **	8771450	−94.79330	29.31000	Galveston Pier 21	G
350	8771510	−94.78940	29.28530	Galveston Pleasure Pier, GoMex	G
351 **	8772440	−95.30830	28.94830	Freeport, Dow Barge Canal	G
352 **	8772447	−95.30250	28.94310	U.S.C.G. Freeport, Entr Channel	G
353 **	8773037	−96.71170	28.40800	Seadrift, San Antonio Bay	G
354 **	8773259	−96.59500	28.64000	Port Lavaca, Lavaca Causeway	G
355 **	8773701	−96.38830	28.45170	Port O'Connor, Matagorda Bay	G
356 **	8774513	−97.02170	28.11830	Copano Bay State Fishing Pier	G
357 **	8774770	−97.04670	28.02170	Rockport, Aransas Bay	G
358 **	8775188	−97.47500	27.85830	White Point Bay	G
359 **	8775237	−97.07330	27.83890	Port Aransas	G
360	8775270	−97.05000	27.82670	Port Aransas, H. Caldwell Pier	G
361 **	8775283	−97.20330	27.82130	Port Ingleside, Corpus Christi Bay	G
362 **	8775296	−97.39000	27.81170	Texas State Aquarium, Corpus	G
363 **	8775421	−97.28000	27.70500	Corpus Christi Naval Air Station	G
364 **	8775792	−97.23670	27.63330	Packery Channel	G
365	8775870	−97.21670	27.58000	Corpus Christi, Gulf Of Mexico	G
366 **	8779748	−97.17670	26.07670	South Padre Island (U.S.C.G)	G
367	8779750	−97.15670	26.06830	Padre Island, Brazos Santiago Pass	G
368 **	8779770	−97.21500	26.06000	Port Isabel, Laguna Madre	G
369	9500966	−97.78050	22.26200	Madero, Tampico Harbor, Mexico	G
370	9650593	−87.87000	15.89300	Puerto Cortes	C
371	9710441	−78.99700	26.71000	Settlement Point, Grand Bahamas	C
372	9751309	−64.72100	18.36800	Leinster Point (Bay), St. John	C
373 *	9751364	−64.70500	17.75000	Christiansted, St. Croix Island	C
374 **	9751373	−64.71480	18.34560	St John'S Island, Coral Harbor	C
375 **	9751381	−64.72400	18.31800	Lameshur Bay, St. John	C
376	9751401	−64.75410	17.69500	Lime Tree Bay, St Croix	C
377	9751467	−64.80400	18.36090	Lovango Cay, St John	C
378	9751494	−64.81800	18.29700	Dog Island, St Thomas	C
379 **	9751567	−64.86905	18.31870	Benner Bay	C
380	9751583	−64.86400	18.34870	Water Bay, Saint Thomas	C
381 *	9751584	−64.88400	17.71300	Fredericksted, St. Croix Island	C
382 **	9751639	−64.92030	18.33570	Charlotte Amalie, St. Thomas	C
383 *	9751768	−64.96270	18.37110	Ruy Point, St Thomas	C
384 *	9751774	−65.03500	18.36300	Botany Bay, St Thomas	C
385	9752235	−65.30200	18.30100	Culebra	C
386	9752619	−65.44400	18.15300	Isabel Segunda, Vieques Island	C
387 *	9752695	−65.47100	18.09395	Esperanza, Vieques Island	C
388	9752962	−65.57000	18.34500	Isla Palominos	C
389 *	9753216	−65.63100	18.33500	Playa De Fajardo	C
390 *	9753641	−65.71102	18.18700	Naguabo	C
391 *	9754228	−65.83300	18.05500	Yabucoa Harbor	C
392 **	9755371	−66.11600	18.45900	San Juan, La Puntilla, San Juan Bay	C
393	9755679	−66.15800	17.92800	Las Mareas	C
394 *	9756639	−66.40700	17.95390	Santa Isabel	C
395	9757809	−66.70210	18.48140	Arecibo, Puerto Rico	C
396	9758053	−66.76200	17.97300	Penuelas, Punta Guayanilla	C

Table A1. *Cont.*

ID	CO-OPS	Longitude	Latitude	Station Name	Region
397 **	9759110	−67.04603	17.97000	Magueyes Island	C
398 **	9759189	−67.18900	18.07500	Puerto Real	C
399 **	9759197	−67.19700	17.95100	Bahia Salinas	C
400 *	9759394	−67.16080	18.21790	Mayaguez, Puerto Rico	C
401	9759412	−67.16500	18.45700	Aguadilla, Crashboat Beach	C
402	9759421	−67.18530	18.16500	Punta Guanajabo, Mayagues	C
403	9759938	−67.93900	18.09000	Mona Island	C
404 *	9761115	−61.82100	17.59040	Barbuda	C
405	IHO	−66.05000	45.23330	Partridge Island	A
406	IHO	−67.04999	45.06667	St Andrews	A
407	IHO	−66.86667	45.04583	Back Bay	A
408	IHO	−65.06665	45.05000	Margretsville	A
409	IHO	−67.01711	44.96622	Fairhaven	A
410	IHO	−66.98333	44.90000	Eastport	A
411	IHO	−66.95354	44.88334	Welshpool	A
412	IHO	−62.75896	44.77344	Murphy Cove	A
413 **	IHO	−66.75010	44.76557	North Head	A
414	IHO	−65.83334	44.66667	Deep Cove	A
415	IHO	−63.56712	44.64378	Halifax	A
416	IHO	−66.79999	44.60000	Outer Wood Island	A
417	IHO	−63.95001	44.49900	Indian Harbour	A
418 **	IHO	−66.10001	44.46390	Sandy Cove	A
419 **	IHO	−68.20001	44.40000	Bar Harbour	A
420	IHO	−68.01666	44.40000	Prospect Harbour	A
421	IHO	−66.39999	44.25000	Lighthouse Cove	A
422	IHO	−66.16666	44.20000	Meteghan	A
423	IHO	−68.88333	44.14642	Pulpit Harbour	A
424	IHO	−64.66210	43.98320	Liverpool	A
425	IHO	−65.10420	43.66480	Lockeport	A
426 **	IHO	−70.24667	43.65667	Portland	A
427	IHO	−65.74290	43.52580	Woods Harbour	A
428	IHO	−66.00000	43.50000	Flat Island	A
429	IHO	−66.00000	43.48333	Seal Island	A
430 **	IHO	−70.74167	43.08000	Portsmouth (Navy Yard)	A
431	IHO	−63.20001	42.81667	Fundy 1	A/D
432	IHO	−63.98334	42.78333	SB2	A/D
433	IHO	−64.36667	42.61666	Fundy 21	A/D
434	IHO	−67.71667	42.46667	Fundy 6	A/D
435 **	IHO	−71.03326	42.35078	Boston (Commonwealth Piers)	A
436	IHO	−65.50000	42.11666	Fundy 22a	A/D
437	IHO	−65.63333	42.05000	Fundy 22b	A/D
438 **	IHO	−71.39694	41.80080	Providence	A
439 *	IHO	−70.50000	41.77482	E Cape Cod Canal	A
440 **	IHO	−70.61667	41.74072	WCape Cod Canal	A
441 **	IHO	−70.62512	41.73333	Buzzards Bay	A
442	IHO	−65.79999	41.73333	Fundy 3	A/D
443 *	IHO	−70.89999	41.60000	New Bedford	A
444	IHO	−71.33334	41.50000	Newport	A
445	IHO	−70.67143	41.52422	Woods Hole (Ocean Inst)	A
446 **	IHO	−72.09900	41.34903	New London	A
447	IHO	−72.35001	41.26667	Connecticut River Ent	A
448 *	IHO	−73.16666	41.16667	Bridgeport	A
449	IHO	−72.20001	41.16521	Plum Island	A
450 *	IHO	−71.96667	41.05000	montauk	A
451 **	IHO	−73.06728	40.95027	Port Jefferson	A
452 *	IHO	−73.78333	40.80000	Willets Point	A
453 **	IHO	−73.85006	40.78285	College Point	A

Table A1. *Cont.*

ID	CO-OPS	Longitude	Latitude	Station Name	Region
454	IHO	−66.83334	40.73333	Fundy 4	A/D
455 **	IHO	−73.23280	40.71533	Bayshore Long Island	A
456 **	IHO	−74.01666	40.70000	New York: Battery	A
457 **	IHO	−74.01666	40.68333	New York: Governor's Island	A
458	IHO	−74.03333	40.60000	New York: Fort Hamilton	A
459	IHO	−74.01666	40.46833	Sandy Hook	A
460	IHO	−67.75000	40.36666	Fundy 23	A/D
461	IHO	−70.89999	40.30000	IAPSO: 30-1.2.32	A/D
462	IHO	−68.63333	40.11667	IAPSO: 30-1.2.1	A/D
463 **	IHO	−75.13333	39.95000	Philadelphia	A
464	IHO	−71.38333	39.95000	IAPSO: 30-1.2.2	A/D
465 **	IHO	−75.58334	39.58333	Delaware City	A
466 **	IHO	−75.56665	39.55000	Reedy Point	A
467 **	IHO	−75.81665	39.53140	Chesapeake City	A
468 **	IHO	−75.88333	39.51667	Court House Point	A
469 **	IHO	−75.98419	39.43576	Elk River Entrance	A
470	IHO	−76.26666	39.28333	Pooles Island Light	A
471 **	IHO	−76.58070	39.26940	Baltimore	A
472	IHO	−72.16666	39.21667	IAPSO: 30-1.2.17	A/D
473	IHO	−71.36667	39.16667	IAPSO: 30-1.2.19	A/D
474	IHO	−76.41666	39.15000	Seven Foot Knoll Light	A
475	IHO	−76.30221	39.04201	Love Point Light	A
476 **	IHO	−76.48191	38.98550	Annapolis	A
477 *	IHO	−74.96000	38.96833	Cape May Ferry Terminal	A
478	IHO	−76.43335	38.90000	Thomas Point Shoal Light	A
479 **	IHO	−77.01725	38.86094	Washington D.C.	A
480 **	IHO	−75.10220	38.78790	Breakwater Harbour	A
481 **	IHO	−75.07045	38.60092	Indian River Inlet	A
482 **	IHO	−76.06341	38.57254	Cambridge	A
483 **	IHO	−76.45001	38.31667	Solomons Island	A
484 **	IHO	−76.41666	38.31667	Drum Point Light	A
485	IHO	−76.95001	38.25000	Colonial Beach	A
486	IHO	−76.75000	38.21667	Colton Point	A
487	IHO	−76.53333	38.13334	Piney Point	A
488	IHO	−76.10001	38.06667	Holland Island Bar Light	A
489	IHO	−76.26666	37.80000	Great Wicomico Light	A
490	IHO	−76.26666	37.56667	Stingray Point Light	A
491	IHO	−73.08334	37.36666	IAPSO: 30-1.2.16	A/D
492 **	IHO	−77.26666	37.31667	City Point Hopewell	A
493 **	IHO	−76.02449	37.26667	Cape Charles	A
494 **	IHO	−76.49882	37.24811	Gloucester Point	A
495	IHO	−76.29999	37.00000	Old Point Comfort	A
496 **	IHO	−76.33334	36.95000	Hampton Roads (Sewall Pt.)	A
497	IHO	−75.96667	36.83333	Virginia Beach	A
498	IHO	−75.50000	35.33333	Avon	A
499 *	IHO	−76.68335	34.71667	Morehead City	A
500 **	IHO	−77.95001	34.23333	Wilmington	A
501 *	IHO	−78.01667	33.91500	Southport	A
502	IHO	−78.89999	33.66667	Myrtle Beach	A
503 **	IHO	−79.91666	32.78333	Charleston	A
504	IHO	−75.61667	32.68333	IAPSO: 30-1.2.3	A/D
505	IHO	−64.64999	32.36666	St. Davids Island	A
506 **	IHO	−80.78279	32.31757	Port Royal Sound	A
507	IHO	−64.83334	32.31667	Ireland Island	A
508 **	IHO	−80.89995	32.03360	Savannah River Entrance	A
509	IHO	−64.43335	32.01667	IAPSO: 30-1.2.18	A/D
510 **	IHO	−81.20050	31.53659	Sapelo Sound	A

Table A1. *Cont.*

ID	CO-OPS	Longitude	Latitude	Station Name	Region
511 **	IHO	−88.04010	30.70830	Mobile	G
512	IHO	−76.41666	30.43333	IAPSO: 30-1.2.11	A/D
513 **	IHO	−88.90330	30.41175	Biloxi	G
514 **	IHO	−87.21667	30.40000	Pensacola	G
515 *	IHO	−81.43259	30.39928	Mayport	A
516 **	IHO	−87.26428	30.34872	Warrington Navy Yard	G
517 **	IHO	−81.61667	30.35000	Jacksonville Dredger Dept.	A
518	IHO	−90.29999	30.29805	Pass Nanchac Light	G
519	IHO	−89.33334	30.30000	Bay St Louis	G
520	IHO	−89.16666	30.23333	Cat Island	G
521 **	IHO	−88.01666	30.23333	Mobile Point Light	G
522 **	IHO	−85.74736	30.16939	Alligator Bayou	G
523	IHO	−84.18335	30.06667	St Marks Light	G
524	IHO	−90.11667	30.02376	West End	G
525 **	IHO	−90.06803	29.91999	New Orleans	G
526	IHO	−93.34736	29.78333	Calcasieu Pass Light	G
527 **	IHO	−94.69040	29.71333	Round Point	G
528	IHO	−84.98334	29.71667	Apalachicola	G
529	IHO	−93.85001	29.70000	Sabine	G
530 **	IHO	−94.98334	29.68333	Morgan Point	G
531 *	IHO	−94.49038	29.51828	Gilchrist	G
532	IHO	−92.03492	29.57862	Lighthouse Point	G
533 **	IHO	−91.54999	29.51667	Point Chevreuil	G
534	IHO	−91.76710	29.48820	South Point	G
535	IHO	−89.16666	29.48333	Breton Island	G
536 **	IHO	−91.27077	29.51204	Shell Island	G
537	IHO	−91.59734	29.50966	Rabbit Island Pass	G
538	IHO	−91.38500	29.37170	Eugene Island	G
539 **	IHO	−89.33334	29.36667	Jack Bay	G
540	IHO	−94.70001	29.33333	Galveston Bay Entrance	G
541	IHO	−91.75000	29.28667	Point au Fer	G
542 **	IHO	−94.78333	29.31667	Galveston	G
543 **	IHO	−89.96667	29.26667	Bayou Rigaud	G
544	IHO	−89.60001	29.25000	Empire Jetty	G
545	IHO	−81.00000	29.23333	Daytona Beach	A
546 **	IHO	−95.00000	29.21667	Carancahua Reef	G
547	IHO	−89.04999	29.21667	Lonesome Bayou	G
548 **	IHO	−81.00000	29.21667	Daytona Beach	A
549	IHO	−83.03167	29.13333	Cedar Kay	G
550	IHO	−89.03333	29.11667	Southeast Pass	G
551	IHO	−89.26666	29.05000	Joseph Bayou	G
552	IHO	−89.16666	29.01667	Port Eads	G
553	IHO	−89.13333	28.98333	South Pass	G
554	IHO	−95.29999	28.93333	Freeport	G
555	IHO	−89.42833	28.93167	Southwest Pass	G
556 *	IHO	−82.66874	28.45132	Indian Bay	G
557	IHO	−76.79999	28.45000	IAPSO: 30-1.2.15	A/D
558	IHO	−67.53333	28.23333	IAPSO: 30-1.2.5	A/D
559	IHO	−69.75000	28.13333	IAPSO: 30-1.2.4	A/D
560 **	IHO	−97.04999	28.01667	Rockport	G
561	IHO	−76.78333	28.01667	IAPSO: 30-1.2.14	A/D
562	IHO	−69.66666	27.98333	IAPSO: 30-1.2.8	A/D
563	IHO	−69.66666	27.96667	IAPSO: 30-1.2.7	A/D
564 **	IHO	−97.39999	27.81493	Nueces Bay	G
565	IHO	−82.61667	27.76667	St Petersburg	G
566 *	IHO	−82.73295	27.53391	Anna Maria	G
567 **	IHO	−82.25000	26.71667	South Boca Grande	G
568	IHO	−84.25000	26.70000	IAPSO: 30-1.2.13	G/D

Table A1. *Cont.*

ID	CO-OPS	Longitude	Latitude	Station Name	Region
569 **	IHO	−81.86667	26.65000	Fort Myers	G
570 **	IHO	−82.06665	26.63333	Matlacha Pass	G
571 **	IHO	−82.08081	26.55000	Tropical Homesites	G
572 **	IHO	−82.18335	26.51667	Captiva Island	G
573 **	IHO	−82.08334	26.48333	St James City	G
574 **	IHO	−82.01666	26.48333	Punta Rassa	G
575	IHO	−69.33334	26.46667	IAPSO: 30-1.2.13	A/D
576 **	IHO	−81.95001	26.45511	Matanzas Pass	G
577 **	IHO	−81.93335	26.45000	Hurricane Bay San Carlos	G
578	IHO	−69.31665	26.45000	IAPSO: 30-1.2.9	A/D
579 **	IHO	−81.90951	26.43333	Estero Island Estero Bay	G
580 **	IHO	−81.85938	26.43120	Mound Key Estero Bay	G
581 **	IHO	−81.89248	26.41690	Ostego Bay	G
582 **	IHO	−81.88324	26.40748	Carlos Point Estero Bay	G
583 **	IHO	−97.35001	26.35000	North Point	G
584 **	IHO	−97.21500	26.06000	Port Isabel	G
585	IHO	−97.14999	26.06667	South Padre Island	G
586	IHO	−79.89999	25.85000	IAPSO: 30-1.2.12	A/D
587	IHO	−79.28333	25.55000	Cat Cay	A
588	IHO	−77.35001	25.08333	Nassau	A
589	IHO	−77.96208	25.04691	Anros Island	A
590	IHO	−76.15000	24.76667	Eleuthera	A
591	IHO	−89.64999	24.76667	IAPSO: 30-1.2.6	G/D
592	IHO	−80.93335	24.76667	Grassy Key	A
593 **	IHO	−81.01666	24.71667	Marathon Shores	A
594	IHO	−82.88333	24.63333	Tortugas	G
595	IHO	−81.79994	24.54559	Key West	G
596	IHO	−75.96631	23.66719	Steventon Great Exuma	A
597	IHO	−82.33334	23.17150	Habana	G
598	IHO	−74.95001	23.00000	Long Island	A
599	IHO	−73.04999	22.33333	Start Point Mayaguana	A
600	IHO	−97.76990	22.25000	Tampico	G
601	IHO	−74.29999	22.16667	Datum Bay	A
602	IHO	−79.97908	21.72682	Casilda	C
603	IHO	−82.91677	21.44490	Carapachibey	C
604	IHO	−71.14999	21.43333	Grand Turk	A
605	IHO	−89.65000	21.30000	Progreso	G
606	IHO	−76.10860	21.11580	Gibara	A
607	IHO	−74.49380	20.36023	Baracoa	A
608	IHO	−75.14999	19.89300	Guantanamo Bay	C
609	IHO	−90.55310	19.85580	Campeche	G
610	IHO	−70.65910	19.78300	Puerto Plata	A
611 **	IHO	−69.31665	19.19590	Samana	A
612	IHO	−96.11160	19.18333	Vera Cruz	G
613 **	IHO	−64.38333	18.72501	Anegada	A
614	IHO	−72.35384	18.55022	Port au Prince	C
615 **	IHO	−69.88333	18.46527	Ciudad Trujillo	C
616 **	IHO	−66.11600	18.45900	San Juan	A
617 **	IHO	−64.61667	18.42723	Tortola	C
618 **	IHO	−68.95001	18.41036	La Romana	C
619 *	IHO	−64.93335	18.33333	St Thomas	C
620	IHO	−65.28333	18.30000	Great Harbor	C
621	IHO	−78.13333	18.20000	Savanna la Mar	C
622	IHO	−94.41666	18.15805	Coatzacoalcos	G
623 **	IHO	−67.04603	17.97000	Magueyes Island	C
624 **	IHO	−61.85111	17.12284	St Johns	C
625	IHO	−64.88333	16.53333	IAPSO: 30-1.3.2	C/D
626	IHO	−64.91666	16.50000	IAPSO: 30-1.3.1	C/D

Table A1. *Cont.*

ID	CO-OPS	Longitude	Latitude	Station Name	Region
627 **	IHO	−61.50000	16.38333	Petit Canal	C
628 *	IHO	−61.69943	16.33476	Sainte Rose	C
629	IHO	−61.26666	16.25000	Saint Francois	C
630	IHO	−61.53702	16.23290	Pointe a Pitre	C
631	IHO	−87.95001	15.83333	Puerto Cortes	C
632 *	IHO	−61.46667	15.56667	Portsmouth	C
633	IHO	−61.04999	14.58333	Fort de France	C
634	IHO	−83.36667	14.01667	Puerto Cabezas	C
635	IHO	−61.00110	14.02240	Castries	C
636	IHO	−61.23334	13.13333	Kingstown St Vincent	C
637 **	IHO	−59.61454	13.08616	Carlisle Bay	A
638	IHO	−61.18335	12.83333	Mustique Grand Bay	C
639	IHO	−61.33334	12.70329	Charlestown Bay	C
640	IHO	−61.35001	12.63333	Tobago Cays	C
641	IHO	−70.05290	12.60000	Aruba Malmok Bay	C
642	IHO	−61.41778	12.59252	Clifton Harbour	C
643	IHO	−70.03554	12.51347	Aruba Oranjestad	C
644	IHO	−61.45709	12.48783	Hillsborough Bay	C
645	IHO	−68.93335	12.10000	Curacao Willemstad	C
646 *	IHO	−61.75652	12.05000	St Georges	C
647	IHO	−68.64999	12.00000	Klein Curacao n.w. Coast	C
648 *	IHO	−70.21667	11.75000	Amuay	C
649 *	IHO	−60.73360	11.16920	Scarborough	A
650	IHO	−71.64651	11.02353	Zaparita	C
651	IHO	−71.58334	11.00000	Malecon	C
652	IHO	−71.56665	10.96667	Zapara Island	C
653	IHO	−71.61667	10.88333	Tablazo	C
654	IHO	−60.93335	10.83689	Toco	A
655	IHO	−71.63333	10.81667	Punta Palmas	C
656 **	IHO	−61.60001	10.68333	Carenage Bay	C
657	IHO	−61.64999	10.66667	Gaspar Grande	C
658 *	IHO	−61.51692	10.64955	Port of Spain	C
659	IHO	−66.93335	10.61667	La Guaira	C
660	IHO	−62.08334	10.61667	Puerto de Hierro	C
661	IHO	−64.20470	10.45000	Cumana	C
662	IHO	−61.01932	10.40000	Nariva River	A
663	IHO	−75.57640	10.38333	Cartagena	C
664	IHO	−61.48334	10.36667	Point Lisas	C
665	IHO	−61.70001	10.18333	Point Fortin	C
666 **	IHO	−62.64310	10.12410	Punta Gorda	C
667 *	IHO	−61.01666	10.15000	Guayaguayare Bay	A
668 *	IHO	−61.64999	10.06667	Erin Bay	C
669	IHO	−62.20001	10.01667	Rio Pedernales	C
670	IHO	−83.03333	10.00267	Puerto Limon	C
671	IHO	−79.91666	9.36667	Colon	C
672	IHO	−79.91666	9.35000	Cristobal (Canal Zone)	C
673 **	IHO	−59.79999	8.41667	Waini Point	A
674 **	IHO	−58.25000	6.95000	Bluejacket Beacon	A
675 **	IHO	−58.04999	6.95000	Demerara Beacon	A
676 **	IHO	−58.41666	6.86667	Parika	A
677 *	IHO	−58.16666	6.83333	Georgetown	A
678 **	IHO	−57.95001	6.78333	Belfield	A
679 **	IHO	−58.61667	6.40000	Bartica	A
680 *	IHO	−57.01666	5.96667	Nickerie River Mouth	A
681 **	IHO	−55.21667	5.98630	Surinam River Entrance Light	A

* Station is approximated by nearest neighbor for harmonic extraction since it is not within the actual bounds of the EC2001 model domain but is near the edge of the domain; ** Station is not included in EC2001 error measures or scatter plots as it is not physically within the EC2001 model domain and is far removed from the domain.

Appendix B

Scatter plots for the 10 stations shown by a black X in Figures 5 and 6 are provided herein. Both the EC2015 Manning's *n* and VDatum friction models are compared to the EC2001 model. Note that other than the Pilottown, LA station (313) and Curacoa, Willemstad (645) stations, the different friction formulations generally create more of a difference in the amplitude response than they do in the phase response. Plots are grouped according to region.
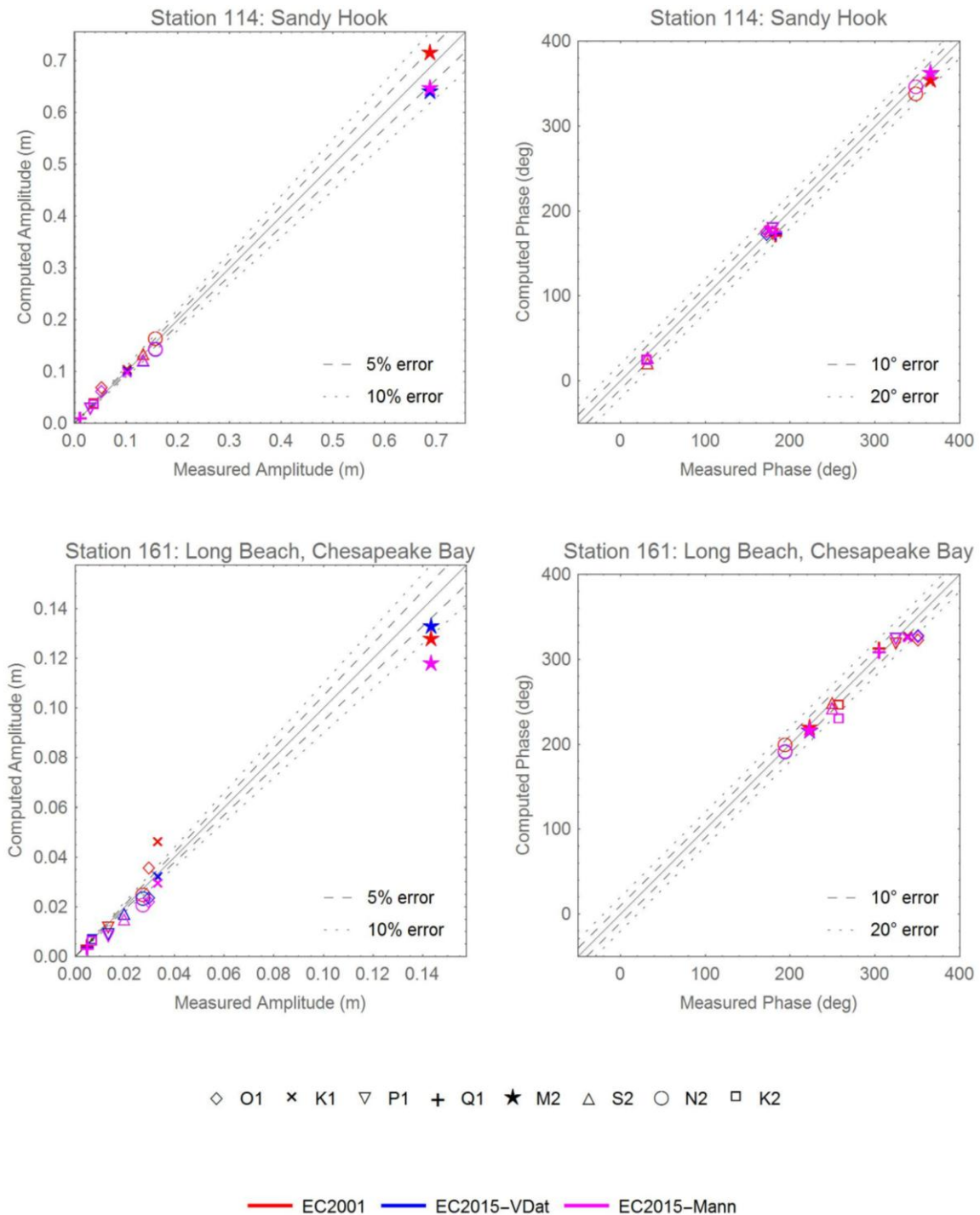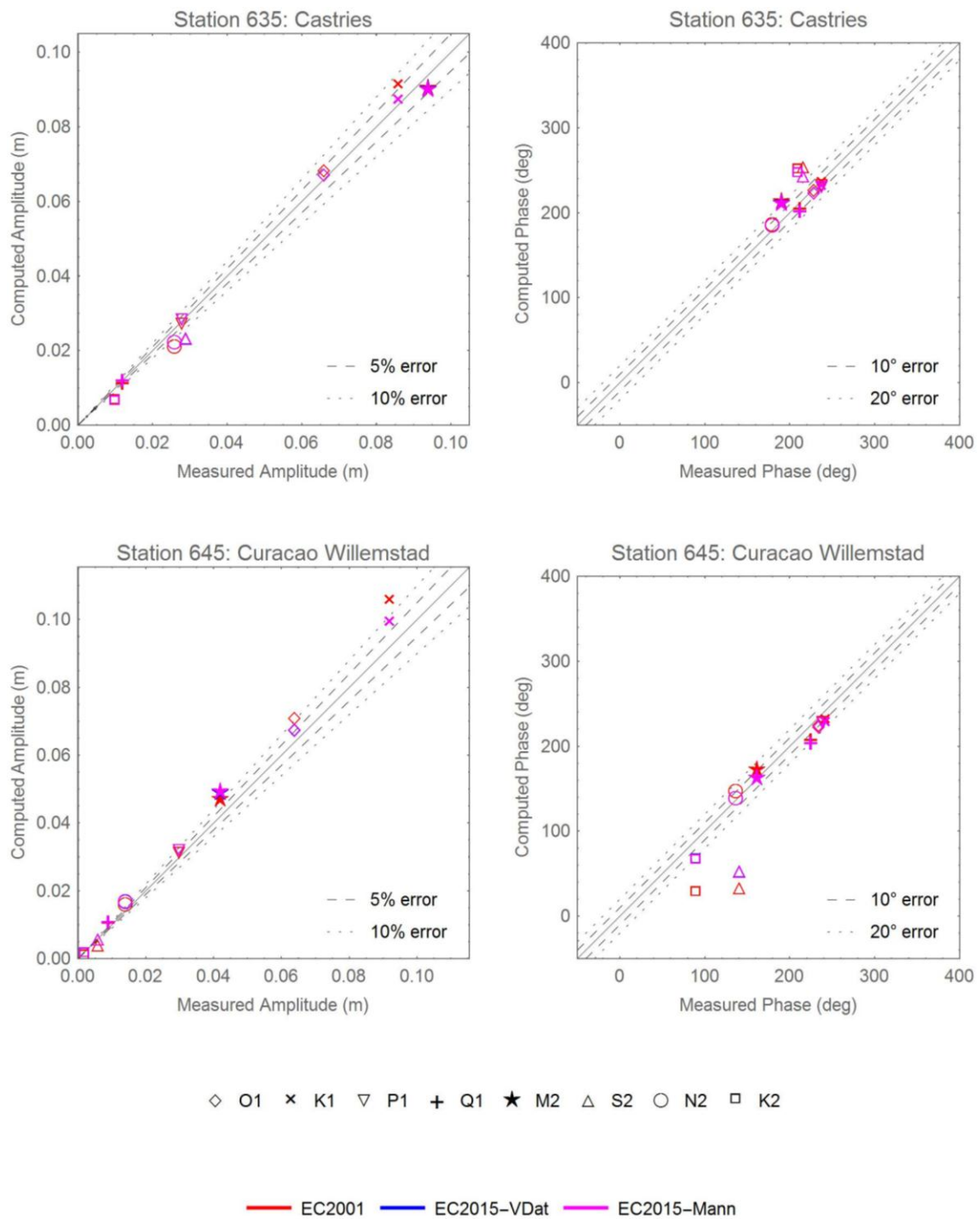

Figure B1. Scatterplots of computed versus measured harmonic data for representative stations along the Atlantic coast.
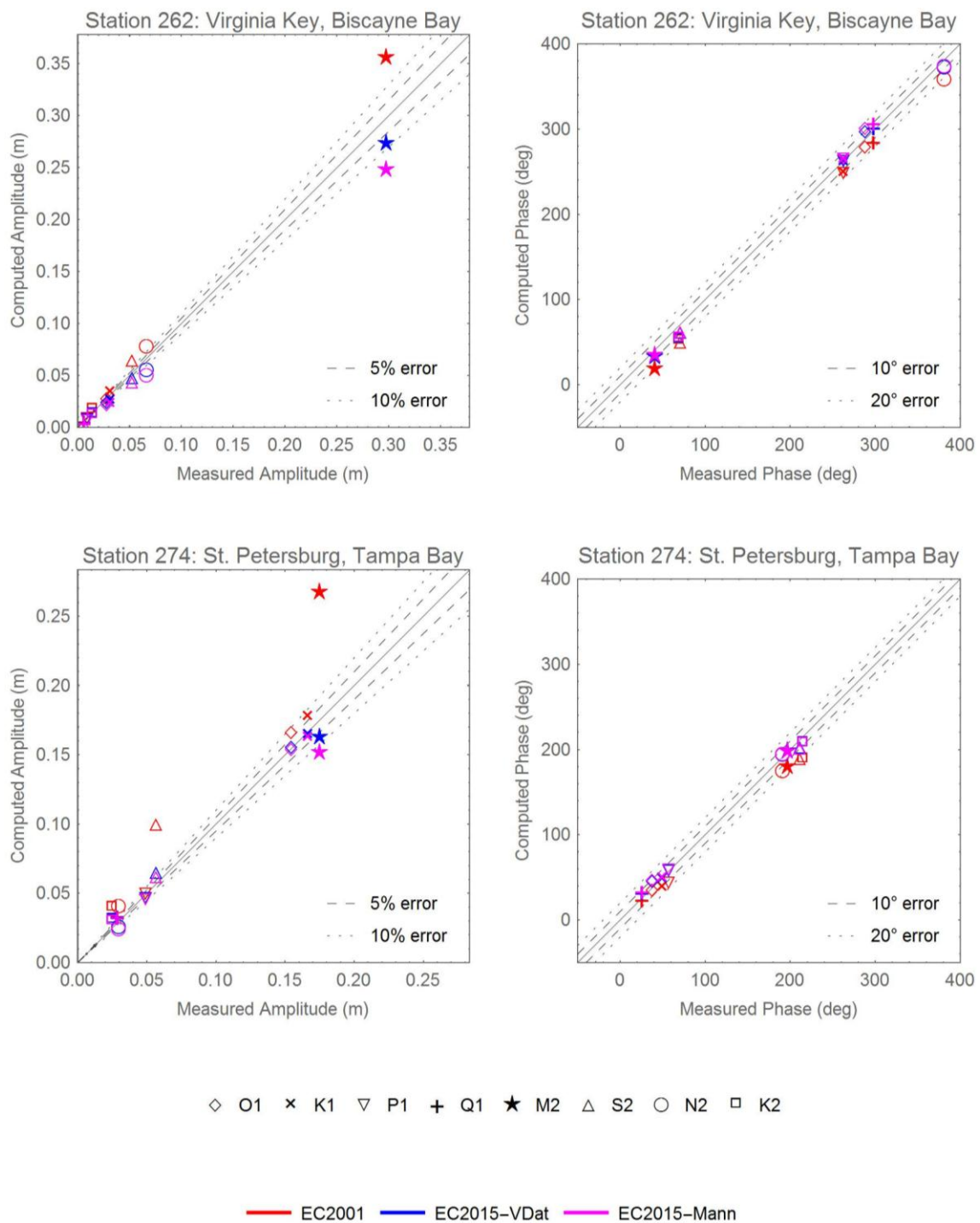
Figure B2. Scatterplots of computed versus measured harmonic data for representative stations along the Florida coast.
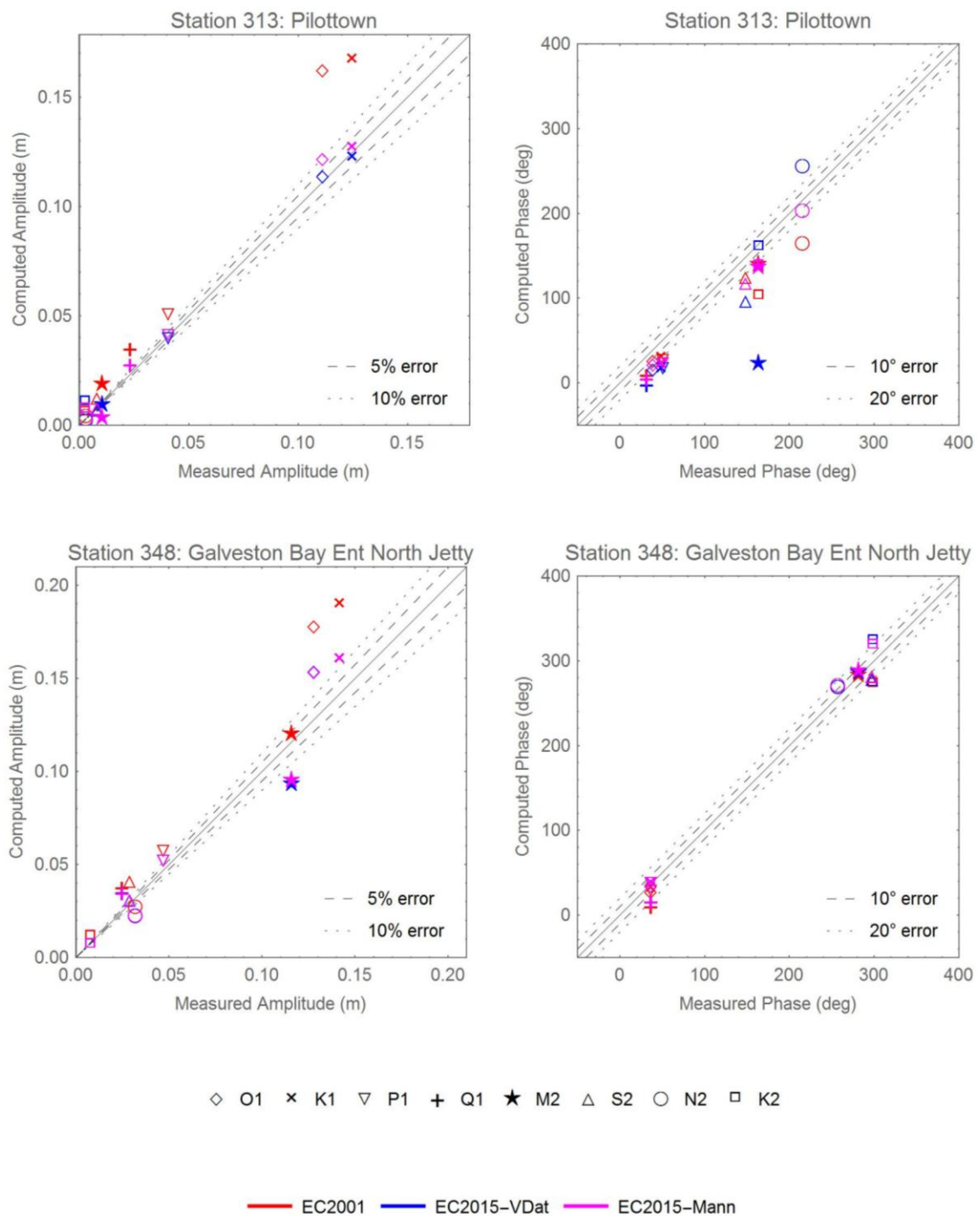
Figure B3. Scatterplots of computed versus measured harmonic data for representative stations along the Gulf of Mexico coast.

Figure B4. Scatterplots of computed versus measured harmonic data for representative stations in the Caribbean Sea.
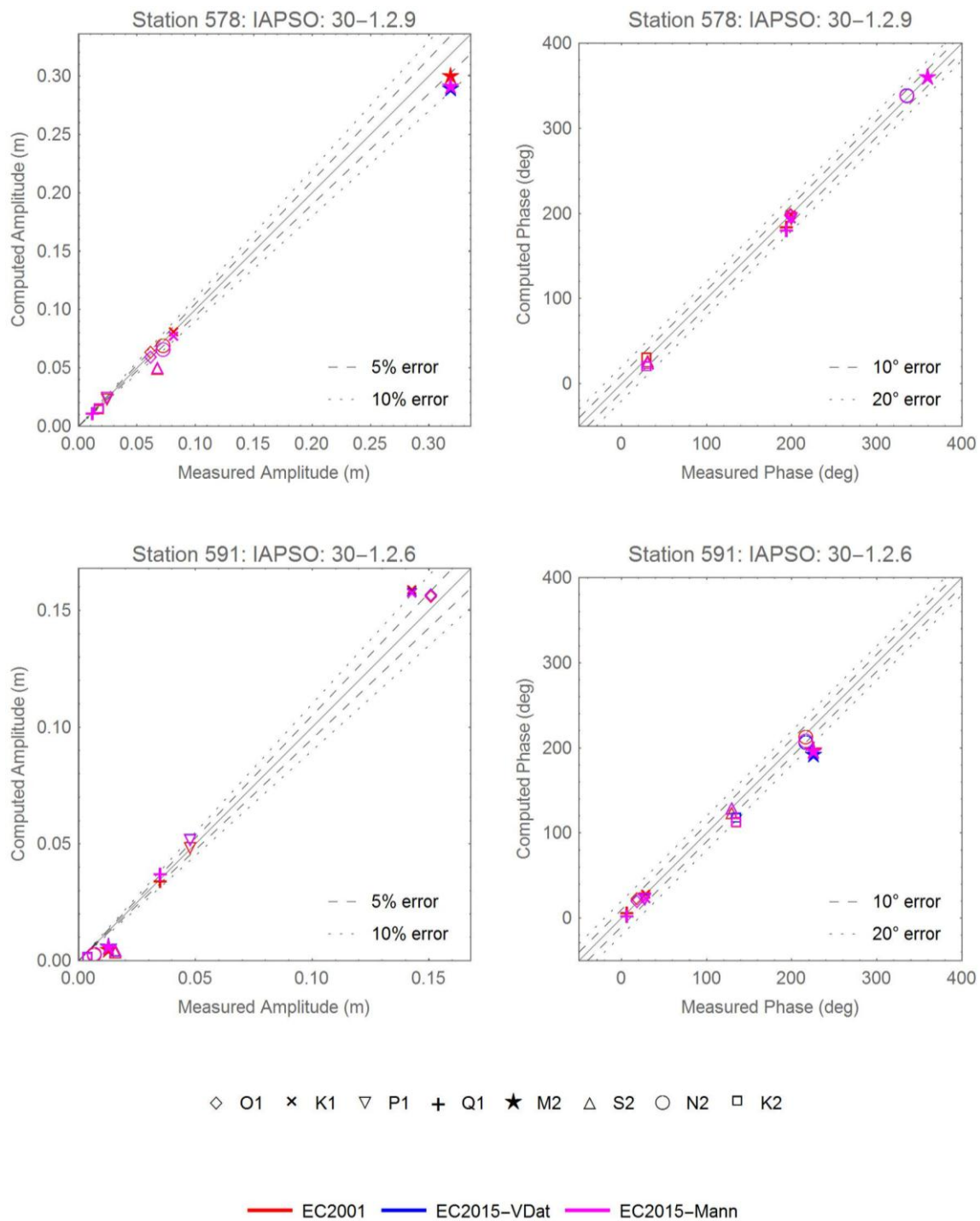
Figure B5. Scatterplots of computed versus measured harmonic data for representative deep IHO stations.

Appendix C

The actual geographic distribution of errors for the K_1 and M_2 constituents are provided at all 681 validation stations in the following seven figures. Although the same regional views given in Figures 5 and 6 are used herein, only the dominant constituent is shown in each subregion: Gulf of Maine, Atlantic Coast and Florida Coast—M_2, Gulf of Mexico and Caribbean Sea—K_1. Symbol shapes denote the magnitude of the errors while the colors represent whether the EC2015 model is over (red)

or underestimating (blue) the amplitudes. Similarly, blue symbols denote locations where the model exhibits a phase lag while red symbols denote a phase lead.
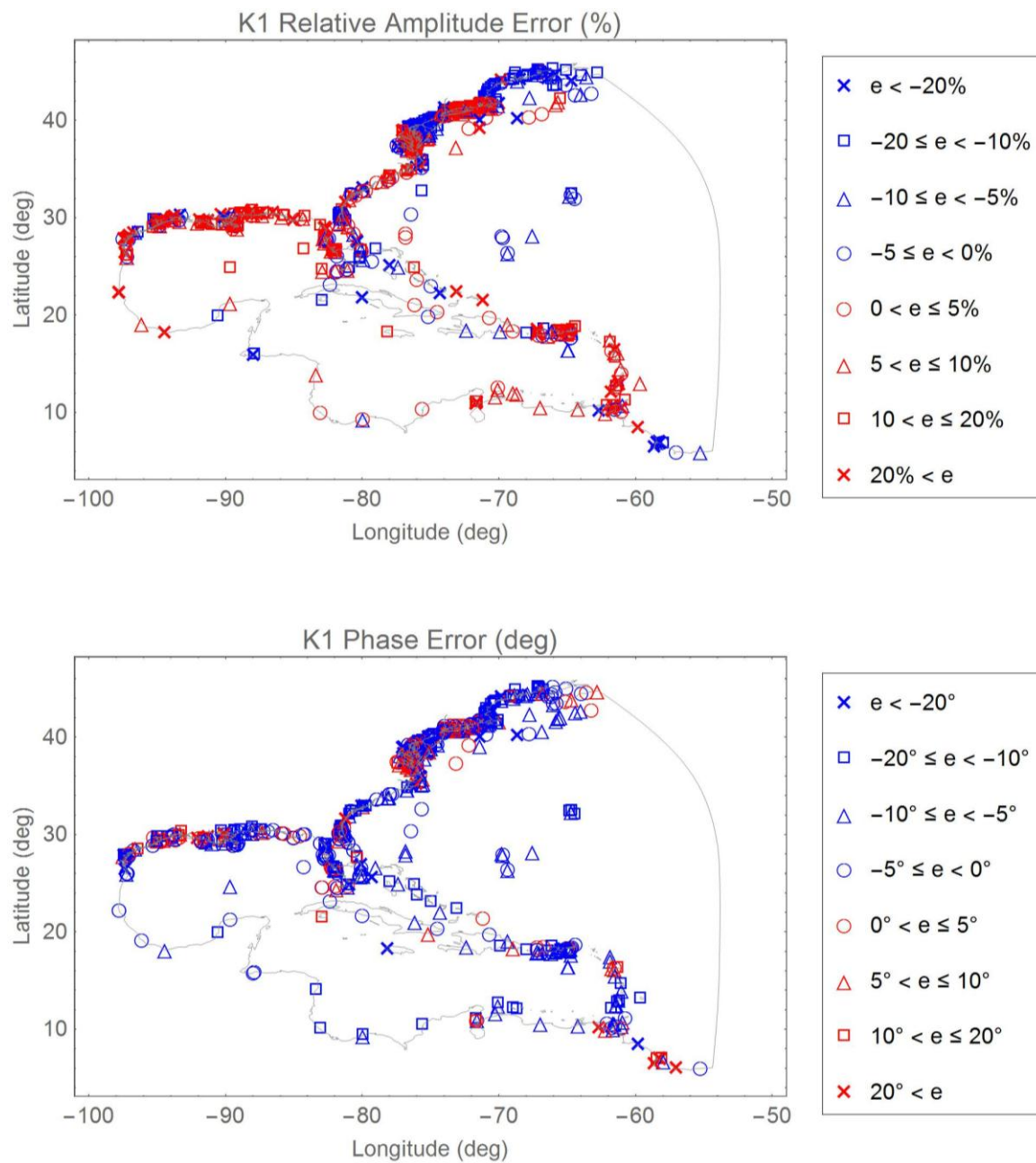
Figure C1. Distribution of relative amplitude and absolute phase errors for the K_1 constituent: global view.
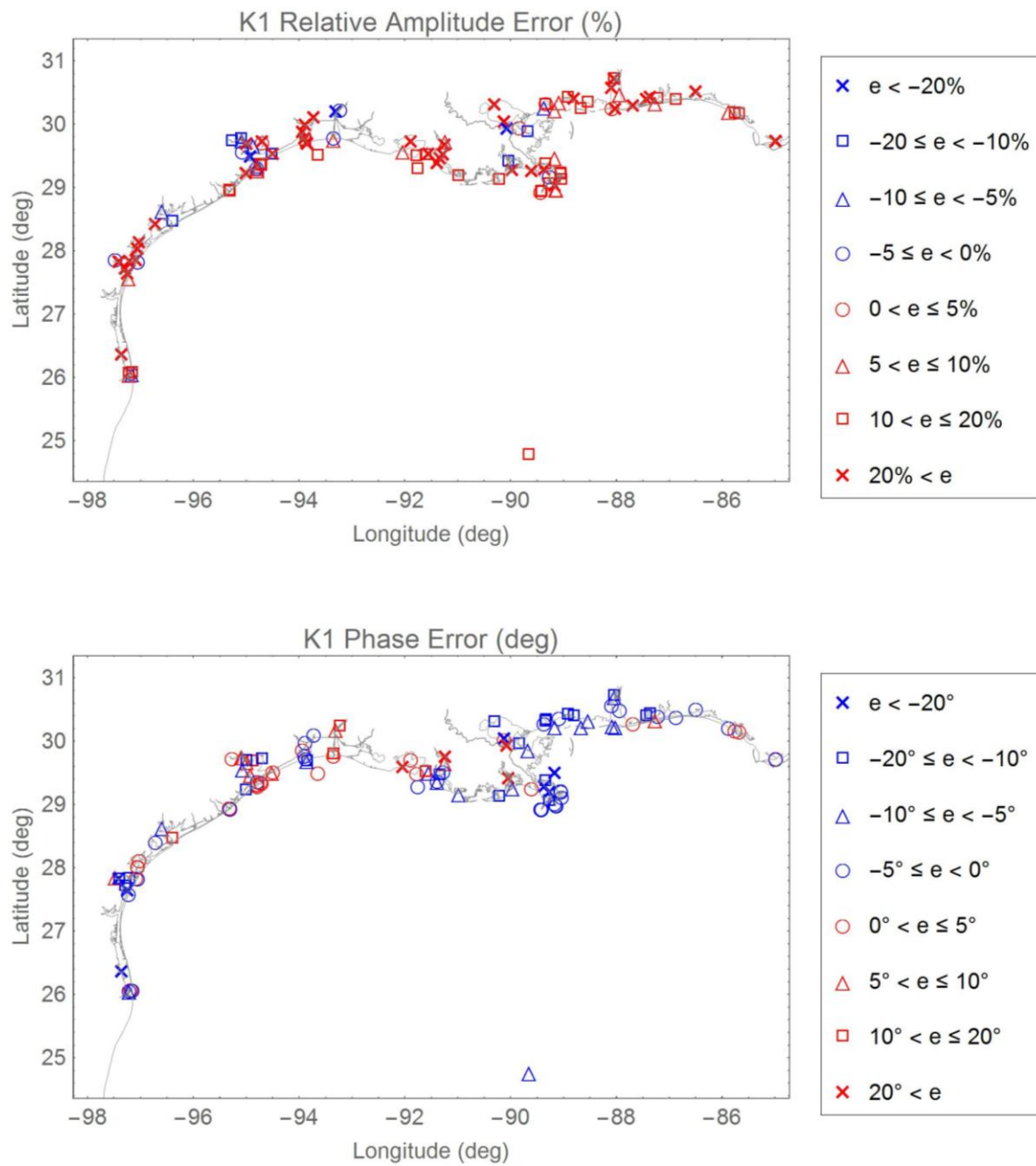
Figure C2. Distribution of relative amplitude and absolute phase errors for the K_1 constituent: Gulf of Mexico.
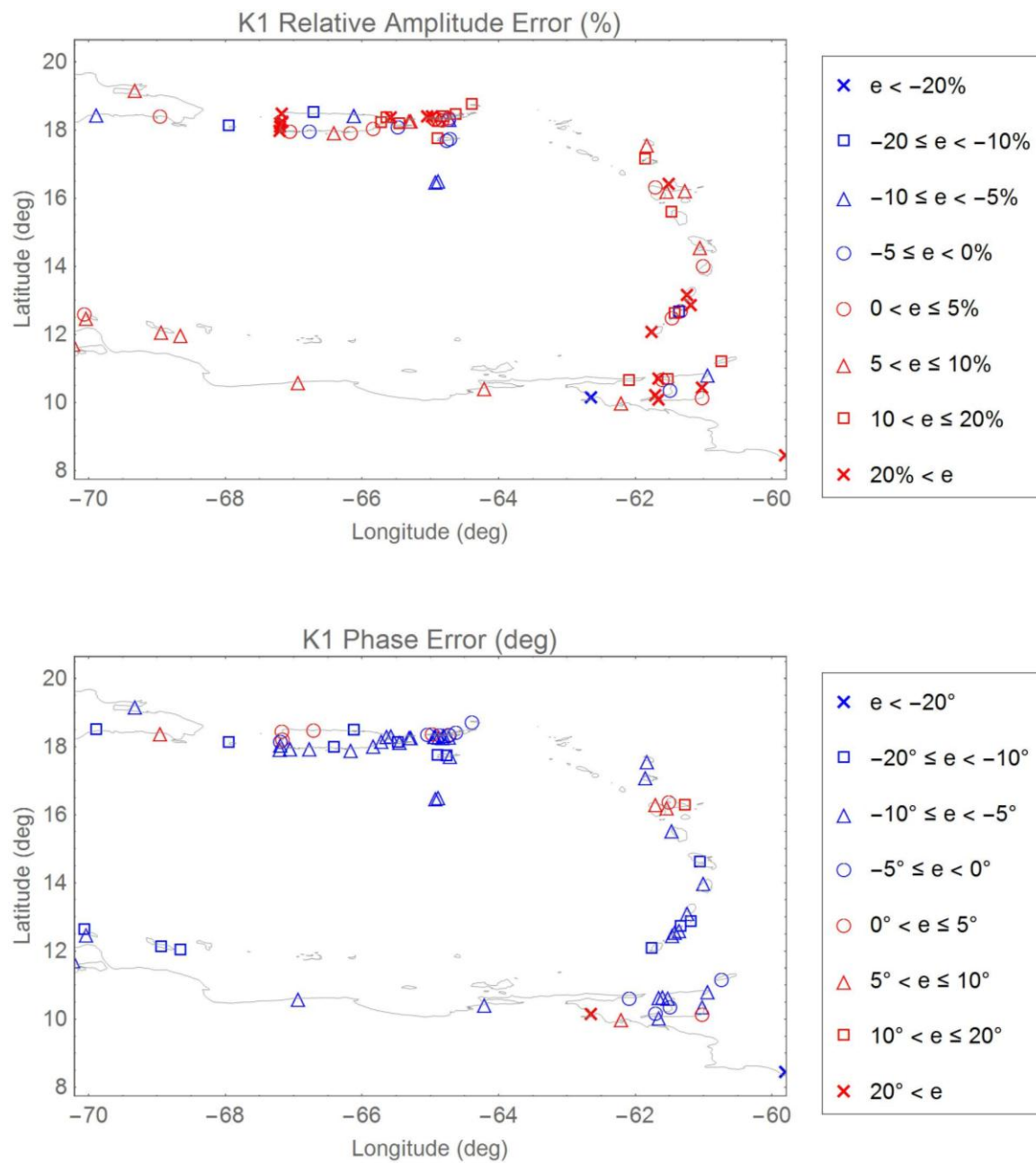
Figure C3. Distribution of relative amplitude and absolute phase errors for the K_1 constituent: Caribbean Sea.
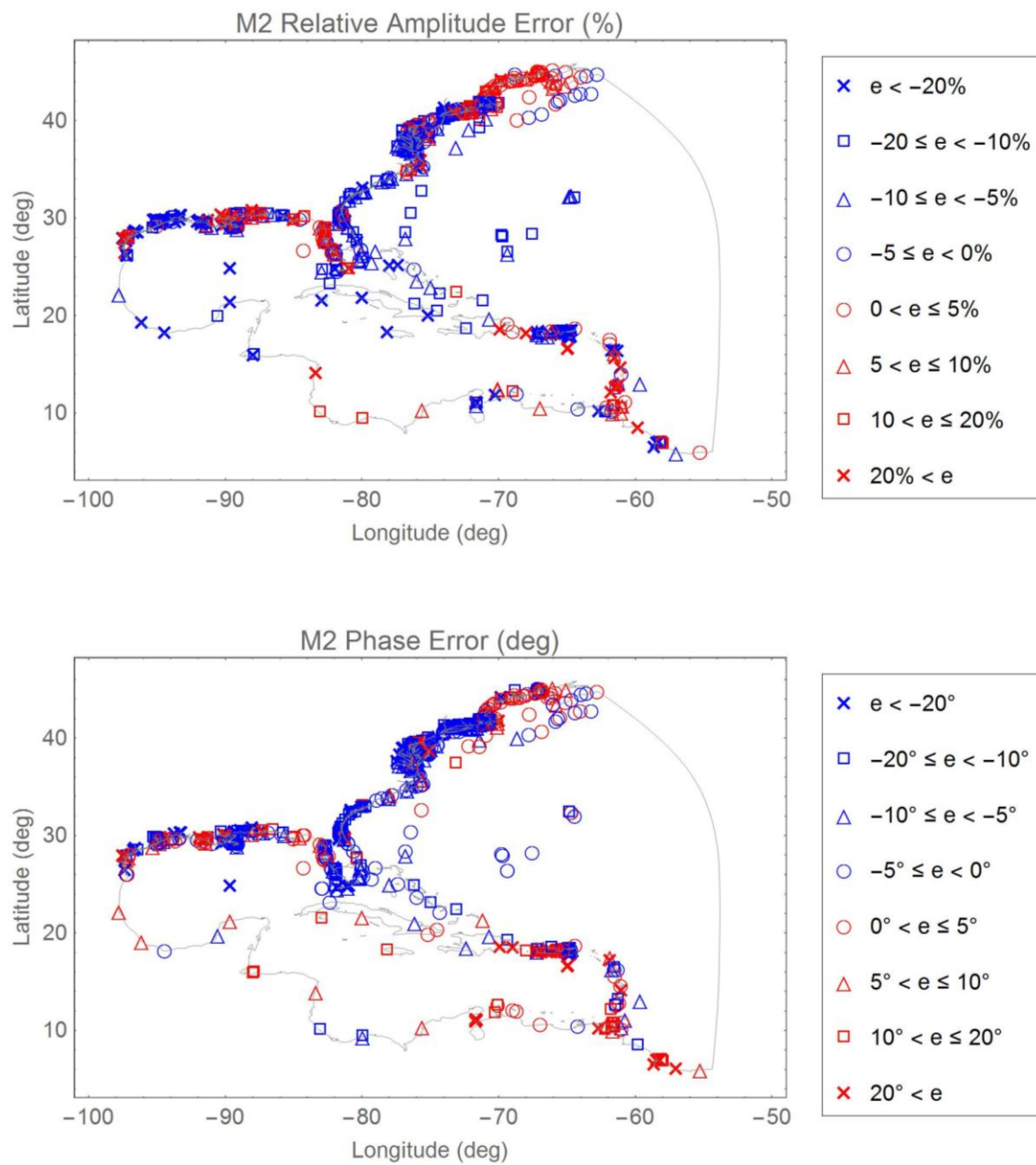
Figure C4. Distribution of relative amplitude and absolute phase errors for the M_2 constituent: global view.
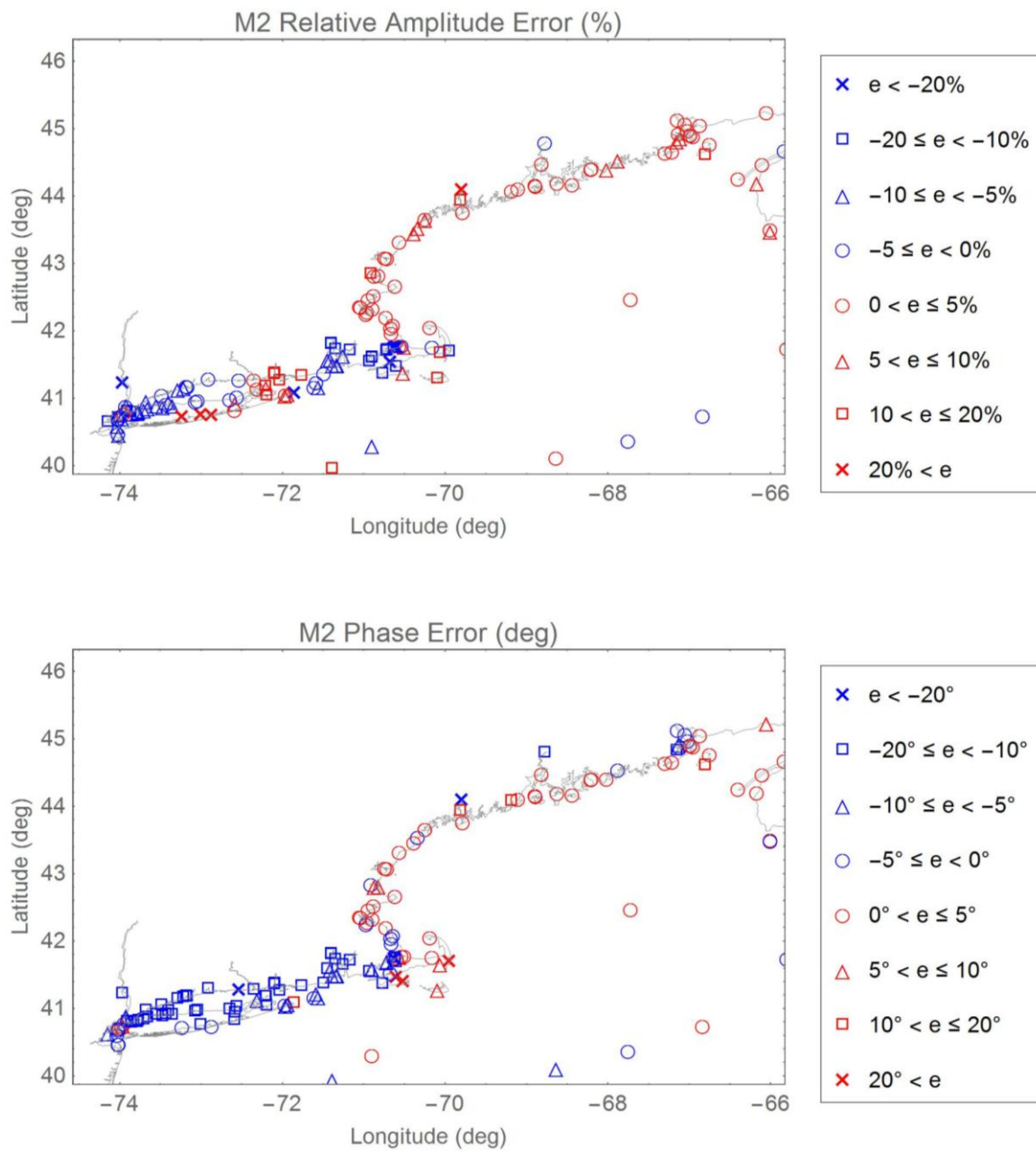
Figure C5. Distribution of relative amplitude and absolute phase errors for the M_2 constituent: Gulf of Maine and New York Bight.
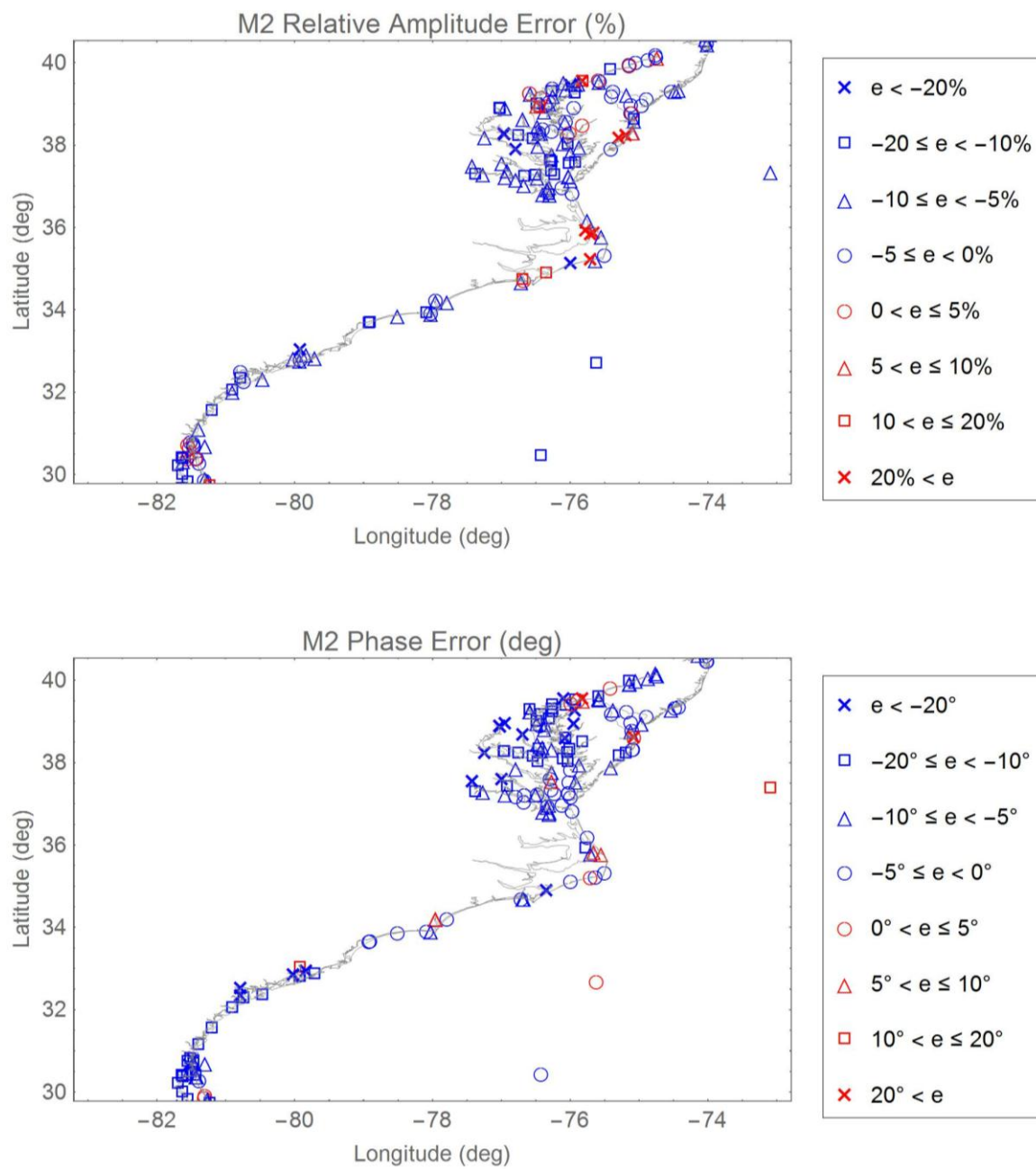
Figure C6. Distribution of relative amplitude and absolute phase errors for the M_2 constituent: Atlantic coast from Delaware to Georgia.
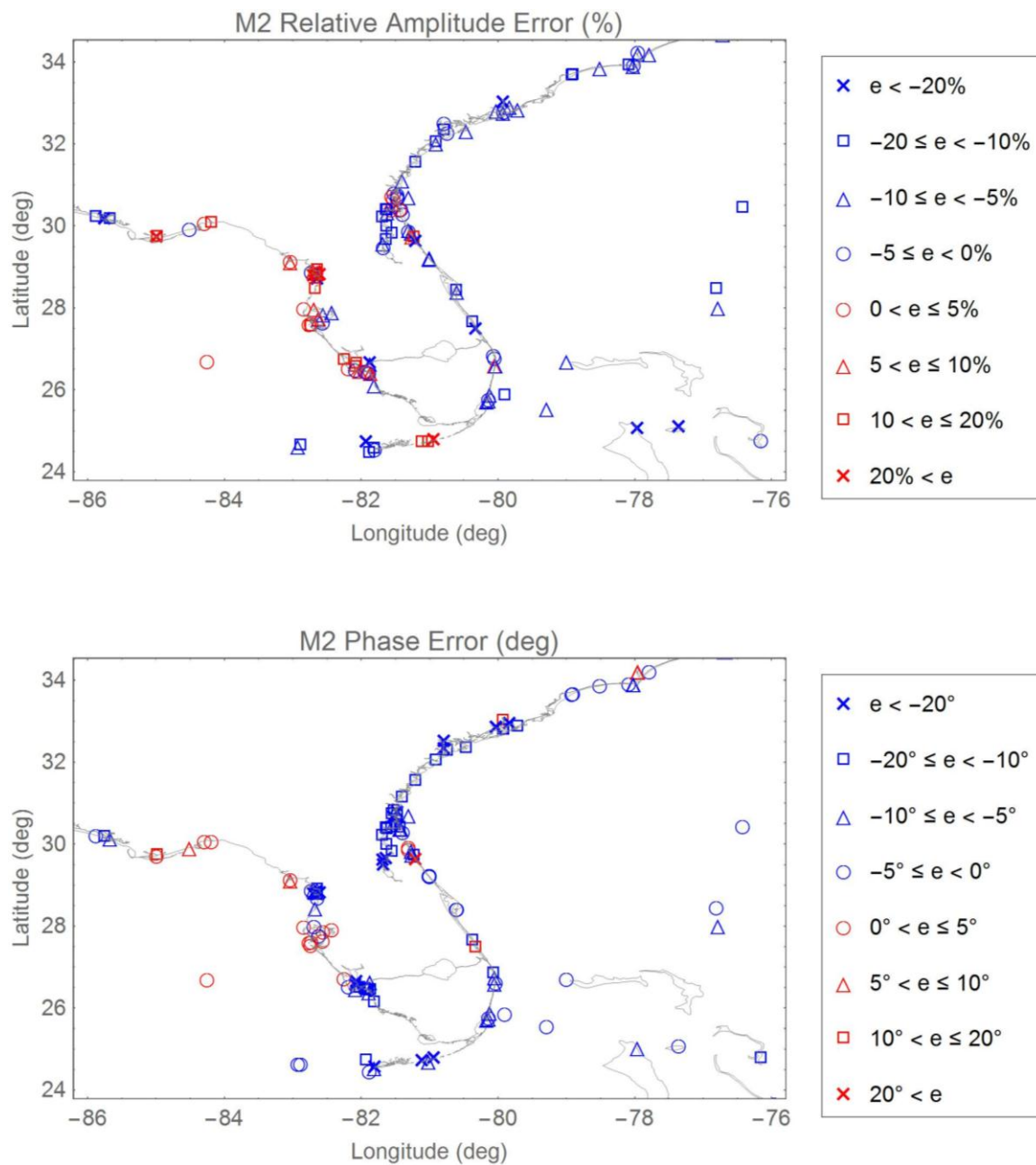
Figure C7. Distribution of relative amplitude and absolute phase errors for the M_2 constituent: Florida coast.

Appendix D

Herein we provide general applicability and usage guidelines for the EC205 tidal database. It is recommended that users read through these sections to understand the limitations of the database before they apply it to their own regions of interest.

Appendix D.1. Applicability Guidelines for the EC2015 Tidal Database

The EC2015 tidal database provides elevation amplitudes and phases throughout the WNAT domain for all 37 constituents frequently used by NOS. Although data for all 37 constituents are included in the database, care should be taken when deciding how many of these constituents are important for the user's intended application. Often, accurate results can be obtained when using only

the primary astronomic tides, particularly if the boundary of interest is in deeper water, far removed from the coastline.

This database does not provide information regarding responses associated with density effects, riverine driven circulation, wind and atmospheric pressure driven events and/or oceanic currents. Vertical and horizontal variations in density can set up steric level differences in sea surface elevation, can drive significant horizontal circulation patterns, and can cause variation in the vertical structure of the currents. These effects tend to be important in estuarine or delta systems with significant freshwater riverine inflows. Furthermore the seasonal heating of the upper layers of the ocean's surface directly drives the expansion in the upper layer water volume that is associated with a seasonal fluctuation of water level. This can be especially significant in the Gulf of Mexico and the Caribbean Sea. It is noted that published tidal constituent data includes these seasonal sea surface expansions as long-term tidal constituents such as the Sa Solar annual and the Ssa Solar semiannual constituents. From a tidal hydrodynamics perspective these long-term constituents (with periods of a year and half a year respectively) are of astronomical origin and should appear as weak tides. They may also be generated through nonlinear interactions that lead to extremely weak responses. Nonetheless, in harmonically-decomposed measured field data, these constituents can appear as significant constituents since the driving radiational heating process is also an annual event. In the Gulf of Mexico, the Sa and Ssa elevation constituents can be almost as large as the dominant diurnal tides while current responses are much smaller due to the long-term period associated with these constituents. Thus it is emphasized that the EC2015 computations are entirely barotropic and do not include any of these density effects.

Rivers were not included in the EC2015 tidal database calculations. The barotropic pressure gradient and mass input effects of the river will be important in the immediate vicinity of the river outlet and will diminish away from the river outlet. Wind driven and/or atmospheric pressure driven effects such as coastal setup and storm surge and any basinwide modes that may be set up by these processes are also not included in the database. These effects can be significant on the shelf as well as within bays and estuaries. Major oceanic circulation patterns such as the Gulf Stream and the associated loop currents and other eddies, which are shed from it, are not included in the database. These currents tend to reside off the shelf in deep ocean waters but can be associated with fast flows in the 1 to 2 m/s range.

Finally the local accuracy of the EC2015 tidal computations will be affected by the accuracy of the geometry and bathymetry locally defined in the WNAT-based EC2015 grid. Geometric and bathymetric inaccuracies in the grid will especially affect the accuracy of the currents. Obviously a missing estuary or island or inaccurate bathymetry will greatly influence the database computations.

Appendix D.2. Usage Guidelines for the EC2015 Tidal Database

The EC2015 tidal constituent database can be applied anywhere within the defined WNAT domain. However, the prevailing hydrodynamics in a specific region will determine how accurately the currents will be predicted. If the surface elevation response and currents are indeed dominated by astronomical tides, then the database will provide an excellent prediction of the response. A good estimate of the accuracy of the EC2015 tides can be obtained by examining the regional error estimates given in Tables 7 and 8, or by examining the error plots provided for the dominant constituents in Appendix C; although plots are only provided for the M_2 and K_1 constituents, in general, all four of the semi-diurnal constituents follow the same regional trends, as do the diurnal constituents. Furthermore how accurately the EC2015 grid and bathymetry describe the region of specific interest influences the accuracy and appropriateness of applying database values.

For locations that are tidally dominated and for which the EC2015 grid accurately describes both local geometry and bathymetry, the database can be directly applied to extract tidal elevations and currents. Because the thirty-seven constituents are computed at every node and are defined within the

framework of a finite element grid, values at any point within the domain can be readily interpolated from the nodal values within which the point lies.

An extraction program, ADCIRC_db_extract.F90, together with the EC2015 finite element grid file, ec2012_v3d_chk.grd, accompany the tidal database. The user must supply an input file that provides the number of extraction points desired followed by the list of coordinates for those points. The extraction program will prompt the user for this input files as well as the name of the grid used to create the database. The program will also prompt the user whether they would like to produce the harmonic constituent output for elevations, velocities or both and then will produce the harmonic extraction output for amplitude and phase at the specified location(s) according to the user's request. Elevation output is stored in elev_hc.out while velocity output is stored in vel_hc.out. Additionally, diagnostic output is written to tides.dia and provides the location of each extraction point in the global mesh as well as the interpolation weights used to calculate the harmonic constituents. The KDTREE2 search algorithms have been incorporated into the new extraction program to facilitate a speedier search response. Finally, the program takes advantage of dynamic allocation in order to avoid the old hardcoded array limitations found in previous extraction routines. The ADCIRC_db_extract.F90 program will work with any old ADCIRC databases that utilized the individual fort.53 and fort.54 file formats.

A time-history of response can be readily Fourier synthesized using the outputs in the elev_hc.out and vel_hc.out files. For example a time-history of water-surface elevation can be computed as

$$\zeta\left(x,y,t\right) = \sum A_i\left(x,y\right) f_i\left(t_0\right) \cos\left[\sigma_i\left(t-t_0\right) + V_i\left(t_0\right) - h_i\left(x,y\right)\right] \tag{D1}$$

where $A_i(x,y)$ and $h_i(x,y)$ are the amplitude and phase, respectively, at the location (x,y) of interest for constituent i, which are provided by the EC2015 tidal database, and the frequency $\sigma_i = 2\pi/T_i$. The frequencies σ_i in rad/sec and periods T_i in hours for each of the 37 constituents included in the database are presented in Table D1. It is important to specify frequencies precisely, at least to eight significant figures. The nodal factor $f_i(t_0)$ and the equilibrium argument, $V_i(t_0)$, relative to reference time t_0 can be computed using program tide_fac.f, which is available as a utility program on the ADCIRC website [60].

Table D1. Frequencies and periods for EC2015 harmonic constituents.

Constituent	Frequency (Rad/s)	Period (h)
M(2)	0.0001405189	12.42
N(2)	0.0001378797	12.66
S(2)	0.0001454441	12.00
O(1)	0.0000675977	25.82
K(1)	0.0000729212	23.93
K(2)	0.0001458423	11.97
L(2)	0.0001431581	12.19
2N(2)	0.0001352405	12.91
R(2)	0.0001456432	11.98
T(2)	0.0001452450	12.02
Lambda(2)	0.0001428049	12.22
Mu(2)	0.0001355937	12.87
Nu(2)	0.0001382329	12.63
J(1)	0.0000755604	23.10
M(1)	0.0000702820	24.83
OO(1)	0.0000782446	22.31
P(1)	0.0000725229	24.07
Q(1)	0.0000649585	26.87

Table D1. *Cont.*

Constituent	Frequency (Rad/s)	Period (h)
2Q(1)	0.0000623193	28.01
Rho(1)	0.0000653117	26.72
M(4)	0.0002810378	6.21
M(6)	0.0004215567	4.14
M(8)	0.0005620756	3.11
S(4)	0.0002908882	6.00
S(6)	0.0004363323	4.00
M(3)	0.0002107784	8.28
S(1)	0.0000727221	24.00
MK(3)	0.0002134401	8.18
2MK(3)	0.0002081166	8.39
MN(4)	0.0002783986	6.27
MS(4)	0.0002859630	6.10
2SM(2)	0.0001503693	11.61
Mf	0.0000053234	327.86
Msf	0.0000049252	354.37
Mm	0.0000026392	661.31
Sa	0.0000001991	8765.82
Ssa	0.0000003982	4382.91

In locations and/or at times where the hydrodynamics is not tidally dominated and/or the EC2015 grid does not provide sufficient geometric and/or bathymetric detail, a regional model that interfaces with the EC2015 model will lead to a better representation of regional flows. Some examples of cases where this may be appropriate include: (a) bays or estuaries not included in the grid; (b) shallow nonlinearly-dominated inlets or estuaries; (c) coastal and/or estuarine regions barotropically and/or baroclinically influenced by a significant riverine discharge; (d) combined wind- and tidally-driven circulation on a shelf. The basic idea is to construct a domain/grid that extends onto or beyond the shelf within the EC2015 domain. The open ocean boundary is then forced using the tidal constituent data from the EC2015 tidal data base. The defined domain may also include additional regional detail in geometric and bathymetric definition, may include additional forcing functions on select boundaries or within the domain, and/or may include additional terms in the governing equations.

The regional model open ocean boundary should be placed away from the region of immediate interest, and its exact position and shape depends on the application. In no case should the boundary be placed at the mouth or entrance to an embayment of interest. The tidal constituents on the open ocean boundary nodes of the regional model are extracted in the same way as a simple point location. It may be necessary to add an additional forcing component to the boundary elevation and/or radiation forcing function to account for additional interior domain processes and forces. In the development of a regional model it is also recommended that the bathymetry along the open boundary match the bathymetry of the EC2015 grid. This will help ensure that the boundary condition extracted from the EC2015 database is physically consistent with the regional model. Failure to match bathymetries along the regional model open boundary can lead to unrealistic gyre formation and/or instabilities in the regional model computations. The bathymetry can depart from that comprising the EC2015 grid away from the open boundary area.

The EC2015 tidal database is available on the ADCIRC website as two separate compressed files: EC2015_elev-only_tidaldatabase.tar, which contains all of the extraction programs, grids, and sample notes but only has the fort.53 elevation harmonics; and EC2015_tidaldatabase.tar, which has everything given in the previous file with the addition of the fort.54 velocity harmonics [24]. You will only need to download one of the files depending upon whether you wish to have access to the velocity data as well.

In addition to the ADCIRC_db_extract.F90 extraction program, the database also includes another utility for "cutting" a portion of the global database out for visualization within SMS (or other tools). The HarmonicResultScope.f90 program works much the same way as ResultScope.f90, for those who are familiar with that ADCIRC utility program. Additional notes about the usage of each of these programs, as well as sample input and output files for each, are included in the TidalExtract/ directory within the database tar file.

References

1. Pandoe, W.; Edge, B. Case Study for a Cohesive Sediment Transport Model for Matagorda Bay, Texas, with Coupled ADCIRC 2D-Transport and SWAN Wave Models. *J. Hydraul. Eng.* **2008**, *134*, 303–314. [CrossRef]

2. Grzegorzewski, A.S.; Johnson, B.D.; Wamsley, T.V.; Rosati, J.D. Sediment transport and morphology modeling of Ship Island, Mississippi, USA, during storm events. In Proceedings of Coastal Dynamics 2013, Arcachon Convention Centre, Arcachon, France, 24–28 June 2013; pp. 1505–1516.

3. Miles, T.; Seroka, G.; Kohut, J.; Schofield, O.; Glenn, S. Glider observations and modeling of sediment transport in Hurricane Sandy. *J. Geophys. Res. Oceans* **2015**, *120*, 1771–1791. [CrossRef]

4. Dietsche, D.; Hagen, S.C.; Bacopoulos, P. Storm Surge Simulations for Hurricane Hugo (1989): On the Significance of Inundation Areas. *J. Waterw. Port Coast. Ocean Eng.* **2007**, *133*, 183–191. [CrossRef]

5. Irish, J.L.; Resio, D.T.; Ratcliff, J.J. The influence of storm size on hurricane surge. *J. Phys. Oceanogr.* **2008**, *38*, 2003–2013. [CrossRef]

6. Kerr, P.C.; Donahue, A.S.; Westerink, J.J.; Luettich, R.A., Jr.; Zheng, L.Y.; Weisberg, R.H.; Huang, Y.; Wang, H.V.; Teng, Y.; Forrest, D.R.; et al. U.S. IOOS coastal and ocean modeling testbed: Inter-model evaluation of tides, waves, and hurricane surge in the Gulf of Mexico. *J. Geophys. Res. Oceans* **2013**, *118*, 5129–5172. [CrossRef]

7. Mattocks, C.; Forbes, C. A real-time, event-triggered storm surge forecasting system for the state of North Carolina. *Ocean Model.* **2008**, *25*, 95–119. [CrossRef]

8. Fleming, J.G.; Fulcher, C.W.; Luettich, R.A.; Estrade, B.D.; Allen, G.D.; Winer, S.H. A Real Time Storm Surge Forecasting System Using ADCIRC. In Proceedings of International Conference on Estuarine and Coastal Modeling 2007, Newport, RI, USA, 5–7 November 2007; Spaulding, M.L., Ed.; ASCE: Reston, VA, USA, 2008; pp. 893–912.

9. Dresback, K.M.; Fleming, J.G.; Blanton, B.O.; Kaiser, C.; Gourley, J.J.; Tromble, E.M.; Luettich, R.A., Jr.; Kolar, R.L.; Hong, Y.; van Cooten, S.; et al. Skill Assessment of a Real-Time Forecast System Utilizing a Coupled Hydrologic and Coastal Hydrodynamic Modeling During Hurricane Irene (2011). *Cont. Shelf Res.* **2013**, *71*, 78–94. [CrossRef]

10. Dietrich, J.C.; Dawson, C.N.; Proft, J.M.; Howard, M.T.; Wells, G.; Fleming, J.G.; Luettich, R.A., Jr.; Westerink, J.J.; Cobell, Z.; Vitse, M.; et al. Real-Time Forecasting and Visualization of Hurricane Waves and Storm Surge Using SWAN + ADCIRC and FigureGen. *Comput. Chall. Geosci.* **2013**, *156*, 49–70.

11. Feyen, J.; Hess, K.; Spargo, E.; Wong, A.; White, S.; Sellars, J.; Gill, S. Development of a continuous bathymetric/topographic unstructured coastal flooding model to study sea level rise in North Carolina. In Proceedings of International Conference on Estuarine and Coastal Modeling 2005, Charleston, SC, USA, 31 October–2 November 2005; Spaulding, M.L., Ed.; ASCE: Reston, VA, USA, 2006; pp. 338–356.

12. Atkinson, J.; McKee Smith, J.; Bender, C. Sea-Level Rise Effects on Storm Surge and Nearshore Waves on the Texas Coast: Influence of Landscape and Storm Characteristics. *J. Waterw. Port Coast. Ocean Eng.* **2013**, *139*, 98–117. [CrossRef]

13. Bilskie, M.V.; Hagen, S.C.; Medeiros, S.C.; Passeri, D.L. Dynamics of sea level rise and coastal flooding on a changing landscape. *Geophys. Res. Lett.* **2014**, *41*, 927–934. [CrossRef]

14. Cheng, T.K.; Hill, D.F.; Beamer, J.; García-Medina, G. Climate change impacts on wave and surge processes in a Pacific Northwest (USA) estuary. *J. Geophys. Res. Oceans* **2015**, *120*, 182–200. [CrossRef]

15. Carr, S.D.; Hench, J.L.; Luettich, R.A.; Forward, R.B.; Tankersley, R.A. Spatial patterns in the ovigerous Callinectes sapidus spawning migration: Results from a coupled behavioral-physical model. *Mar. Ecol. Prog. Ser.* **2005**, *294*, 213–226. [CrossRef]

16. Oliveira, A.; Fortunato, A.B.; Pinto, L. Modeling the hydrodynamics and the fate of passive and active tracers in the Guadiana estuary. *Estuar. Coast. Shelf Sci.* **2006**, *70*, 76–84. [CrossRef]

17. Reyns, N.B.; Eggleston, D.B.; Luettich, R.A. Secondary dispersal of early juvenile blue crabs within a wind-driven estuary. *Limnol. Oceanogr.* **2006**, *51*, 1982–1995. [CrossRef]

18. Tromble, E.; Kolar, R.; Dresback, K.; Luettich, R. River Flux Boundary Conditions in a Coupled Hydrologic-Hydrodynamic Modeling System. In Proceedings of International Conference on Estuarine and Coastal Modeling 2011, St. Augustine, FL, USA, 7–9 November 2011; Spaulding, M.L., Ed.; ASCE: Reston, VA, USA, 2013; pp. 510–527.

19. Dietrich, J.C.; Trahan, C.J.; Howard, M.T.; Fleming, J.G.; Weaver, R.J.; Tanaka, S.; Yu, L.; Luettich, R.A., Jr.; Dawson, C.N.; Westerink, J.J.; et al. Surface Trajectories of Oil Transport along the Northern Coastline of the Gulf of Mexico. *Cont. Shelf Res.* **2012**, *41*, 17–47. [CrossRef]

20. Alizad, K.; Hagen, S.C.; Morris, J.T.; Bacopoulos, P.; Bilskie, M.V.; Weishampel, J.F.; Medeiros, S.C. A coupled two-dimensional hydrodynamic-marsh model with biological feedback. *Ecol. Model.* **2016**, *327*, 29–43. [CrossRef]

21. Lyard, F.; Lefevre, F.; Letellier, T.; Francis, O. Modelling the Global Ocean Tides: Modern Insights from FES2004. *Ocean Dyn.* **2006**, *56*, 394–415. [CrossRef]

22. Westerink, J.J.; Luettich, R.A.; Scheffner, N.W. *ADCIRC: An Advanced Three-Dimensional Circulation Model for Shelves, Coasts, and Estuaries, Report 3: Development of a Tidal Constituent Database for the Western North Atlantic and Gulf of Mexico*; Technical Report DRP 92-6; U.S. Army Engineer Research and Development Center, Coastal and Hydraulics Laboratory: Vicksburg, MS, USA, 1993. Available online: http://www.unc.edu/ims/adcirc/publications/1993/1993_Westerink02.pdf (accessed on 27 June 2016).

23. Mukai, A.Y.; Westerink, J.J.; Luettich, R.A.; Mark, D. *Eastcoast 2001: A Tidal Constituent Database for the Western North Atlantic, Gulf of Mexico and Caribbean Sea*; Technical Report ERDC/CHL TR-02-24; U.S. Army Engineer Research and Development Center, Coastal and Hydraulics Laboratory: Vicksburg, MS, USA, 2002; p. 201. Available online: http://www.unc.edu/ims/adcirc/publications/2002/2002_Mukai01.pdf (accessed on 27 June 2016).

24. ADCIRC Tidal Databases—ADCIRC. Available online: http://adcirc.org/products/adcirc-tidal-databases/ (accessed on 1 July 2016).

25. Westerink, J.J.; Luettich, R.A.; Muccino, J.C. Modelling tides in the western North Atlantic using unstructured graded grids. *Tellus A* **1994**, *46*, 178–199. [CrossRef]

26. Blain, C.A.; Westerink, J.J.; Luettich, R.A. The influence of domain size on the response characteristics of a hurricane storm surge model. *J. Geophys. Res.* **1994**, *99*, 18467–18479. [CrossRef]

27. Bathymetric Data Viewer. Available online: http://maps.ngdc.noaa.gov/viewers/bathymetry/ (accessed on 8 September 2016).

28. Schureman, P. *Manual of Harmonic Analysis and Prediction of Tides*; Special Publication 98, Coast and Geodetic Survey; U.S. Department of Commerce: Washington, DC, USA, 1958; p. 317.

29. Kinnmark, I.P.E. *The Shallow Water Wave Equations: Formulations, Analysis and Application*; Springer: Berlin, Germany, 1986.

30. Luettich, R.A.; Westerink, J.J.; Scheffner, N.W. *ADCIRC: An Advanced Three-Dimensional Circulation Model for Shelves, Coasts, and Estuaries; Report 1: Theory and Methodology of ADCIRC-2DDI and ADCIRC-3DL*; Technical Report CERC-TR-DRP-92-6; U.S. Army Corps of Engineers, U.S. Department of the Army: Washington, DC, USA, 1992.

31. Kolar, R.L.; Gray, W.G.; Westerink, J.J.; Luettich, R.A. Shallow Water Modeling in Spherical Coordinates: Equation Formulation, Numerical Implementation and Application. *J. Hydraul. Res.* **1994**, *32*, 3–24. [CrossRef]

32. Bunya, S.; Dietrich, J.C.; Westerink, J.J.; Ebersole, B.A.; Smith, J.M.; Atkinson, J.H.; Jensen, R.; Resio, D.T.; Luettich, R.A.; Dawson, C.; et al. A High-Resolution Coupled Riverine Flow, Tide, Wind, Wind Wave, and Storm Surge Model for Southern Louisiana and Mississippi. Part 1: Model Development and Validation. *Mon. Weather Rev.* **2010**, *138*, 345–377. [CrossRef]

33. OSU Tidal Data Inversion. Available online: http://volkov.oce.orst.edu/tides/global.html (accessed on 27 June 2016).

34. NOAA/NOS's VDatum 3.6: Vertical Datums Transformation. Available online: http://vdatum.noaa.gov/welcome.html (accessed on 27 June 2016).

35. Hess, K.; Spargo, E.; Wong, A.; White, S.; Gill, S. *VDatum for Central Coastal North Carolina: Tidal Datums, Marine Grids, and Sea Surface Topography*; NOAA Technical Report NOS CS 21; U.S. Department of Commerce: Silver Spring, MD, USA, 2005. Available online: http://vdatum.noaa.gov/download/publications/2005_ TechReport_CS21.pdf (accessed on 16 June 2016).

36. Spargo, E.; White, S.; Hess, K. *VDatum for the Northeast Gulf of Mexico from Mobile Bay, Alabama, to Cape San Blas, Florida: Tidal Datum Modeling and Population of the Marine Grids*; NOAA Technical Report NOS CS 14; U.S. Department of Commerce: Silver Spring, MD, USA, 2008. Available online: http://vdatum.noaa. gov/download/publications/TM_NOS-CS14_FY08_28_EmilyHess_NEGulfOfMexico.pdf (accessed on 16 June 2016).

37. Yang, Z.; Myers, E.; Wong, A.; White, S. *VDatum for Chesapeake Bay, Delaware Bay and Adjacent Coastal Water Areas: Tidal Datums and Sea Surface Topography*; NOAA Technical Report NOS CS 15; U.S. Department of Commerce: Silver Spring, MD, USA, 2008. Available online: http://vdatum.noaa.gov/download/ publications/TM_NOS-CS15_FY08_26_Yang_VDatumCHES-DEL.pdf (accessed on 16 June 2016).

38. Yang, Z.; Myers, E.; White, S. *VDatum for Eastern Louisiana and Mississippi Coastal Waters: Tidal Datums, Marine Grids, and Sea Surface Topography*; NOAA Technical Memorandum NOS CS 19; U.S. Department of Commerce: Silver Spring, MD, USA, 2010. Available online: https://vdatum.noaa.gov/download/publications/CS_19_ FY09_26_Zizang_VDatum_NewOrleans_techMemor.pdf (accessed on 16 June 2016).

39. Yang, Z.; Myers, E.; White, S. *VDatum for Great South Bay, New York Bight and New York Harbor: Tidal Datums, Marine Grids, and Sea Surface Topography*; NOAA Technical Memorandum NOS CS 21; U.S. Department of Commerce: Silver Spring, MD, USA, 2010. Available online: https://vdatum.noaa.gov/download/ publications/CS_21_FY09_25_Zizang_VDatum_GreatSouthBay_techMemor.pdf (accessed on 16 June 2016).

40. Yang, Z.; Myers, E.; Jeong, I.; White, S. *VDatum for Coastal Waters from the Florida Shelf to the South Atlantic Bight: Tidal Datums, Marine Grids, and Sea Surface Topography*; NOAA Technical Memorandum NOS CS 27; U.S. Department of Commerce: Silver Spring, MD, USA, 2012. Available online: https://vdatum.noaa.gov/ download/publications/TM_NOS-CS27_FY12-14_VDatum_FL_SA_zyang.pdf (accessed on 16 June 2016).

41. Xu, J.; Myers, E.; Jeong, I.; White, S. *VDatum for Coastal Waters of Texas and Western Louisiana: Tidal Datums and Topography of the Sea Surface*; NOAA Technical Memorandum NOS CS 29; U.S. Department of Commerce: Silver Spring, MD, USA, 2013. Available online: https://vdatum.noaa.gov/download/publications/TM_ NOS-CS29_FY13_Xu_TexasWesternLouisiana.pdf (accessed on 16 June 2016).

42. Yang, Z.; Myers, E.; Jeong, I.; White, S. *VDatum for the Gulf of Maine: Tidal Datums and Topography of the Sea Surface*; NOAA Technical Memorandum NOS CS 31; U.S. Department of Commerce: Silver Spring, MD, USA, 2013. Available online: http://vdatum.noaa.gov/download/publications/TM_NOS_CS_31_FY13_04_ Yang_VDatumGulfOfMaine.pdf (accessed on 16 June 2016).

43. Wang, J.; Myers, E.; Jeong, I.; White, S. *VDatum for the Coastal Waters of Puerto Rico and the U. S. Virgin Islands: Tidal Datums, Marine Grid, and Sea Surface Topography*; NOAA Technical Memorandum NOS CS 33; U.S. Department of Commerce: Silver Spring, MD, USA, 2013. Available online: https://vdatum. noaa.gov/download/publications/TM_NOS_CS33_FY14_02_JWang_VDatumPuertoRico.pdf (accessed on 16 June 2016).

44. VDatum Manual for Development and Support of NOAA's Vertical Datum Transformation Tool, VDatum. Version 1.01. 2012. Available online: http://www.nauticalcharts.noaa.gov/csdl/publications/Manual_2012. 06.26.doc (accessed on 27 June 2016).

45. Bacopoulos, P.; Parrish, D.M.; Hagen, S.C. Unstructured mesh assessment for tidal model of the South Atlantic Bight and its estuaries. *J. Hydraul. Res.* **2011**, *49*, 487–502. [CrossRef]

46. Amante, C.; Eakins, B.W. *ETOPO1 1 Arc-Minute Global Relief Model: Procedures, Data Sources and Analysis*; NOAA Technical Memorandum NESDIS NGDC-24; National Geophysical Data Center, NOAA: Boulder, CO, USA, 2009. Available online: https://www.ngdc.noaa.gov/mgg/global/relief/ETOPO1/docs/ETOPO1.pdf (accessed on 2 November 2012).

47. ETOPO1 Global Relief. Available online: http://www.ngdc.noaa.gov/mgg/global/global.html (accessed on 27 June 2016).

48. Becker, J.J.; Sandwell, D.T.; Smith, W.H.F.; Braud, J.; Binder, B.; Depner, J.; Fabre, D.; Factor, J.; Ingalls, S.; Kim, S.-H.; et al. Global Bathymetry and Elevation Data at 30 Arc Seconds Resolution: SRTM30_PLUS. *Mar. Geod.* **2009**, *32*, 355–371. [CrossRef]

49. Sandwell, D.T.; Müller, R.D.; Smith, W.H.F.; Garcia, E.; Francis, R. New global marine gravity model from CryoSat-2 and Jason-1 reveals buried tectonic structure. *Science* **2014**, *346*, 65–67. [CrossRef]

50. Satellite Geodesy, IGPP, SIO, UCSD | Global Topography | SRTM30, Multibeam and Predicted. Available online: http://topex.ucsd.edu/WWW_html/srtm30_plus.html (accessed on 27 June 2016).

51. Global Tide - FES: Aviso+. Available online: http://www.aviso.altimetry.fr/en/data/products/auxiliary-products/global-tide-fes.html (accessed on 27 June 2016).

52. Egbert, G.D.; Bennett, A.F.; Foreman, M.G.G. TOPEX/POSEIDON tides estimated using a global inverse model. *J. Geophys. Res.* **1994**, *99*, 24821–24852. [CrossRef]

53. Egbert, G.D.; Erofeeva, S.Y. Efficient inverse modeling of barotropic ocean tides. *J. Atmos. Oceanic Technol.* **2002**, *19*, 183–204. [CrossRef]

54. Carrère, L.; Lyard, F.; Cancet, M.; Roblou, L.; Guillot, A. FES2012: A new global tidal model taking advantage of nearly 20 years of altimetry measurements. In Proceedings of meeting "20 Years of Progress in Radar Altimetry Symposium", Venice, Italy, 24–29 September 2012.

55. USGS Coastal and Marine Geology—usSEABED. Available online: http://walrus.wr.usgs.gov/usseabed/index.html (accessed on 29 June 2016).

56. Kolar, R.L.; Westerink, J.J.; Cantekin, M.E.; Blain, C.A. Aspects of nonlinear simulations using shallow-water models based on the wave continuity equation. *Comput. Fluids* **1993**, *23*, 523–538. [CrossRef]

57. NOAA Tides and Currents. Available online: http://tidesandcurrents.noaa.gov/ (accessed on 8 September 2016).

58. *IHO Tidal Constituent Bank: Station Catalogue*; Department of Fisheries and Oceans: Ottawa, ON, Canada, 1979.

59. Qi, S. Use of International Hydrographic Organization Tidal Data for Improved Tidal Prediction. Master's Thesis, Portland State University, Portland, OR, USA, December 2012.

60. ADCIRC Utility Programs—ADCIRC. Available online: http://adcirc.org/home/related-software/adcirc-utility-programs/ (accessed on July 2016).